Periodic FMMs and Calderon's preconditioning in acoustics and elastodynamics(Dissertation_全文)

AUTHOR(S):

Isakari, Hiroshi

Periodic FMMs and Calderon's preconditioning in acoustics and elastodynamics

ISAKARI Hiroshi

Periodic FMMs and Calderon's preconditioning in acoustics and elastodynamics

ISAKARI Hiroshi

Graduate School of Engineering
Kyoto University

January 2012

Acknowledgements

The author expresses the deepest gratitude to Professor Naoshi Nishimura at Computational Mechanics Laboratory of Kyoto University, for his enthusiastic guidance, considerable encouragement and invaluable discussion that make the research of great achievement. The author will not forget Professor Nishimura's advice "Beautiful formulations give us good results, so keep trying to deduce beautiful equations".

The author especially would like to express his appreciation to Professor Takeshi Tamura who was, before his death, the author's Ph.D. supervisor. It was the author's privilege and pressure to learn from Professor Tamura.

The author thanks Professor Toyoaki Miyagawa and Professor Tomoaki Utsunomiya for their reviews and criticisms.

The author also thanks Professor Shun-ichi Kobayashi at Geotechnical Engineering Laboratory of Kanazawa University whose wide range of knowledge about mechanics was great impact to the author.

The author also thanks Professor Hitoshi Yoshikawa at Computational Mechanics Laboratory of Kyoto University whose opinions and information have helped the author very much throughout the production of this study.

The author also thanks Professor Jun Saito at Applied Mechanics Laboratory of Kyoto University who provided carefully considered feedback and valuable comments.

The author pays his respect to Dr. Yoshihiro Otani, who is known as a pioneer in periodic FMMs.

The author has also greatly benefited from members of his laboratory. The author thanks the members of Applied Mechanics and Computational Mechanics Laboratory. Especially, the author would like to extend his gratitude to Mr. Kazuki Niino for discussions about Calderon's preconditioning. The author also enjoyed the discussions about elastodynamics with Mr. Hisashi Shidooka and Mr. Shuntaro Sawine.

The author would like to thank JSPS for a grant that made it possible to complete this study.

Finally, the author would also like to express his gratitude to his family and all his friends for their moral support and warm encouragements.

Contents

1 Introduction **3**
- 1.1 Introduction . . . 3
- 1.2 Organisation of thesis . . . 4

2 A periodic FMM for elastodynamics in 3D **6**
- 2.1 Introduction . . . 6
- 2.2 Formulation . . . 6
  - 2.2.1 Statement of the problem . . . 6
  - 2.2.2 Boundary integral equation method . . . 7
  - 2.2.3 Fast multipole method . . . 8
  - 2.2.4 Periodic FMM . . . 12
  - 2.2.5 Far fields . . . 15
- 2.3 Numerical examples . . . 16
  - 2.3.1 Infinite domain . . . 17
  - 2.3.2 Scattering by elastic inclusions . . . 17
  - 2.3.3 Scattering by a periodic void . . . 18
- 2.4 Conclusions . . . 19

3 A periodic FMM for acoustics-elastodynamics coupled problems **22**
- 3.1 Introduction . . . 22
- 3.2 Formulation . . . 22
  - 3.2.1 Statement of the problem . . . 22
  - 3.2.2 Boundary integral equations . . . 23
- 3.3 Numerical examples . . . 24
  - 3.3.1 Scattering by a slab immersed in water . . . 24
  - 3.3.2 Scattering by periodically perforated slab . . . 26
  - 3.3.3 Scattering by spherical inclusions . . . 27
- 3.4 Conclusions . . . 28

4 Calderon's preconditioning for periodic FMM for elastodynamics in 3D **29**
- 4.1 Introduction . . . 29
- 4.2 PMCHWT formulation for elastic problems . . . 29
  - 4.2.1 Boundary integral equations for the periodic boundary value problems . . . 29
- 4.3 Calderon's formulae and the Calderon preconditioning . . . 30
  - 4.3.1 The case of $\mu^{(1)} = \mu^{(2)}$ . . . 31
  - 4.3.2 The case of $\mu^{(1)} \neq \mu^{(2)}$ . . . 32
- 4.4 Numerical examples . . . 33
  - 4.4.1 Scattering by a doubly periodic layer of spherical scatters . . . 34
  - 4.4.2 Performance around anomalies . . . 42
  - 4.4.3 Scattering by a phononic crystal with the NaCl-type structure . . . 43
- 4.5 Conclusions . . . 46

5 Calderon's preconditioning for acoustics-elastodynamics coupled problems **49**
- 5.1 Introduction . . . 49
- 5.2 PMCHWT formulation and Calderon's preconditioning . . . 49
- 5.3 Other formulations based on the Burton-Miller method and Calderon's preconditioning . . . 51
- 5.4 Numerical examples . . . 52

5.4.1 Scattering by periodically perforated tungsten slab immersed in water 52
5.4.2 Scattering by spherical inclusion immersed in water 53
5.5 Conclusion 55

6 Conclusions **56**

Chapter 1

Introduction

1.1 Introduction

In the field of science and engineering, it is required to solve boundary value problems (BVPs) of partial differential equations (PDEs). As a numerical solver for BVPs, we can mention Finite Difference Method (FDM), Finite Element Method (FEM) and Boundary Integral Equation Method (BIEM, also called Boundary Element Method or BEM). With BIEM, we translate the PDEs into boundary integral equations (BIEs) and discretise them into linear algebraic equations. In the discretisation, we only have to consider the boundary of a domain. This remarkable feature keeps the size of the linear equations small in BIEM. It is also notable that, among various numerical solvers for PDEs, the BIEM is particularly effective for wave scattering problems because of the following reasons:

- Exterior problems are easily handled since discretisation of the domain is not required.
- Any artificial treatment to obtain a numerical solution which satisfies radiation conditions is not needed since the solution is expressed in terms of a superposition of the fundamental solution which satisfies the radiation conditions.

When we use the BIEM, however, we have to solve the linear equations with dense coefficient matrices and the complexity for computing these matrices is $O(N^2)$ where N is the number of unknowns. This complexity problem, however, is now almost solved because of the developments of the so called fast BIEMs, which use acceleration techniques such as Fast Multipole Methods (FMMs) [1] to decrease the computational complexity of BIEM to $O(N(\log N)^\alpha)$ ($\alpha \geq 0$). The FMM is originally proposed by Rokhlin [2] as an acceleration technique for BIEM for Laplace's equation in 2D and then further developed for N body problems by Greengard and Rokhlin [3]. Because of this work, the FMM is made known widely. After that, the FMM is studied for variety of wave problems as found in [4, 5], for example. Especially in the field of elastodynamics, applications of the FMM for BIEM have been studied after some pioneering works [6, 7]. Combined with the FMM, the BIEM is now considered as a fast solver for large scale wave scattering problems.

As an attempt to further increase the applicability of fast BIEMs, we have been investigating applications of FMM accelerated BIEMs to periodic wave scattering problems (periodic FMM) these few years. This is partly because of increased attention to periodic structures [8] such as photonic crystals [9] and metamaterials [10] in optics. The photonic crystal, for instance, is a periodic structure of dielectric materials having a geometric periodicity comparable to the wavelength of light. One can design a photonic crystal which prohibits the propagation of waves in a certain frequency range called a stopband. As another interesting phenomenon related to periodic problems, we can mention the Wood's anomaly [11]. This is a phenomenon in which a slight change of incident angle or frequency of the incident wave may cause a drastic change on the scattered field. This phenomenon is somehow related to guided modes in periodic structures [12]. It is also known that near Wood's anomaly the accuracy and the convergence of numerical solver will decline [11]. In spite of this difficulties, we have confirmed the efficiency of the periodic FMM through studies for periodic wave scattering problems in electromagnetics [13, 14]. From these investigations, we conclude that the periodic FMM can be a powerful designing tool for metamaterials and photonic crystals in the field of nanophotonics.

Stopband and/or some other interesting phenomena due to periodicity will be observed also in the field of elasticity. Actually, materials which have stopbands for elastic waves are called phononic crystals [15].

The phononic crystal can be used as a Surface Acoustic Wave (SAW) filter, a sound-proof device and a anti-vibration device. In elasticity, however, there are few studies of numerical solvers for periodic problems compared with the case of optics. To design phononic crystals effectively, we have to develop fast and accurate numerical solvers for the periodic boundary value problems for elastodynamics.

In view of these circumstances, the author will extend the periodic FMM to elastodynamics in 3D in this thesis. The author first considers the phononic crystal in which both inclusions and the exterior matrix are made of elastic materials. Through numerical analyses of basic academic problems, the accuracy and efficiency of the proposed method will be confirmed.

Bearing the application of phononic crystals to sound-proof device in mind, we think that it is also important to study the behaviour of sound wave scattered by phononic crystals. This problem is, however, no longer a pure elastodynamic problem because sound waves have longitudinal components only. It is natural to treat this problem as an acoustic-elastic coupled problem, in which the sound pressure is governed by Helmholtz' equation in the acoustic field while the displacement is governed by Navier-Cauchy's equation in the elastodynamic field. As another reason for an importance of the acoustic-elastic coupled periodic problem, we can mention that material constants of exterior domain should be considerably different from those of inclusion [15] for periodic structure to have special properties due to the periodicity. Because of this aspect, the exterior domain is often made of fluid (water, hydrargyrum, etc.) while the inclusion is made of metal. The author will present an FMM for this acoustics-elastodynamics coupled problem, together with numerical examples in this thesis.

When we deal with realistic phononic crystals we may encounter large-scale problems, which include over millions of degrees of freedom. This is partly because multi-layered phononic crystals are often considered to produce sufficiently wide stopbands [16]. When we use FMM, we ordinarily use iterative methods such as GMRES or BiCG for solving linear equations $A\boldsymbol{x} = \boldsymbol{b}$ obtained as discretised boundary integral equations since the FMM gives us a fast method of computation of not A itself but $A\boldsymbol{x}$. Unfortunately, the number of iteration of the iterative methods is unpredictable since the FMM does not assure the fast convergence of the iterative methods. It is obvious that the computational cost for solving such equations heavily depends on the iteration number of these solvers. This is especially true in periodic wave problems, because the iteration number is known to increase sharply around the so called Wood's anomaly [11].

Use of preconditioners is a common technique to decrease the number of iterations. Indeed, we can find many such attempts in literature, some of which propose general purpose preconditioners, while others consider techniques applicable to particular numerical methods. As an example of the latter type of preconditioners suitable especially for BIEM, we can mention approaches based on Calderon's formulae proposed originally by Steinbach and Wendland in Laplace's equation [17]. This method is applied to Helmholtz' equation by Christiansen and Nédélec [18] and more recently by Antoine and Boubendir [19]. Niino and Nishimura confirmed the efficiency of the Calderon preconditioning for periodic wave scattering problems for Helmholtz' equation [20, 21]. Niino and Nishimura pointed out that the efficiency of the approach proposed by Antoine and Boubendir [19] can be enjoyed simply by ordering the matrices properly without using preconditioners. In the present study, the author will extend the Calderon preconditioners to periodic FMMs for elastodynamics and acoustics-elastodynamics coupled problems in 3D and apply the method to relatively large problems whose degrees of freedom is over one million.

1.2 Organisation of thesis

This thesis is organised as follows.

- Chapter 2
  In chapter 2, we investigate a periodic FMM for elastodynamics in 3D. To avoid fictitious eigenfrequency, we use the Burton-Miller method. We verify the proposed method by comparing the obtained numerical results with analytic solutions for an infinite domain. We then apply the proposed method to scattering problems for two periodic arrays of elastic inclusions and holes, and compare the obtained energy transmittances with analytical and experimental result from previous studies. We observe good agreements. Through these numerical analyses, we confirm the occurrence of Wood's anomaly in elastodynamics.

  The material in this chapter is taken from Isakari et al.[22].

- Chapter 3
  In chapter 3, an FMM for periodic boundary value problems of Helmholtz-elastodynamics coupled

field is investigated as an extension of studies on periodic FMMs. Both Helmholtz and elastodynamic field are solved by FMM. The efficiency and accuracy of the proposed method are confirmed through three kinds of basic numerical tests. The materials dealt with are a polymethyl methacrylate slab, a periodically perforated tungsten slab and periodically set spherical elastic inclusions all of which are immersed in water. The numerical results are well verified by comparing with analytical solutions or results from previous studies.

The material in this chapter is taken from Isakari et al.[23].

- Chapter 4
  In chapter 4, we investigate preconditioning approaches based on Calderon's formulae for periodic boundary value problems for elastodynamics in 3D formulated in Chapter 2. The efficiency of the proposed preconditioners are then tested with some numerical examples in section 4.4, where a variety of scattering problems by periodic structures are considered.

  The material in this chapter is taken from Isakari et al.[24].

- Chapter 5
  In chapter 5, we investigate the Calderon preconditioning for acoustics-elastodynamics coupled problems formulated in chapter 3.

- Chapter 6
  In chapter 6 we state conclusions.

Chapter 2

A periodic FMM for elastodynamics in 3D

2.1 Introduction

In this chapter, we investigate a periodic FMM for elastodynamics in 3D. To avoid fictitious eigenvalue problem, we use the Burton-Miller method [25]. We verify the proposed method by comparing the obtained numerical results with analytic solutions for an infinite domain. We then apply the proposed method to scattering problems for two periodic arrays of elastic inclusions and holes, and compare the obtained energy transmittances with analytical and experimental result from previous studies. We observe good agreements. Through these numerical analyses, we confirm the occurrence of Wood's anomaly in elastodynamics.

The material in this chapter is taken from Isakari et al.[22].

2.2 Formulation

2.2.1 Statement of the problem

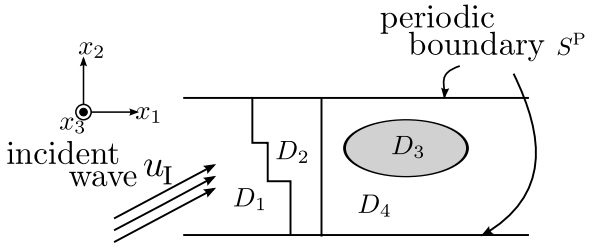

Figure 2.1: Periodic boundary value problems.

Let D be a domain defined by

$$D = ((-\infty, \infty) \otimes [-\zeta_2/2, \zeta_2/2] \otimes [-\zeta_3/2, \zeta_3/2]), \tag{2.1}$$

which is further subdivided into N subdomains $D = D_1 \cup D_2 \cup \cdots \cup D_N$ (Fig. 2.1). We consider doubly periodic problems in which the periodic lengths are ζ_2 along the x_2 axis and ζ_3 along the x_3 axis, respectively. The domain D is impinged upon by an incident plane wave denoted by $\boldsymbol{u}_{\mathrm{I}}$.

We are interested in obtaining the displacement u_i, which is governed by the following Navier-Cauchy's equation in each subdomain D_m:

$$\mu^{(m)} u_{i,jj} + (\lambda^{(m)} + \mu^{(m)}) u_{j,ij} + \rho^{(m)} \omega^2 u_i = 0, \tag{2.2}$$

where $\rho^{(m)}$ is the density and $\lambda^{(m)}$ and $\mu^{(m)}$ are Lamé's constants of the domain D_m and ω is the frequency, respectively. Using these quantities, we define the elasticity tensor $C_{ijpq}^{(m)}$ by

$$C_{ijpq}^{(m)} = \lambda^{(m)}\delta_{ij}\delta_{pq} + \mu^{(m)}(\delta_{ip}\delta_{jq} + \delta_{iq}\delta_{jp}).$$

We assume as boundary conditions the continuity of the displacements u_i and the tractions $t_i = C_{ijpq}^{(m)}u_{p,q}n_j$ across $\partial D_k \cap \partial D_m$ where n_j is the unit normal vector on $\partial D_k \cap \partial D_m$. Furthermore, we require the radiation condition to the scattered field.

On the periodic boundaries given by $S^{\mathrm{P}} = \{\boldsymbol{x} |\ |x_2| = \dfrac{\zeta_2}{2} \text{ or } |x_3| = \dfrac{\zeta_3}{2}\}$, we require the following periodic boundary conditions:

$$u_i\left(x_1, \frac{\zeta_2}{2}, x_3\right) = e^{\mathrm{i}\beta_2} u_i\left(x_1, -\frac{\zeta_2}{2}, x_3\right), \tag{2.3}$$

$$\frac{\partial u_i}{\partial x_2}\left(x_1, \frac{\zeta_2}{2}, x_3\right) = e^{\mathrm{i}\beta_2} \frac{\partial u_i}{\partial x_2}\left(x_1, -\frac{\zeta_2}{2}, x_3\right), \tag{2.4}$$

$$u_i\left(x_1, x_2, \frac{\zeta_3}{2}\right) = e^{\mathrm{i}\beta_3} u_i\left(x_1, x_2, -\frac{\zeta_3}{2}\right), \tag{2.5}$$

$$\frac{\partial u_i}{\partial x_3}\left(x_1, x_2, \frac{\zeta_3}{2}\right) = e^{\mathrm{i}\beta_3} \frac{\partial u_i}{\partial x_3}\left(x_1, x_2, -\frac{\zeta_3}{2}\right), \tag{2.6}$$

where $\beta_i = k_{\mathrm{I}} p_i \zeta_i$ $(i = 2, 3)$ are the phase differences of the incident wave, k_{I} is the wave number and p_i is a unit vector defining the directions of propagation of the incident wave $\boldsymbol{u}_{\mathrm{I}}$, respectively. Note that the values of β_i $(i = 2, 3)$ used in this thesis may differ from the non-dimensional Floquet wavenumbers used in the theory of periodic structures by $2n\pi$ where n is an integer [12].

2.2.2 Boundary integral equation method

The boundary integral equations which are equivalent to the periodic boundary value problem are as follows:

$$\frac{1}{2}(\boldsymbol{u} + \alpha\boldsymbol{t}) = (\boldsymbol{u}_{\mathrm{I}} + \alpha\boldsymbol{t}_{\mathrm{I}})\delta_{1m} + (\mathcal{U}^{(m)} + \alpha\mathcal{T}^{*(m)})\boldsymbol{u} - (\mathcal{T}^{(m)} + \alpha\mathcal{W}^{(m)})\boldsymbol{t}, \tag{2.7}$$

where m is the subdomain number, $\boldsymbol{u}^{\mathrm{I}}$ and $\boldsymbol{t}^{\mathrm{I}}$ are the incident wave and its traction, respectively. α is the coefficient of the Burtion-Miller method. Also, $\mathcal{U}^{(m)}$, $\mathcal{T}^{(m)}$, $\mathcal{T}^{*(m)}$ and $\mathcal{W}^{(m)}$ are integral operators defined as follows:

$$(\mathcal{U}^{(m)}\boldsymbol{v})_i = \int_{\partial D} \Gamma_{ij}^{\mathrm{P}(m)}(\boldsymbol{x} - \boldsymbol{y}) v_j(y) dS_y, \tag{2.8}$$

$$(\mathcal{T}^{(m)}\boldsymbol{v})_i = \text{v.p.} \int_{\partial D} \Gamma_{Iij}^{\mathrm{P}(m)}(\boldsymbol{x} - \boldsymbol{y}) v_j(y) dS_y, \tag{2.9}$$

$$(\mathcal{T}^{*(m)}\boldsymbol{v})_i = \text{v.p.} \int_{\partial D} T_{ij}^{(m)} \Gamma_{jk}^{\mathrm{P}(m)}(\boldsymbol{x} - \boldsymbol{y}) v_k(y) dS_y, \tag{2.10}$$

$$(\mathcal{W}^{(m)}\boldsymbol{v})_i = \text{p.f.} \int_{\partial D} T_{ij}^{(m)} \Gamma_{Ijk}^{\mathrm{P}(m)}(\boldsymbol{x} - \boldsymbol{y}) v_k(y) dS_y, \tag{2.11}$$

and "v.p." and "p.f." stand for Cauchy's principal value and the finite part of divergent integrals, respectively. The traction operator $T_{ij}^{(m)}$ is defined as $T_{ij}^{(m)} = C_{ipjq}^{(m)} n_p \partial_q$ and $\Gamma_{ij}^{\mathrm{P}(m)}$ and $\Gamma_{Iij}^{\mathrm{P}(m)}$ are Green's function and the kernel of double layer, both of which satisfy the periodic boundary conditions in Eq.(2.3)–(2.6) and the radiation condition. These kernel functions are given in terms of the following lattice sums:

$$\Gamma_{ij}^{\mathrm{P}(m)}(\boldsymbol{x} - \boldsymbol{y}) = \lim_{R\to\infty} \sum_{\boldsymbol{\omega}\in\mathcal{L}(R)} \Gamma_{ij}^{(m)}(\boldsymbol{x} - \boldsymbol{y} - \boldsymbol{\omega}) e^{\mathrm{i}\boldsymbol{\beta}\cdot\boldsymbol{\omega}}, \tag{2.12}$$

$$\Gamma_{Iij}^{\mathrm{P}(m)}(\boldsymbol{x} - \boldsymbol{y}) = \lim_{R\to\infty} \sum_{\boldsymbol{\omega}\in\mathcal{L}(R)} \Gamma_{Iij}^{(m)}(\boldsymbol{x} - \boldsymbol{y} - \boldsymbol{\omega}) e^{\mathrm{i}\boldsymbol{\beta}\cdot\boldsymbol{\omega}}, \tag{2.13}$$

where $\mathcal{L}$ stands for the following lattice points:

$$\mathcal{L}(R) = \{(0, \omega_2, \omega_3) | \omega_2 = p\zeta_2, \omega_3 = q\zeta_3,\ |p|, |q| \le R,\ p, q \in \mathbb{Z}\},$$

and $\Gamma_{ij}^{(m)}$ and $\Gamma_{Iij}^{(m)}$ represent the fundamental solution and the kernel of double layer for three dimensional elastodynamics given by:

$$\Gamma_{ij}^{(m)}(\boldsymbol{x}-\boldsymbol{y}) = \frac{1}{4\pi\mu^{(m)}}\left[\frac{e^{\mathrm{i}k_{\mathrm{T}}^{(m)}|\boldsymbol{x}-\boldsymbol{y}|}}{|\boldsymbol{x}-\boldsymbol{y}|}\delta_{ij} + \frac{1}{k_{\mathrm{T}}^{(m)2}}\frac{\partial^2}{\partial y_i \partial y_j}\left(\frac{e^{\mathrm{i}k_{\mathrm{T}}^{(m)}|\boldsymbol{x}-\boldsymbol{y}|}}{|\boldsymbol{x}-\boldsymbol{y}|} - \frac{e^{\mathrm{i}k_{\mathrm{L}}^{(m)}|\boldsymbol{x}-\boldsymbol{y}|}}{|\boldsymbol{x}-\boldsymbol{y}|}\right)\right], \tag{2.14}$$

$$\Gamma_{Iij}^{(m)}(\boldsymbol{x}-\boldsymbol{y}) = \frac{\partial}{\partial y_l}\Gamma_{ik}^{(m)}(\boldsymbol{x}-\boldsymbol{y})C_{klmj}n_m(y). \tag{2.15}$$

In these formulae, $k_{\mathrm{L}}^{(m)}$ and $k_{\mathrm{T}}^{(m)}$ stand for the wave numbers of longitudinal and transverse waves of the subdomain D_m defined by:

$$k_{\mathrm{L}}^{(m)} = \omega\sqrt{\frac{\rho^{(m)}}{\lambda^{(m)}+2\mu^{(m)}}}, \quad k_{\mathrm{T}}^{(m)} = \omega\sqrt{\frac{\rho^{(m)}}{\mu^{(m)}}}.$$

We note that the above formulation has no irregular frequency since it is based on the Burton-Miller method [25], which is known to have unique solution when the coefficient α has non-zero imaginary part.

2.2.3 Fast multipole method

Formulation

As preliminary descriptions, we give an outline of the fast multipole method for non-periodic problems in this section. The reader is referred to Rokhlin [2], Nishimura [1], etc. for further details.

We first note that FMM is a fast method to calculate the integrals which appear in the boundary integral equations (2.7). Hence, we usually use iterative methods such as GMRES and BiCG to solve linear equations $A\boldsymbol{x} = \boldsymbol{b}$ which is obtained as discretised integral equations (2.7) since these iterative solvers include the computation of $A\boldsymbol{x}$.

In FMM for wave problems in frequency domain, there are two kinds of expansions of the integral kernels as follows:

- FMM based on the series expansion of the fundamental solutions (low frequency FMM)
- FMM based on the diagonal form (for high frequency problems) [5]

We here use the low frequency FMM in this thesis since most of periodic problems of interest can appropriately be solved with this formulation. We henceforth state the formulation of the low frequency FMM for elastodynamics in 3D. To this end, we prepare the equations for the multipole expansion of the fundamental solutions $G_{\mathrm{L,T}}$ of three dimensional Helmholtz' equation since the FMM for elastodynamics can be formulated similarly to that for Helmholtz' equation. The fundamental solution of the three dimensional Helmholtz' equation with wave number $k_{\mathrm{L,T}}$ can be expanded into the following form:

$$\begin{aligned} G_{\mathrm{L,T}}(\boldsymbol{x}-\boldsymbol{y}) &= \frac{e^{\mathrm{i}k_{\mathrm{L,T}}|\boldsymbol{x}-\boldsymbol{y}|}}{4\pi|\boldsymbol{x}-\boldsymbol{y}|} \\ &= \frac{\mathrm{i}k_{\mathrm{L,T}}}{4\pi}\sum_{n=0}^{\infty}\sum_{m=-n}^{n}(2n+1)(-1)^m I_n^{-m}(\overrightarrow{Oy}, k_{\mathrm{L,T}})O_n^m(\overrightarrow{Ox}, k_{\mathrm{L,T}}), \end{aligned} \tag{2.16}$$

where we have assumed $|\overrightarrow{Ox}| > |\overrightarrow{Oy}|$. This expansion is known as Gegenbauer's addition theorem [26]. Also, the functions I_n^m and O_n^m denote entire solutions of Helmholtz' equation and radiating solutions of Helmholtz' equation which are singular at the origin, respectively. They are expressed as follows:

$$I_n^m(\overrightarrow{Ox}, k_{\mathrm{L,T}}) = j_n(k_{\mathrm{L,T}}|\overrightarrow{Ox}|)Y_n^m\left(\frac{\overrightarrow{Ox}}{|\overrightarrow{Ox}|}\right), \tag{2.17}$$

$$O_n^m(\overrightarrow{Ox}, k_{\mathrm{L,T}}) = h_n^{(1)}(k_{\mathrm{L,T}}|\overrightarrow{Ox}|)Y_n^m\left(\frac{\overrightarrow{Ox}}{|\overrightarrow{Ox}|}\right), \tag{2.18}$$

where j_n and $h_n^{(1)}$ are the spherical Bessel function of the nth order and the spherical Hankel function of the 1st kind and the nth order, respectively. Y_n^m is the spherical harmonic function. We note that in this

thesis we define Y_n^m in the following manner:

$$Y_n^m(\hat{x}) = \sqrt{\frac{(n-m)!}{(n+m)!}} P_n^m(\cos\theta) e^{\mathrm{i}m\phi},$$

where (r, θ, ϕ) represents the spherical coordinate of the point $\boldsymbol{x}$, $\hat{x}$ represents $\hat{x} = \dfrac{\overrightarrow{Ox}}{r}$. Also, P_n^m is the associated Ledgendre function defined as follows:

$$P_n^m(x) = (1-x^2)^{m/2} \frac{d^m}{dx^m} P_n(x) \quad (m \geq 0), \tag{2.19}$$

$$P_n^{-m}(x) = (-1)^m \frac{(n-m)!}{(n+m)!} P_n^m(x) \quad (m \geq 0), \tag{2.20}$$

where P_n is the Ledgendre polynomial.

I_n^m and O_n^m can be expanded into the following form:

$$I_n^m(\overrightarrow{Ox}, k_{\mathrm{L,T}}) = \sum_{n'=0}^{\infty} \sum_{m'=-n'}^{n'} (2n'+1) U_{n,n'}^{m,m'}(\overrightarrow{OO'}, k_{\mathrm{L,T}}) I_{n'}^{m'}(\overrightarrow{O'x}, k_{\mathrm{L,T}}), \tag{2.21}$$

$$O_n^m(\overrightarrow{Ox}, k_{\mathrm{L,T}}) = \sum_{n'=0}^{\infty} \sum_{m'=-n'}^{n'} (2n'+1) T_{n,n'}^{m,m'}(\overrightarrow{OO'}, k_{\mathrm{L,T}}) I_{n'}^{m'}(\overrightarrow{O'x}, k_{\mathrm{L,T}}), \tag{2.22}$$

where we have assumed $|\overrightarrow{OO'}| > |\overrightarrow{O'x}|$ in Eq.(2.22). In these expansions, $U_{n,n'}^{m,m'}$ and $T_{n,n'}^{m,m'}$ are the functions defined as follows:

$$U_{n,n'}^{m,m'}(\overrightarrow{Ox}, k_{\mathrm{L,T}}) = \sum_{n''=0}^{\infty} \sum_{m''=-n''}^{n''} (2n''+1) E_{n,n',n''}^{m,m',m''} I_{n''}^{m''}(\overrightarrow{Ox}, k_{\mathrm{L,T}}), \tag{2.23}$$

$$T_{n,n'}^{m,m'}(\overrightarrow{Ox}, k_{\mathrm{L,T}}) = \sum_{n''=0}^{\infty} \sum_{m''=-n''}^{n''} (2n''+1) E_{n,n',n''}^{m,m',m''} O_{n''}^{m''}(\overrightarrow{Ox}, k_{\mathrm{L,T}}), \tag{2.24}$$

$$E_{n,n',n''}^{m,m',m''} = \frac{\mathrm{i}^{n'+n''-n}}{4\pi} (-1)^{m'+m''} \int_{|\hat{x}|=1} Y_n^m(\hat{x}) Y_{n'}^{-m'}(\hat{x}) Y_{n''}^{-m''}(\hat{x}) dS_{\hat{x}}. \tag{2.25}$$

We note that $U_{n,n'}^{m,m'}$ and $T_{n,n'}^{m,m'}$ have the following properties:

$$U_{n,n'}^{-m,-m'}(\overrightarrow{Ox}) = (-1)^{m+m'} U_{n',n}^{m',n}(-\overrightarrow{Ox}), \tag{2.26}$$

$$T_{n,n'}^{-m,-m'}(\overrightarrow{Ox}) = (-1)^{m+m'} T_{n',n}^{m',n}(-\overrightarrow{Ox}). \tag{2.27}$$

We are now interested in computing the following integral $V_i(\boldsymbol{x})$:

$$V_i(x) = \int_S \Gamma_{ij}(\boldsymbol{x}-\boldsymbol{y}) t_j(y) dS_y - \text{v.p.} \int_S \Gamma_{Iij}(\boldsymbol{x}-\boldsymbol{y}) u_j(y) dS_y, \tag{2.28}$$

where S is the subset of the boundary ∂D which is far from the observation point x. $V_i(\boldsymbol{x})$ is an integral which appears in the boundary integral equations for non-periodic problems in the case that the coefficient of the Burton-Miller method α is 0. The fundamental solution of three dimensional elastodynamics (2.14) can be rewritten in the following form:

$$\Gamma_{ij}(\boldsymbol{x}-\boldsymbol{y}) = \frac{1}{\mu k_{\mathrm{T}}^2} \left(e_{ipr} \frac{\partial}{\partial x_p} e_{jqr} \frac{\partial}{\partial y_q} G_{\mathrm{T}}(\boldsymbol{x}-\boldsymbol{y}) + \frac{\partial}{\partial x_i} \frac{\partial}{\partial y_j} G_{\mathrm{L}}(\boldsymbol{x}-\boldsymbol{y}) \right), \tag{2.29}$$

in the case of $x \neq y$. When $|\overrightarrow{Yx}| > |\overrightarrow{Yy}|$ is hold, Gegenbauer's addition theorem (Eq.(2.16)) and the representation of the fundamental solution Eq.(2.29) give the following multipole expansion of $V_i(x)$:

$$V_i(x) = \frac{\mathrm{i}}{4\pi\mu k_{\mathrm{T}}^2} \sum_{n=0}^{\infty} \sum_{m=-n}^{n} (2n+1) \left\{ k_{\mathrm{L}} M_{n,m}^{\mathrm{L}}(Y) \frac{\partial}{\partial x_i} O_n^m(\overrightarrow{Yx}, k_{\mathrm{L}}) + k_{\mathrm{T}} M_{r;n,m}^{\mathrm{T}}(Y) e_{ipr} \frac{\partial}{\partial x_p} O_n^m(\overrightarrow{Yx}, k_{\mathrm{T}}) \right\}, \tag{2.30}$$

where $M^{\mathrm{L}}_{n,m}$ and $M^{\mathrm{T}}_{r;n,m}$ are the multipole moments defined as follows:

$$M^{\mathrm{L}}_{n,m}(Y) = \int_S (-1)^m \left\{ t_j(y)\frac{\partial}{\partial y_j} - u_j(y)n_k(y)\left(\lambda\delta_{jk}\frac{\partial}{\partial y_l}\frac{\partial}{\partial y_l} + 2\mu\frac{\partial}{\partial y_j}\frac{\partial}{\partial y_k}\right)\right\} I_n^{-m}(\overrightarrow{Yy}, k_{\mathrm{L}})dS_y, \tag{2.31}$$

$$M^{\mathrm{T}}_{r;n,m}(Y) = \int_S (-1)^m \left\{ t_j(y)e_{jqr}\frac{\partial}{\partial y_q} - u_j(y)n_k(y)\mu\left(e_{kqr}\frac{\partial}{\partial y_j}\frac{\partial}{\partial y_q} + e_{jqr}\frac{\partial}{\partial y_k}\frac{\partial}{\partial y_q}\right)\right\} I_n^{-m}(\overrightarrow{Yy}, k_{\mathrm{T}})dS_y. \tag{2.32}$$

In the case of $|\overrightarrow{YX}| > |\overrightarrow{Xx}|$, Eq.(2.30) can be further expanded into the following form (the local expansion) in light of Eq.(2.22):

$$V_i(\boldsymbol{x}) = \frac{\mathrm{i}}{4\pi\mu k_{\mathrm{T}}^2}\sum_{n'=0}^{\infty}\sum_{m'=-n'}^{n'}(2n'+1)\left\{k_{\mathrm{L}}L^{\mathrm{L}}_{n',m'}(X)\frac{\partial}{\partial x_i}I_{n'}^{m'}(\overrightarrow{Xx}, k_{\mathrm{L}}) + k_{\mathrm{T}}L^{\mathrm{T}}_{r;n',m'}(X)e_{ipr}\frac{\partial}{\partial x_p}I_{n'}^{m'}(\overrightarrow{Xx}, k_{\mathrm{T}})\right\}, \tag{2.33}$$

where $L^{\mathrm{L}}_{n,m}$ and $L^{\mathrm{T}}_{r;n,m}$ are the coefficients of the local expansion defined as follows (M2L formulae):

$$L^{\mathrm{L}}_{n',m'}(X) = \sum_{n=0}^{\infty}\sum_{m=-n}^{n}(2n+1)T_{n,n'}^{m,m'}(\overrightarrow{YX}, k_{\mathrm{L}})M^{\mathrm{L}}_{n,m}(Y), \tag{2.34}$$

$$L^{\mathrm{T}}_{r;n',m'}(X) = \sum_{n=0}^{\infty}\sum_{m=-n}^{n}(2n+1)T_{n,n'}^{m,m'}(\overrightarrow{YX}, k_{\mathrm{T}})M^{\mathrm{T}}_{r;n,m}(Y). \tag{2.35}$$

The FMM algorithm requires us to shift the origin of the multipole moment and the coefficient of the local expansion. This can be achieved by expanding I_n^m in equations (2.31), (2.32), (2.33) as follows:

$$M^{\mathrm{L}}_{n,m}(Y) = \sum_{n'=0}^{\infty}\sum_{m'=-n'}^{n'}(2n'+1)U_{n',n}^{m',m}(\overrightarrow{Y'Y}, k_{\mathrm{L}})M^{\mathrm{L}}_{n',m'}(Y'), \tag{2.36}$$

$$M^{\mathrm{T}}_{r;n,m}(Y) = \sum_{n'=0}^{\infty}\sum_{m'=-n'}^{n'}(2n'+1)U_{n',n}^{m',m}(\overrightarrow{Y'Y}, k_{\mathrm{T}})M^{\mathrm{T}}_{r;n',m'}(Y'), \tag{2.37}$$

$$L^{\mathrm{L}}_{n,m}(X) = \sum_{n'=0}^{\infty}\sum_{m'=-n'}^{n'}(2n'+1)U_{n',n}^{m',m}(\overrightarrow{X'X}, k_{\mathrm{L}})L^{\mathrm{L}}_{n',m'}(X'), \tag{2.38}$$

$$L^{\mathrm{T}}_{r;n,m}(X) = \sum_{n'=0}^{\infty}\sum_{m'=-n'}^{n'}(2n'+1)U_{n',n}^{m',m}(\overrightarrow{X'X}, k_{\mathrm{T}})L^{\mathrm{T}}_{r;n',m'}(X'). \tag{2.39}$$

We note that we have used Eq.(2.26) to obtain equations (2.36), (2.37).

When the coefficient of the Burton-Miller method α is not zero, one computes the following one instead of Eq.(2.28):

$$V_i(x) = \text{v.p.}\int_S(\Gamma_{ij} + \alpha T_{ik}\Gamma_{kj})(\boldsymbol{x}-\boldsymbol{y})t_j(y)dS_y - \text{p.f.}\int_S(\Gamma_{Iij} + \alpha T_{ik}\Gamma_{Ikj})(\boldsymbol{x}-\boldsymbol{y})u_j(y)dS_y, \tag{2.40}$$

To this end, one only has to replace Eq.(2.33) by the following equations:

$$\begin{aligned} V_i(\boldsymbol{x}) = \frac{\mathrm{i}}{4\pi\mu k_{\mathrm{T}}^2}\sum_{n'=0}^{\infty}\sum_{m'=-n'}^{n'}(2n'+1)\Bigg\{&k_{\mathrm{L}}L^{\mathrm{L}}_{n',m'}(X)\left(\frac{\partial}{\partial x_i}I_{n'}^{m'}(\overrightarrow{Xx}, k_{\mathrm{L}}) + \alpha T_{ik}\frac{\partial}{\partial x_k}I_{n'}^{m'}(\overrightarrow{Xx}, k_{\mathrm{L}})\right)\\ &+k_{\mathrm{T}}L^{\mathrm{T}}_{r;n',m'}(X)\left(e_{ipr}\frac{\partial}{\partial x_p}I_{n'}^{m'}(\overrightarrow{Xx}, k_{\mathrm{T}}) + \alpha T_{ik}e_{kpr}\frac{\partial}{\partial x_p}I_{n'}^{m'}(\overrightarrow{Xx}, k_{\mathrm{T}})\right)\Bigg\}, \end{aligned} \tag{2.41}$$

and any modification for the other formulae is not required.

We remark that a naive computation of equations (2.33)-(2.39) truncating the infinite series with p terms gives $O(p^4)$ complexity even when $U_{n,n'}^{m,m'}, T_{n,n'}^{m,m'}$ are precomputed. In our implementation, however, we reduce this complexity to $O(p^3)$ by using rotations of the coordinates and recursive formulae as discussed in Gumerov and Duraiswami [27]

Algorithm

We now discuss how to apply the FMM for BIEM.

1. Make "cell-tree" structure.
   To determine which element is sufficiently far from the observation point, so that the multipole expansion is valid, we introduce a cell-tree structure (Fig. 2.2). An octree is used for three dimensional problems. We first make a cube which circumscribes ∂D and call this cube the cell of level 0. we then take a cell (a parent cell) of level l ($l \geq 0$) and divide it into 8 equal sub cubes whose edge length is half of that of the parent cell and call any of them a cell (a child cell) of level $l+1$ if some collocation points of boundary element belong to this cube. We continue to subdivide the cells unless the number of boundary elements belonging to the cell is smaller than a given number N_{leaf}. A childless cell is called a leaf. Fig. 2.2 shows the above procedure. We note that this figure shows the case for two dimensional problems with quadtree. We also note that N_{leaf} is set to be $N_{\text{leaf}} = 2$ in the figure, while in our implementation, we usually set N_{leaf} to be several dozen.

   We now define some terminologies at each level which represent how far the cells are from the target cell which includes the observation point. Fig. 2.3 shows a case at level 3.

   - Adjacent cell: A cell which shares at least one edge with the target cell.
   - Interaction list: A set of cells which are not adjacent cells of the target cells while their parents are adjacent to the parent of the target cell.
   - Far cell: A cell which is neither adjacent cells nor in the interaction lists.

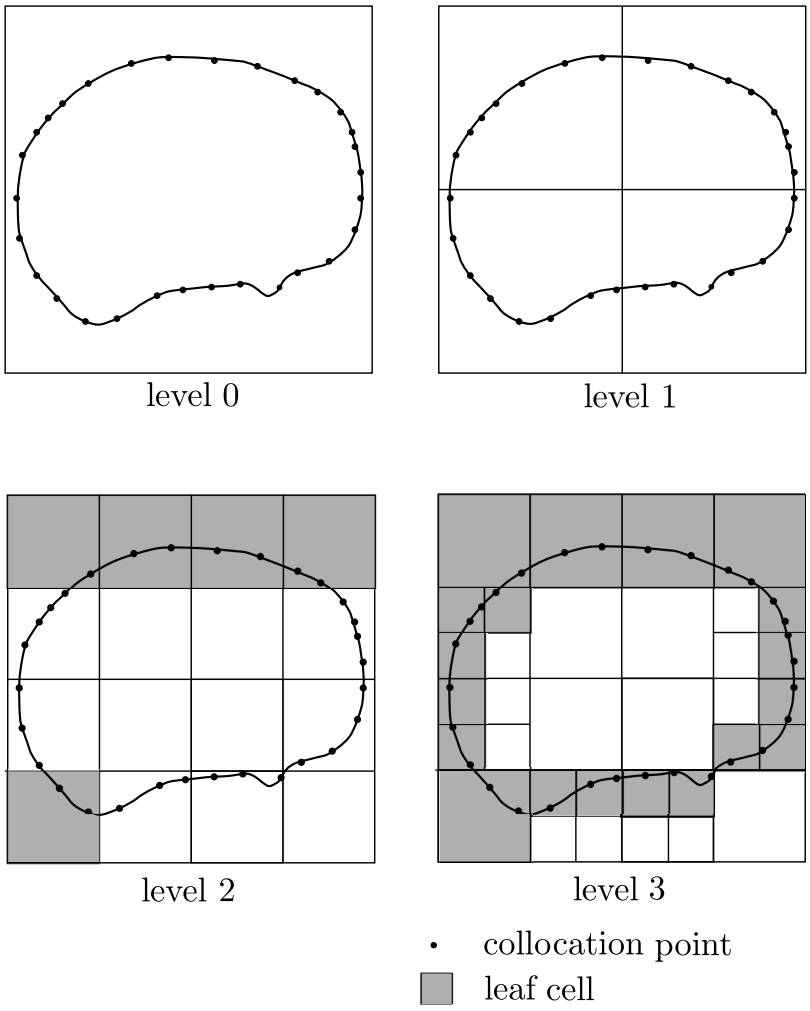

Figure 2.2: Cell-tree structure.

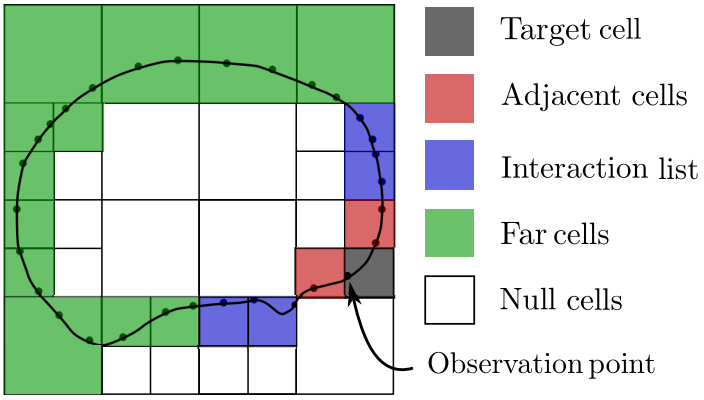

Figure 2.3: Definition of adjacent cells, interaction lists and far cells in the case at level 3.

2. Execute the upward pass
   We compute the multipole moments at the centre of each cells at level l ($l \geq 2$) in the upward pass.
   (a) The multipole moments for a leaf cell are computed by Eq.(2.31) and (2.32).
   (b) The multipole moments for a non-leaf cell are computed from its children's multipole moments. We first shift the centre of the children's moments from the centre of the child to that of the current cell by using M2M formulae (2.36) and (2.37). We then sum up all children's moments.

3. Execute the downward pass
   We compute the coefficient of the local expansion at the centre of each leaf and evaluate the integral which appears in RHS of Eq.(2.28) (or (2.40)) with the full integral range ∂D in the downward pass.
   (a) We convert the multipole moments of non-leaf cells in the interaction list to the coefficient of the local expansion at the centre of the target cell by using M2L formulae (2.34) and (2.35) and sum them up.
   (b) If the current cell is at level l ($l \geq 3$), we shift the centre of the coefficient of the local expansion from the centre of the parent cell to that of the current cell via L2L formulae (2.38) and (2.39).
   (c) For leaf cells, we compute the local expansion in Eq.(2.33) (or (2.41)).
   (d) For leaf cells, we compute the contribution from elements in the cell itself, adjacent cells and leaf cells in the interaction lists by direct integration using Eq.(2.8)–(2.11).
   (e) We complete the evaluation of the integral as the sum of the results of (c) and (d).

   These procedures give us the LHS of (2.7) for given $\boldsymbol{u}$ and $\boldsymbol{t}$. Hence, we can now solve the linear algebraic equations obtained as discretised (2.7) using an iterative method.

2.2.4 Periodic FMM

In this section, we discuss how to extend the FMM described in the above section to periodic problems. From the lattice sum expression Eq.(2.12) for the Green's function Γ^{P}_{ij}, we see that the periodic boundary value problems can be interpreted as an ordinary problem with an infinite repetition of the replicas of the unit cell (Fig. 2.4).

We now take the unit cell as the level 0 cell in FMM and divide the set of replica cells into those adjacent to the unit cell (denoted by C_{N}) and others (denoted by C_{F}). We note that the unit cell may not be a cube. To deal with non-cubic cell, we only have to change the definition of the adjacent cell, the interaction list and the far cells. The reader is referred to Otani and Nishimura [28] for further details on the treatment of non-cubic cell. Corresponding to C_{N} and C_{F}, the sum in Γ^{P}_{ij} is divided into the contribution from C_{N}, denoted by $\Gamma^{\mathrm{PN}}_{ij}$ which includes the contributions from the unit cell itself, and those from C_{F}, denoted by $\Gamma^{\mathrm{PF}}_{ij}$. Namely, we have

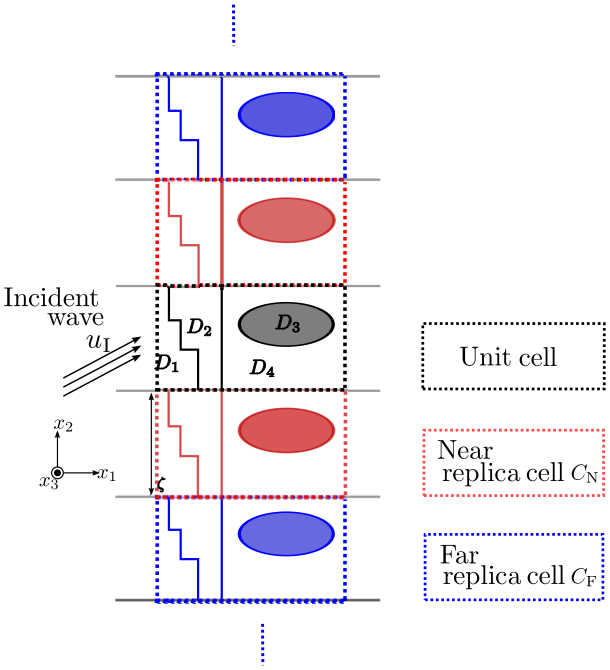

Figure 2.4: Replica cells.

$$\Gamma_{ij}^{\mathrm{P}}(\boldsymbol{x}-\boldsymbol{y}) = \Gamma_{ij}^{\mathrm{PN}}(\boldsymbol{x}-\boldsymbol{y}) + \Gamma_{ij}^{\mathrm{PF}}(\boldsymbol{x}-\boldsymbol{y}), \tag{2.42}$$

where

$$\Gamma_{ij}^{\mathrm{PN}}(\boldsymbol{x}-\boldsymbol{y}) = \sum_{\boldsymbol{\omega}\in\mathcal{L}'} \Gamma_{ij}(\boldsymbol{x}-\boldsymbol{y}-\boldsymbol{\omega}) e^{\mathrm{i}\boldsymbol{\beta}\cdot\boldsymbol{\omega}}, \tag{2.43}$$

$$\Gamma_{ij}^{\mathrm{PF}}(\boldsymbol{x}-\boldsymbol{y}) = \sum_{\boldsymbol{\omega}\in\mathcal{L}''} \Gamma_{ij}(\boldsymbol{x}-\boldsymbol{y}-\boldsymbol{\omega}) e^{\mathrm{i}\boldsymbol{\beta}\cdot\boldsymbol{\omega}}, \tag{2.44}$$

and $\mathcal{L}'$ is the set of centroid of the cells belonging to C_{N} and $\mathcal{L}'' = \mathcal{L}\backslash\mathcal{L}'$. With $\Gamma_{ij}^{\mathrm{PN}}$ and $\Gamma_{ij}^{\mathrm{PF}}$, the integral which appears in the RHS of Eq.(2.7) can be evaluated as follows:

- The contribution from $\Gamma_{ij}^{\mathrm{PN}}$
  The contribution from $\Gamma_{ij}^{\mathrm{PN}}$ can be evaluated by introducing the cell-tree structure in C_{N}.
  1. Change the definition of the adjacent cells, interaction list and far cells as indicated in Fig. 2.5.
  2. Execute the ordinary upward pass from the deepest level to level 0 in the unit cell. In this process, we compute the multipole moments of cells in each level l ($l > 0$).
  3. Execute the ordinary downward pass from level 0 to the deepest level. We note that the multipole moments in the replica cells C_{N} and their children, which are required to compute the coefficients of the local expansion in Eq.(2.34) and (2.35) can be obtained as $M_{\mathrm{L,T}}e^{in\beta_i}$ by virtue of the periodic boundary conditions in Eq.(2.3)–(2.6), where $M_{\mathrm{L,T}}$ is the multipole moments of descendant cells of the unit cell and n is either 1 or -1. The displacements and tractions in replica cells, which are required to compute the direct integration, can be obtained in the same manner.

- The contribution from $\Gamma_{ij}^{\mathrm{PF}}$
  We now derive a formula to compute the contribution from $\Gamma_{ij}^{\mathrm{PF}}$ (periodic M2L formula). To this

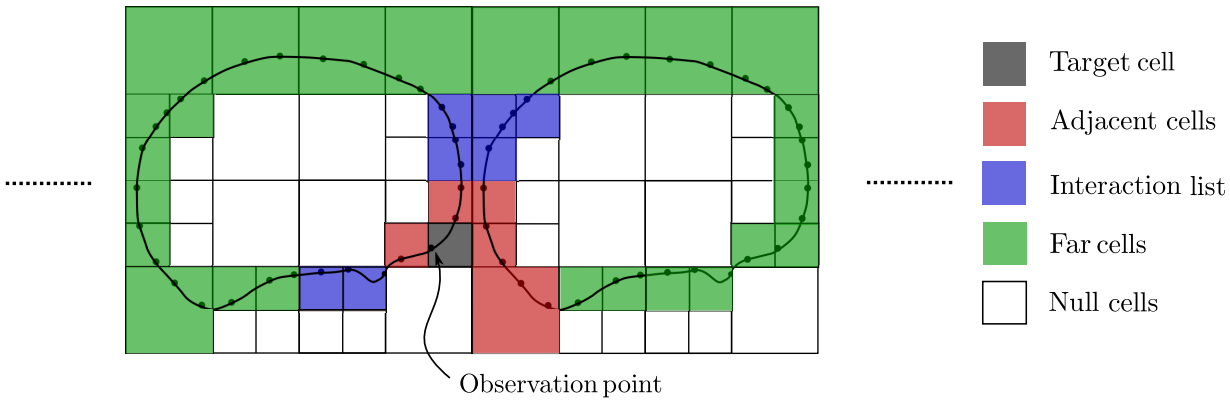

Figure 2.5: Interaction list for periodic FMM.

end, we consider the following potential $V(x)$ with the Helmholtz' periodic kernel.

$$V(x) = \int_{\partial D} G^{\mathrm{PF}}(\boldsymbol{x}-\boldsymbol{y})\phi(y)dS, \tag{2.45}$$

$$G^{\mathrm{PF}}(\boldsymbol{x}-\boldsymbol{y}) = \sum_{\boldsymbol{\omega}\in\mathcal{L}''} \frac{e^{\mathrm{i}k|\boldsymbol{x}-\boldsymbol{y}-\boldsymbol{\omega}|}}{4\pi|\boldsymbol{x}-\boldsymbol{y}-\boldsymbol{\omega}|} e^{\mathrm{i}\boldsymbol{\beta}\cdot\boldsymbol{\omega}}, \tag{2.46}$$

where ϕ is a density function. Since we have now $|\overrightarrow{Ox}-\overrightarrow{O\omega}| > |\overrightarrow{Oy}|$ and $|\overrightarrow{O\omega}| > |\overrightarrow{Ox}|$, we can expand $V(x)$ as follows:

$$V(x) = \frac{\mathrm{i}k}{4\pi} \sum_{n'=0}^{\infty} \sum_{m'=-n'}^{n'} (2n'+1) I_{n'}^{m'}(\overrightarrow{Ox}) \left(\sum_{n=0}^{\infty} \sum_{m=-n}^{n} \sum_{\boldsymbol{\omega}\in\mathcal{L}''} (2n+1) T_{n,n'}^{m,m'}(-\boldsymbol{\omega}) e^{\mathrm{i}\boldsymbol{\beta}\cdot\boldsymbol{\omega}} M_{n,m}(O) \right), \tag{2.47}$$

where $M_{n,m}(O)$ is the multipole moment of the unit cell defined as follows:

$$M_{n,m}(O) = \int_{\partial D} (-1)^m I_n^{-m}(\overrightarrow{Oy})\phi(x)dS, \tag{2.48}$$

and O is the centre of the unit cell. We have used Eq.(2.16) and (2.22) to derive (2.47). By extending the above observation to the elastodynamic kernel, one may obtain the following periodic M2L formulae:

$$L_{n,m}^{\mathrm{L}}(O) = \sum_{n=0}^{\infty} \sum_{m=-n}^{n} (2n+1) T^{\mathrm{P}\,m',m}_{n',n}(k_{\mathrm{L}}) M_{n',m'}^{\mathrm{L}}(O), \tag{2.49}$$

$$L_{r;n,m}^{\mathrm{T}}(O) = \sum_{n=0}^{\infty} \sum_{m=-n}^{n} (2n+1) T^{\mathrm{P}\,m',m}_{n',n}(k_{\mathrm{T}}) M_{r;n',m'}^{\mathrm{T}}(O), \tag{2.50}$$

where $M_{n',m'}^{\mathrm{L}}(O), M_{r;n',m'}^{\mathrm{T}}(O)$ are the multipole moment of the unit cell, and $L_{n',m'}^{\mathrm{L}}(O), L_{r;n',m'}^{\mathrm{T}}(O)$ are the coefficient of the local expansion of the unit cell. $T^{\mathrm{P}\,m,m'}_{n,n'}(k_{\mathrm{L,T}})$ is the coefficient of the periodic M2L formulae defined as follows:

$$T^{\mathrm{P}\,m,m'}_{n,n'}(k_{\mathrm{L,T}}) = \sum_{\omega\in\mathcal{L}''} T_{n,n'}^{m,m'}(-\omega, k_{\mathrm{L,T}}) e^{\mathrm{i}\boldsymbol{\beta}\cdot\boldsymbol{\omega}}. \tag{2.51}$$

$T^{\mathrm{P}\,m,m'}_{n,n'}(k_{\mathrm{L,T}})$ can be computed with recursive formulae [27, 28] whose initial value is as follows:

$$T^{\mathrm{P}\,0,m'}_{0,n'}(k_{\mathrm{L,T}}) = (-1)^{n'+m'} \left(\sum_{\omega\in\mathcal{L}''} O_{n'}^{m'}(-\omega, k_{\mathrm{L,T}}) e^{\mathrm{i}\boldsymbol{\beta}\cdot\boldsymbol{\omega}} \right). \tag{2.52}$$

We note, however, it is quite impractical to compute the lattice sums which appear in RHS of Eq.(2.52) as they are since the convergence of this series is extremely slow. In our implementation, we have precomputed them with the help of Fourier analysis, the details of which are found in Otani and Nishimura [14]

2.2.5 Far fields

In the limit of $x_1 \to \pm\infty$ ($S^{\pm}$, see Fig. 2.6), the displacement fields $\boldsymbol{u}$ allow the following expressions in terms of the superposition of plane waves:

$$u_i^{\pm} = \delta_{\pm} u_i^{\mathrm{I}} + \sum_n A_n^{\mathrm{L}\pm} (d_n^{\mathrm{L}\pm})_i e^{\mathrm{i}k_{\mathrm{L}} \boldsymbol{p}_n^{\mathrm{L}\pm} \cdot \boldsymbol{x}} + \sum_n A_n^{\mathrm{T}\pm} (d_n^{\mathrm{T}\pm})_i e^{\mathrm{i}k_{\mathrm{T}} \boldsymbol{p}_n^{\mathrm{T}\pm} \cdot \boldsymbol{x}}, \tag{2.53}$$

where n is a multiple index defined by $n = (n_2, n_3)$, $\delta_+ = 0$ and $\delta_- = 1$. Also, $\boldsymbol{d}_n^{\mathrm{L,T}\pm}$ is the unit

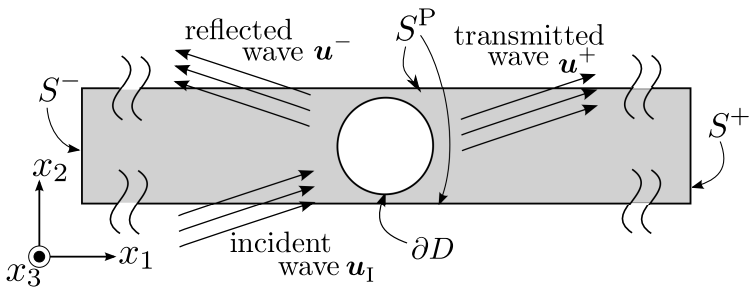

Figure 2.6: Far fields.

vector which represents the direction of motion of the scattered wave and $\boldsymbol{p}_n^{\mathrm{L,T}\pm}$ is the unit vector which represents the direction of propagation of the scattered wave given by

$$\boldsymbol{p}_n^{\mathrm{L,T}\pm} = \frac{1}{k_{\mathrm{L,T}}} \begin{pmatrix} \pm\sqrt{k_{\mathrm{L,T}}^2 - \left(\frac{\beta_2 + 2n_2\pi}{\zeta_2}\right)^2 - \left(\frac{\beta_3 + 2n_3\pi}{\zeta_3}\right)^2} \\ \left(\frac{\beta_2 + 2n_2\pi}{\zeta_2}\right) \\ \left(\frac{\beta_3 + 2n_3\pi}{\zeta_3}\right) \end{pmatrix}. \tag{2.54}$$

The summation which appears in Eq.(2.53) is taken over such n_2, n_3 that the vector $\boldsymbol{p}_n^{\mathrm{L,T}\pm}$ is real. Then, we obtain the following formulae for the amplitude of the plane waves of far fields in Eq.(2.53):

$$A_n^{\mathrm{L,T}\pm} = \frac{\Omega_n^{\mathrm{L,T}\pm}}{I_n^{\mathrm{L,T}\pm}}, \tag{2.55}$$

$$\Omega_n^{\mathrm{L,T}\pm} = \int_{\partial D} e^{-\mathrm{i}k_{\mathrm{L,T}} \boldsymbol{p}_n^{\mathrm{L,T}\pm} \cdot \boldsymbol{x}} \Big(\boldsymbol{t} \cdot \boldsymbol{d}_n^{\mathrm{L,T}\pm} + \mathrm{i}k_{\mathrm{L,T}} \Big[\lambda (\boldsymbol{u} \cdot \boldsymbol{n})(\boldsymbol{d}_n^{\mathrm{L,T}\pm} \cdot \boldsymbol{p}_n^{\mathrm{L,T}\pm}) + \mu \big((\boldsymbol{u} \cdot \boldsymbol{d}_n^{\mathrm{L,T}\pm})(\boldsymbol{n} \cdot \boldsymbol{p}_n^{\mathrm{L,T}\pm}) + (\boldsymbol{u} \cdot \boldsymbol{p}_n^{\mathrm{L,T}\pm})(\boldsymbol{n} \cdot \boldsymbol{d}_n^{\mathrm{L,T}\pm}) \big) \Big] \Big) dS, \tag{2.56}$$

$$I_n^{\mathrm{L,T}\pm} = 2\mathrm{i}k_{\mathrm{L,T}} \zeta_2 \zeta_3 \big((\lambda + \mu)(d_n^{\mathrm{L,T}\pm})_1 \boldsymbol{d}_n^{\mathrm{L,T}\pm} \cdot \boldsymbol{p}_n^{\mathrm{L,T}\pm} + \mu (p_n^{\mathrm{L,T}\pm})_1 \big), \tag{2.57}$$

where $\boldsymbol{u}$, $\boldsymbol{t}$ are the displacement and traction at ∂D which are computed by the FMM, respectively.

Let $\check{u}_j = \mathrm{Re}[u_j e^{-\mathrm{i}\omega t}]$ be the corresponding solution in time domain to solution u_j in frequency domain. We define the time averaged rate of energy $< P_{S_e} >$ which pass thorough the inspection surface S_e as follows:

$$< P_{S_e} > = \frac{1}{T} \int_{t'}^{t'+T} P_{S_e} dt, \tag{2.58}$$

$$P_{S_e} = \int_{S_e} \dot{\check{u}}_i T_{jk} \check{u}_k dS, \tag{2.59}$$

where T is the period given by $T = 2\pi/\omega$. We then obtain the time averaged rate of energy of the plane wave which consists of the Eq.(2.53) as follows:

$$< P_n^{\mathrm{L,T}\pm} >= \frac{\omega k_{\mathrm{L,T}} \zeta_2 \zeta_3 |A_n^{\mathrm{L,T}\pm}|^2}{2} \left((\lambda+\mu)(\boldsymbol{n}^{\pm} \cdot \boldsymbol{d}_n^{\mathrm{L,T}\pm})(\boldsymbol{p}_n^{\mathrm{L,T}\pm} \cdot \boldsymbol{d}_n^{\mathrm{L,T}\pm}) + \mu \boldsymbol{n}^{\pm} \cdot \boldsymbol{p}_n^{\mathrm{L,T}\pm} \right), \tag{2.60}$$

where $\boldsymbol{n}^{\pm}$ are the normals of S_e. For the field which can be described as a superposition of plane waves like Eq.(2.53), the following energy conservation law holds:

$$\mathcal{E} := \sum_{\alpha=\mathrm{L}\pm,\mathrm{T}\pm} \sum_n \frac{< P_n^{\alpha} >}{< P^{\mathrm{I}} >} = 1, \tag{2.61}$$

where $< P^{\mathrm{I}} >$ represents the time averaged energy of the incident wave. We also define the energy transmittance $\mathcal{T}$ and reflectance $\mathcal{R}$ in the following manner:

$$\mathcal{T} := \sum_n < P_n^{\mathrm{L}+} > + \sum_n < P_n^{\mathrm{T}+} >, \tag{2.62}$$

$$\mathcal{R} := \sum_n < P_n^{\mathrm{L}-} > + \sum_n < P_n^{\mathrm{T}-} >. \tag{2.63}$$

2.3 Numerical examples

In this section, we present some numerical results, which verify the accuracy and applicability of the periodic FMM for elastodynamics in 3D. We consider the problems of plane waves entering the domain including elastic spherical scatterers which are set periodically (Fig. 2.7). We first state techniques common to all the examples to follow.

- We use the collocation method with locally constant elements for discretisation. In the discretisation, we divided the surface of elastic inclusion ∂D in the unit cell in Fig. 2.8 into $N = 18000$ triangular elements.
- We utilise Flexible GMRES, which is known as FGMRES [29], as the solver for the algebraic equations. The error tolerance for the convergence of FGMRES is set to be 10^{-5} times the initial residual.
- As a preconditioner for the algebraic equations, we use the part of the matrix computed directly in the FMM algorithm as the (right) preconditioner. The inversion in the process of preconditioning is carried out approximately using GMRES (with FGMRES for the main solver) which we terminate either after 10 iterations or when the norm of the error is less than 10^{-1} times its initial value.
- For the calculation we use Fujitsu HX supercomputer ('Thin' SMP cluster) at Academic Center for Computing and Media Studies of Kyoto University. The code is OpenMP parallelised and the number of CPUs is 16.

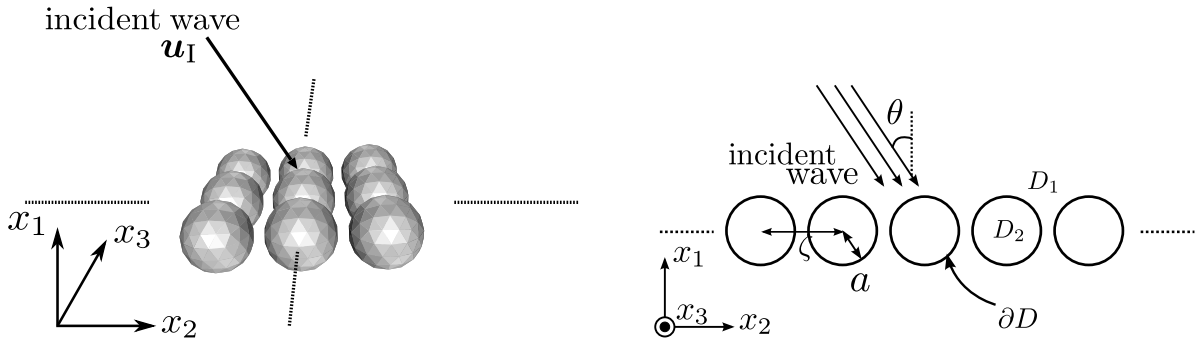

Figure 2.7: Periodic spherical scatters.

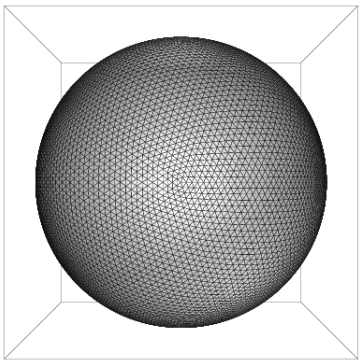

Figure 2.8: Unit cell.

2.3.1 Infinite domain

We first analysed the plane waves propagating in the infinite domain, that is, we set all the material constants of the inclusion the same as those of the exterior domain. This is for the purpose of verification of our numerical codes. We note that in this case the analytical solution is the incident wave itself. We set the numerical constants as follows: the periodic length $\zeta_2 = \zeta_3 = 2.0$, the radius of the scatterer $a = 0.175\zeta$, Lamé's constants $\lambda = \mu = 1.0$, the density $\rho = 1.0$, the frequency of the incident wave $\omega = 8.0$. The incident angle of the incident wave changes from 0.0° to 90.0°. We note that the wave vector of the incident wave is laid in $x_1 - x_2$ plane (Fig. 2.7).

Table 2.1 shows the maximum value with respect to the incident angle of the relative error of the displacements for the case of P-wave and S-wave incidence. The relative error is defined as follows:

$$\mathrm{err} = \sqrt{\frac{\sum_{i=1}^{N}\sum_{j=1}^{3}|u_{j;i}^{\mathrm{num}} - u_{j;i}^{\mathrm{ana}}|^2}{\sum_{i=1}^{N}\sum_{j=1}^{3}|u_{j;i}^{\mathrm{ana}}|^2}}, \tag{2.64}$$

where $u_{j;i}^{\mathrm{num/ana}}$ are the jth components of the displacements at the ith element of the numerical/analytical solutions. In both cases, the relative error is smaller than 1%. To further verify the accuracy of the proposed method, we show the total energy $\mathcal{E}$ (Eq.(2.61)) which indicates the satisfaction level of the energy conservation law in Fig. 2.9. We observe the disturbance occur near 90° where the incidence is grazing. However, we confirm that the error is still smaller than 1%.

Table 2.1: The maximum value of the relative error of the displacement in the case of infinite domain.

Incident wave	The maximum value of the relative error (%)
P-wave	0.241
S-wave	0.463

2.3.2 Scattering by elastic inclusions

We next consider a scattering by periodic elastic inclusions. The structure under consideration consists of steel inclusions in an infinite polyester matrix. The material parameters for this case are as shown in Table 2.2. We set the periodic length to be $\zeta_2 = \zeta_3 = 2.0(= \zeta_{2,3})$ and the radius of the inclusion to be either $a = 0.15\zeta_{2,3}$ or $0.31\zeta_{2,3}$. For the incident wave we consider a plane P-wave of normal incidence.

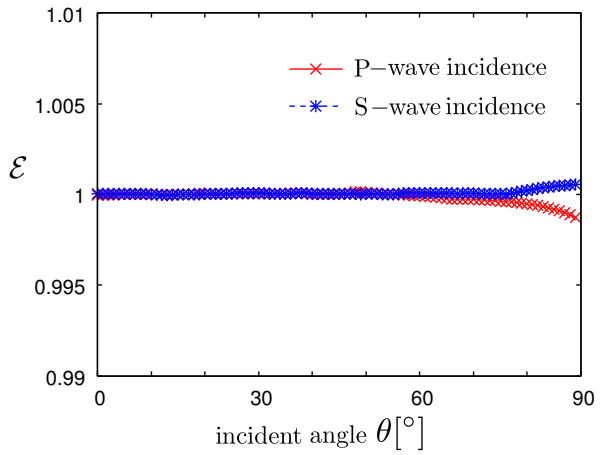

Figure 2.9: Total energy $\mathcal{E}$ versus the incident angle in the case of infinite domain.

This problem has been studied by Maslov et al.[30] who have provided both experimental results and an approximate solution. For this model, we have computed the response in the frequency range of $\omega = 0.2$–8.2.

Table 2.2: Material parameters used in the analysis for the elastic inclusion problem.

	Inclusion (steel)	Exterior matrix (polyester)
Density ρ	6.393	1.000
Lamé's constant λ	1.496	2.453
Lamé's constant μ	47.02	1.000

We compare our numerical results with the approximate and experimental results by Maslov et al.[30]. Fig. 2.10 shows the transmission coefficient $A_0^{\mathrm{L}+}/A^{\mathrm{I}}$ and reflection coefficients $A_0^{\mathrm{L}-}/A^{\mathrm{I}}$ versus frequency in the case of $a = 0.15\zeta_{2,3}$. As seen in Fig. 2.10, our results agree well with the approximate solutions and the experimental results obtained by Maslov et al. Both transmission coefficient and reflection coefficient show an extremum around the non dimensional frequency of $k_{\mathrm{T}}^{(1)}\zeta_{2,3}/2\pi = 0.95$. We believe that this is the resonance type anomaly because near this frequency, the total energy $\mathcal{E}$ also show the maximum value as shown in Fig. 2.11.

Fig. 2.12 shows the transmission and reflection coefficients and Fig. 2.13 shows the total energy in the case of $a = 0.31\zeta_{2,3}$. The numerical results in this case seem to be less accurate than in the case of $a = 0.15\zeta_{2,3}$. However, the agreement is still satisfactory. We note that the difference between our results and the approximate solution obtained by Maslov et al. is to be expected since their approximate solution is obtained with only a few terms of spherical harmonics and is valid only in low frequency problems where $k_{\mathrm{L}}^{(1)}a < 1$ holds. Around $k_{\mathrm{T}}^{(1)}\zeta_{2,3}/2\pi = 0.95$, we observe that $A_0^{\mathrm{L}+}/A^{\mathrm{I}}$ decreases in a relatively wide range. We think that a kind of anomaly occurs around this frequencies because the total energy shows extrema around this frequencies as shown in Fig. 2.13.

2.3.3 Scattering by a periodic void

We finally consider the scattering by holes. Namely, the stiffness property of the inclusion is set to be zero in Fig. 2.7. We use the following parameters for this model, the periodic length $\zeta_{2,3} = 2.0$, the radius of the hole $a = 0.4\zeta_{2,3}$, Lamé's constant $\lambda = 1.0$, $\mu = 1.0$ and the density $\rho = 1.0$ for an exterior domain. The incident wave is P-wave and the incident angle is 0.0°.

Fig. 2.14 shows the far field patterns on the transmission side for $k_{\mathrm{T}}\zeta_{2,3}$ slightly smaller and larger than $k_{\mathrm{T}}\zeta_{2,3} = 2\pi$ and 4π. The sudden changes of the patterns observed at these wave numbers indicate

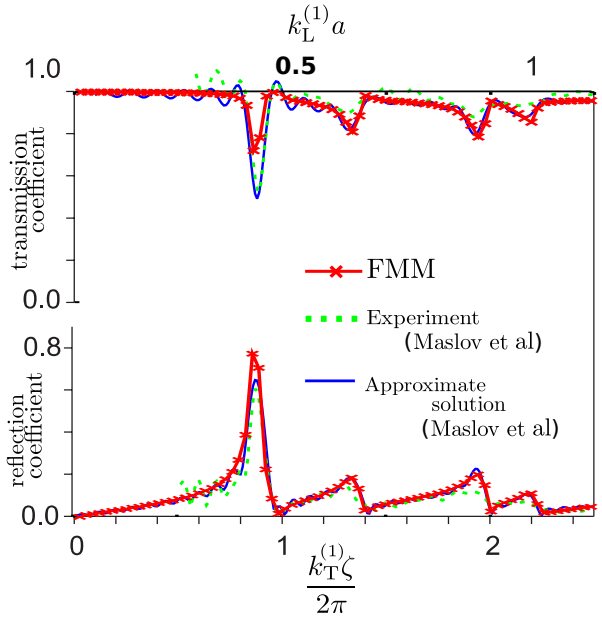

Figure 2.10: Transmission and reflection coefficients versus frequency in the case of $a = 0.15\zeta_{2,3}$.

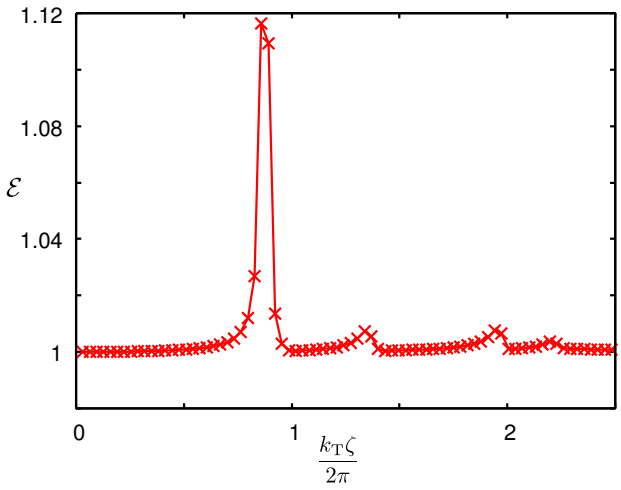

Figure 2.11: Total energy versus frequency in the case of $a = 0.15\zeta_{2,3}$.

the occurrence of Wood's anomaly (Rayleigh's anomaly to be precise) in elastodynamics. According to Eq.(2.54), the number of plane wave which consists of the far field Eq.(2.53) changes across $k_{\mathrm{T}}n\zeta_{2,3}$ where n is integer.

2.4 Conclusions

We have formulated and implemented a periodic FMM for elastodynamics in 3D. Through the numerical analyses, we have verified our method in the problems related to waves scattered by a doubly periodic layer of scatters. Wood's anomaly, which is well known in the fields of nanophotonics, is observed also in elastodynamics.

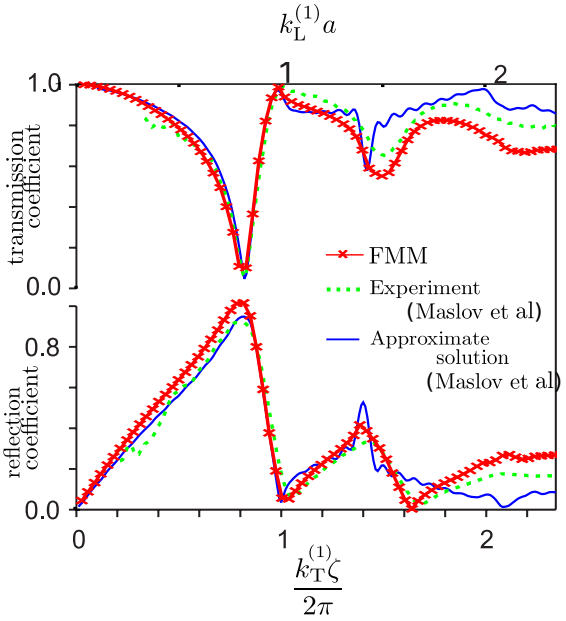

Figure 2.12: Transmission and reflection coefficients versus frequency in the case of $a = 0.31\zeta_{2,3}$.

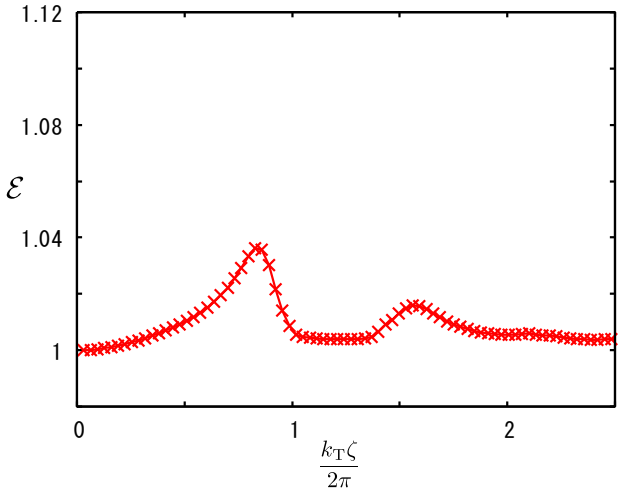

Figure 2.13: Total energy versus frequency in the case of $a = 0.15\zeta_{2,3}$.

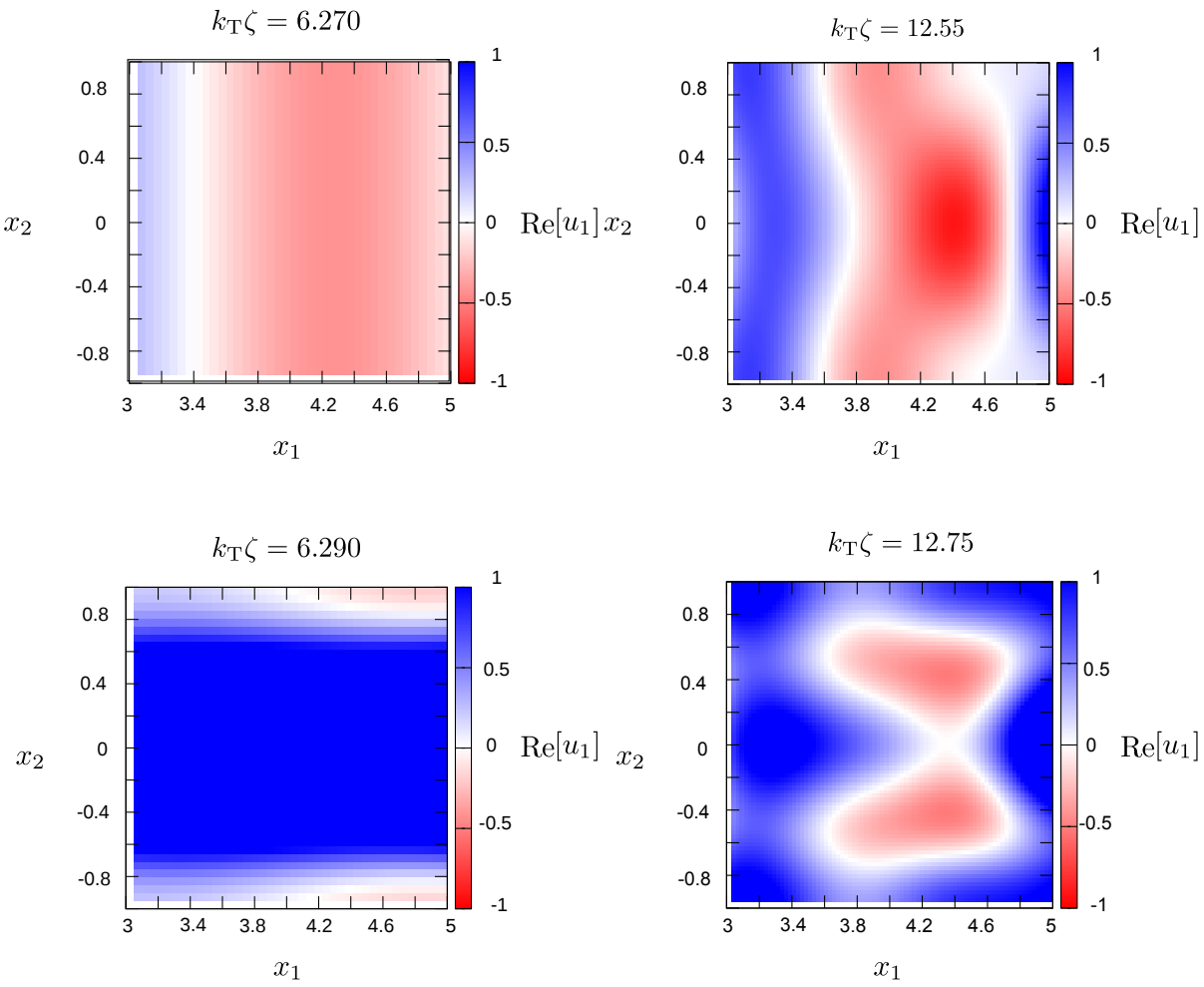

Figure 2.14: Far field patterns of $\mathrm{Re}[u_1]$ in the case of scattering by periodic voids (left: $k_{\mathrm{T}}\zeta_{2,3} \simeq 2\pi$, right: $k_{\mathrm{T}}\zeta_{2,3} \simeq 4\pi$).

Chapter 3

A periodic FMM for acoustics-elastodynamics coupled problems

3.1 Introduction

An FMM for periodic boundary value problems of Helmholtz-elastodynamics coupled field is investigated as an extension of studies on periodic FMMs. Both Helmholtz and elastodynamic fields are solved by FMM. The efficiency and accuracy of the proposed method are confirmed through three kinds of basic numerical tests. The materials dealt with are a polymethyl methacrylate slab, a periodically perforated tungsten slab and periodically set spherical elastic inclusions all of which are immersed in water. The numerical results are well verified with analytical solutions or results from previous studies.

3.2 Formulation

In this section, we formulate an acoustics-elastodynamics coupled problem and the associated BIEM in frequency domain. We choose the time dependence as $e^{-\mathrm{i}\omega t}$, where ω is the frequency.

3.2.1 Statement of the problem

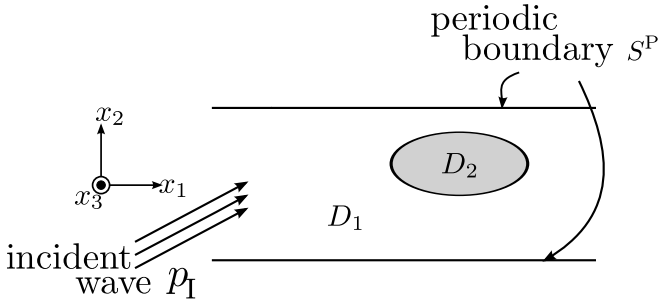

Figure 3.1: Periodic boundary value problems.

Let D be a domain defined by

$$D = ((-\infty, \infty) \otimes [-\zeta_2/2, \zeta_2/2] \otimes [-\zeta_3/2, \zeta_3/2]), \tag{3.1}$$

which is further subdivided into two subdomains $D = D_1 \cup D_2$ (Fig. 3.1). We here assume that D_1 and D_2 are composed of an inviscid fluid and an elastic material, respectively. We consider doubly periodic problems in which the periodic lengths are ζ_2 along the x_2 axis and ζ_3 along the x_3 axis, respectively. The

domain D is impinged upon by an incident sound pressure denoted by $p_{\rm I}$. We here consider a plane wave incidence.

The sound pressure p is governed by the following Helmholtz' equation in D_1:

$$p_{,jj} + k^{(1)2} p = 0, \tag{3.2}$$

where $k^{(1)} = \omega\sqrt{\dfrac{\rho^{(1)}}{\lambda^{(1)}}}$ is the wavenumber of D_1, $\lambda^{(1)}$ is the bulk modulus and $\rho^{(1)}$ is the density. The displacement u_i is governed by the following Navier-Cauchy's equation in D_2:

$$\mu^{(2)} u_{i,jj} + (\lambda^{(2)} + \mu^{(2)}) u_{j,ij} + \rho^{(2)} \omega^2 u_i = 0, \tag{3.3}$$

where $\rho^{(2)}$ is the density, $\lambda^{(2)}$, $\mu^{(2)}$ are the Lamé's constants. Using these quantities, we define the elasticity tensor $C^{(2)}_{ijpq}$ by

$$C^{(2)}_{ijpq} = \lambda^{(2)} \delta_{ij} \delta_{pq} + \mu^{(2)} (\delta_{ip}\delta_{jq} + \delta_{iq}\delta_{jp}).$$

We assume the following as boundary conditions at the boundary $\partial D_1 \cap \partial D_2$:

- The equilibrium of force

$$t_i + p n_i = 0, \tag{3.4}$$

  where $t_i = C^{(2)}_{ijpq} u_{p,q} n_j$ is the traction in D_2, n_i is the outward unit normal vector on the surface of the domain D_1.

- The continuity of the normal component of the displacement rates as follows:

$$-\mathrm{i}\omega u_i n_i = v_i n_i, \tag{3.5}$$

  where v_i is the particle velocity in the domain D_1.

We note that in virtue of Eq.(3.4) the tangential component of the traction is always to be zero since the domain D_1 is composed of inviscid fluid. On the other hand, in light of the equation of motion in the domain D_1, the particle velocity v_i is associated with the sound pressure p in the following manner:

$$\frac{\partial p}{\partial n} = \mathrm{i}\rho^{(1)} \omega v_i n_i. \tag{3.6}$$

Furthermore, we require the radiation condition to the scattered field.

On the periodic boundaries given by $S^{\rm P} = \{\boldsymbol{x} |\ |x_2| = \dfrac{\zeta_2}{2} \text{ or } |x_3| = \dfrac{\zeta_3}{2}\}$, we require the following periodic boundary conditions:

$$p\left(x_1, \frac{\zeta_2}{2}, x_3\right) = e^{\mathrm{i}\beta_2} p\left(x_1, -\frac{\zeta_2}{2}, x_3\right), \tag{3.7}$$

$$\frac{\partial p}{\partial x_2}\left(x_1, \frac{\zeta_2}{2}, x_3\right) = e^{\mathrm{i}\beta_2} \frac{\partial p}{\partial x_2}\left(x_1, -\frac{\zeta_2}{2}, x_3\right), \tag{3.8}$$

$$p\left(x_1, x_2, \frac{\zeta_3}{2}\right) = e^{\mathrm{i}\beta_3} p\left(x_1, x_2, -\frac{\zeta_3}{2}\right), \tag{3.9}$$

$$\frac{\partial p}{\partial x_3}\left(x_1, x_2, \frac{\zeta_3}{2}\right) = e^{\mathrm{i}\beta_3} \frac{\partial p}{\partial x_3}\left(x_1, x_2, -\frac{\zeta_3}{2}\right), \tag{3.10}$$

where $\beta_i = k_{{\rm I}i}\zeta_i$ $(i = 2, 3)$ are the phase differences of the incident wave and $\boldsymbol{k}_{\rm I}$ is the wave number vector of the incident wave.

3.2.2 Boundary integral equations

The boundary integral equations which are equivalent to the above periodic boundary value problem are as follows:

$$\frac{1}{2}\left(p + \alpha \frac{\partial p}{\partial n_x}\right) = p_{\rm I} + \alpha \frac{\partial p_{\rm I}}{\partial n_x} + (\mathcal{S} + \alpha \mathcal{D}^*) \frac{\partial p}{\partial n_y} - (\mathcal{D} + \alpha \mathcal{N}) p, \tag{3.11}$$

$$\frac{1}{2}\boldsymbol{u} = \mathcal{T}\boldsymbol{u} - \mathcal{U}\boldsymbol{t}, \tag{3.12}$$

where p_{I} is the incident sound pressure, α is the coefficient of the Burton-Miller method. Also, $\mathcal{S}$, $\mathcal{D}$, $\mathcal{D}^*$, $\mathcal{N}$, $\mathcal{U}$ and $\mathcal{T}$ are integral operators defined as follows:

$$\mathcal{S}v = \int_{\partial D} G^{\mathrm{P}(1)}(\boldsymbol{x}-\boldsymbol{y})v(y)dS_y, \tag{3.13}$$

$$\mathcal{D}v = \int_{\partial D} \frac{\partial G^{\mathrm{P}(1)}(\boldsymbol{x}-\boldsymbol{y})}{\partial n_y}v(y)dS_y, \tag{3.14}$$

$$\mathcal{D}^*v = \int_{\partial D} \frac{\partial G^{\mathrm{P}(1)}(\boldsymbol{x}-\boldsymbol{y})}{\partial n_x}v(y)dS_y, \tag{3.15}$$

$$\mathcal{N}v = \text{p.f.}\int_{\partial D} \frac{\partial^2 G^{\mathrm{P}(1)}(\boldsymbol{x}-\boldsymbol{y})}{\partial n_x \partial n_y}v(y)dS_y, \tag{3.16}$$

$$(\mathcal{U}\boldsymbol{v})_j = \int_{\partial D} \Gamma^{(2)}_{jk}(\boldsymbol{x}-\boldsymbol{y})v_k(y)dS_y, \tag{3.17}$$

$$(\mathcal{T}\boldsymbol{v})_j = \text{v.p.}\int_{\partial D} \Gamma^{(2)}_{Ijk}(\boldsymbol{x}-\boldsymbol{y})v_k(y)dS_y, \tag{3.18}$$

and "v.p." and "p.f." stand for Cauchy's principal value and the finite part of divergent integrals, respectively. $G^{\mathrm{P}(1)}$ is Green's function which satisfies the periodic boundary conditions in Eq.(3.7)–(3.10) and the radiation condition. $G^{\mathrm{P}(1)}$ is given in terms of the following lattice sums:

$$G^{\mathrm{P}(1)}(\boldsymbol{x}-\boldsymbol{y}) = \lim_{R\to\infty}\sum_{\boldsymbol{\omega}\in\mathcal{L}(R)} \frac{e^{\mathrm{i}k^{(1)}|\boldsymbol{x}-\boldsymbol{y}-\boldsymbol{\omega}|}}{|\boldsymbol{x}-\boldsymbol{y}-\boldsymbol{\omega}|}e^{\mathrm{i}\boldsymbol{\beta}\cdot\boldsymbol{\omega}}, \tag{3.19}$$

where $\mathcal{L}$ stands for the following lattice points:

$$\mathcal{L}(R) = \{(0,\omega_2,\omega_3)|\omega_2 = p\zeta, \omega_3 = q\zeta,\ |p|,|q| \le R,\ p,q\in\mathbb{Z}\}. \tag{3.20}$$

Also, $\Gamma^{(2)}_{jk}$, $\Gamma^{(2)}_{Ijk}$ are the fundamental solution and the kernel of double layer of three dimensional elastodynamics, both of which satisfy the radiation condition.

We solve the following system of equations composed with the boundary integral equations in (3.11), (3.12) and the boundary conditions (Eq.(3.4), (3.5)):

$$\begin{pmatrix} p_{\mathrm{I}} + \alpha\dfrac{\partial p_{\mathrm{I}}}{\partial n_x} \\ 0 \\ \mathbf{0} \\ \mathbf{0} \end{pmatrix} = \begin{pmatrix} -\mathcal{S} - \alpha\left(\mathcal{D}^* - \dfrac{\mathcal{I}}{2}\right) & \left(\mathcal{D} + \dfrac{\mathcal{I}}{2}\right) + \alpha\mathcal{N} & \mathbf{0} & \mathbf{0} \\ \mathcal{I} & \mathbf{0} & \mathbf{0} & -\rho^{(1)}\omega^2\boldsymbol{n}^T \\ \mathbf{0} & \mathbf{0} & \mathcal{U} & -\mathcal{T} + \dfrac{\mathcal{I}}{2} \\ \mathbf{0} & \boldsymbol{n} & \mathcal{I} & \mathbf{0} \end{pmatrix} \begin{pmatrix} \dfrac{\partial p}{\partial n} \\ p \\ \boldsymbol{t} \\ \boldsymbol{u} \end{pmatrix}, \tag{3.21}$$

where $\mathcal{I}$ stands for the identity operator.

3.3 Numerical examples

In this section, we show some numerical examples with the proposed method and confirm the validity, accuracy and efficiency of the method.

In all the examples to follow, we used the collocation method with locally constant elements in discretisation of the integral equations in (3.21). As a preconditioner we use the part of the matrix computed directly in the FMM algorithm and the components which represent Eq.(3.4) and (3.5) as the (right) preconditioner unless otherwise noted. The inversion in the process of preconditioning is carried out approximately using GMRES (with FGMRES for the main solver) which we terminate either after 10 iterations or when the norm of the error is less than 10^{-1} times its initial value. For the calculation we use Fujitsu HX supercomputer ('Thin' SMP cluster) at Academic Center for Computing and Media Studies of Kyoto University. The code is OpenMP parallelised and the number of CPUs is 16.

3.3.1 Scattering by a slab immersed in water

We first verify our approach by solving problems with known analytical solutions. The model we consider is the slab shown in Fig. 3.2 whose thickness is 0.800. The slab is made of polymethyl methacrylate

(PMMA) and the exterior matrix is water whose material constants are shown in Table 3.1. The incident sound pressure is the plane wave whose frequency is $\omega = 8.0$. We have computed the response in the incident angle range from 0° to 89° and the resolution of incident angle is set to be 1°. This slab problem can be formulated as a periodic problem with arbitrary geometric period. We here set $\zeta_{2,3} = 1.000$. In discretisation, we divide the interface between slab and water into 20(40) triangular elements per one period. The number of element is 4096(16384), hence the total degrees of freedom is 32768(131072). We here set the coefficient of the Burton-Miller method to be $\alpha = 0$ since the fictitious eigenvalue problem will not occur for this problem. This can be easily seen since the complementary domain of each subdomain includes infinity. We note that any preconditioner is not used for this problem.

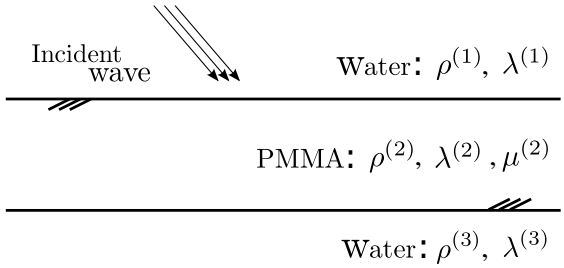

Figure 3.2: Slab immersed in water.

Table 3.1: Material parameters for the slab problem.

	Density ρ	λ	μ
PMMA	1.000	2.161	0.540
Water	1.000	1.000	–

Table 3.2 shows the maximum value of the relative error of the sound pressure p and the displacement $\boldsymbol{u}$ defined as follows:

$$\mathrm{err}(p) = \sqrt{\frac{\sum_{j=1}^{N} |p_{;j}^{\mathrm{num}} - p_{;j}^{\mathrm{ana}}|^2}{\sum_{j=1}^{N} |p_{;j}^{\mathrm{ana}}|^2}}, \tag{3.22}$$

$$\mathrm{err}(\boldsymbol{u}) = \sqrt{\frac{\sum_{j=1}^{N}\sum_{i=1}^{3} |u_{i;j}^{\mathrm{num}} - u_{i;j}^{\mathrm{ana}}|^2}{\sum_{j=1}^{N}\sum_{i=1}^{3} |u_{i;j}^{\mathrm{ana}}|^2}}, \tag{3.23}$$

where $p_{;i}^{\mathrm{num/ana}}$ are the sound pressure at the ith element of the numerical/analytical solutions and $u_{j;i}^{\mathrm{num/ana}}$ are the jth components of the displacements at the ith element of the numerical/analytical solutions, respectively. As shown in Table 3.2, the error of the sound pressure and the displacement is sufficiently small. From this result we conclude that the present method is sufficiently accurate for engineering purposes. We also note that the maximum value of the computational time is 157 sec (548 sec) for the case of 20(40) elements per periodic length.

Table 3.2: The maximum value of average error of pressure and displacement for slab problem.

A number of elements per unit wave length	pressure p	displacement $\boldsymbol{u}$
20	2.000×10^{-2}	1.084×10^{-2}
40	1.065×10^{-2}	5.648×10^{-3}

3.3.2 Scattering by periodically perforated slab

We next consider the scattering by a slab which is periodically perforated with circular holes (Fig. 3.3). The radius of holes is 0.1875, the thickness of the slab is 0.3750 and the period is $\zeta_{2,3} = 1.000$. We here consider a tungsten slab and water as the outer domain, respectively. We note that the material constants of tungsten is extremely different from those of water (Table 3.3). We here consider the normal incidence. We have computed the response in the frequency range from 3.0 to 16.0 with the frequency resolution of 0.1. Fig. 3.4 shows the unit cell for this problem. We divided the interface with 28054 triangular elements, hence the total degrees of freedom is 224432. For this problem, we set the coefficient of the Burton-Miller to be $\alpha = 0$. Fig. 3.5 shows the transmittance curve versus normalised wavelength $\dfrac{\Lambda}{\zeta_{2,3}} = \dfrac{2\pi}{k^{(1)}\zeta_{2,3}}$

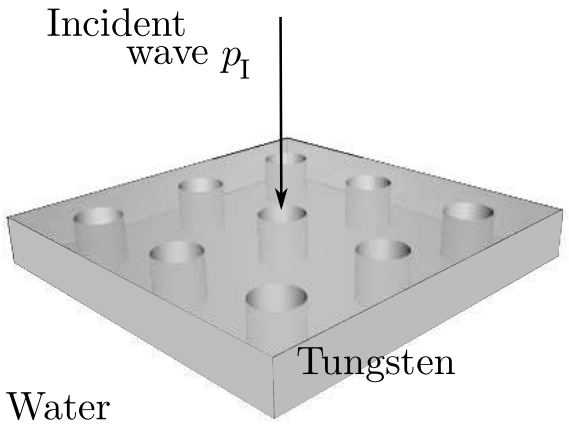

Figure 3.3: Perforated slab immersed in water.

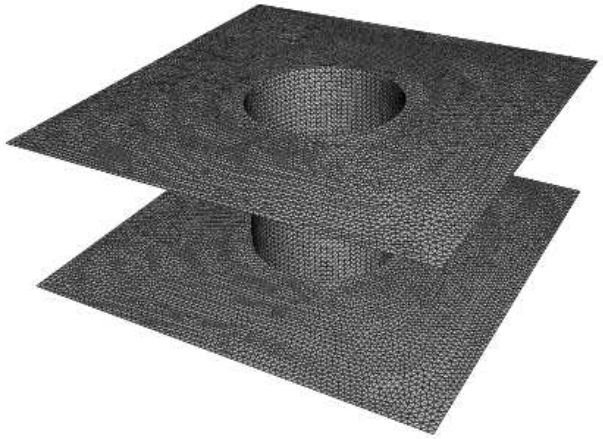

Figure 3.4: Unitcell for perforated slab problems.

Table 3.3: Material parameters for the perforated slab problem.

	Density ρ	λ	μ
Tungsten	13.80	145.6	64.85
Water	1.000	1.000	–

obtained by periodic FMM and the approximate analytical result by Estrada et al.[31], in which the slab

is modeled as rigid body. The results with the proposed method are different from the reference in the low frequency range. However, the agreement is satisfactory since the effect of the deformation of the slab is considered to be larger in low frequency. The maximum value of the number of iteration of GMRES and the computational time were 1259 and 22275 sec, respectively.

We note that the fictitious eigenvalue problem might occur for this problem. However, it is easily seen that fictitious eigenvalue problem will not occur in the case of $\Lambda/\zeta_{2,3} > 0.75$ (twice the thickness of the slab) for a slab without holes and this limit wavelength is considered to be smaller for the perforated slab. Hence, it is reasonable for the majority of the cases in Fig. 3.5 that α has been set to be zero. We also note that the accuracy does not decline even in the case of short wavelength. With these observations, we conclude that it is appropriate that we have set $\alpha = 0$.

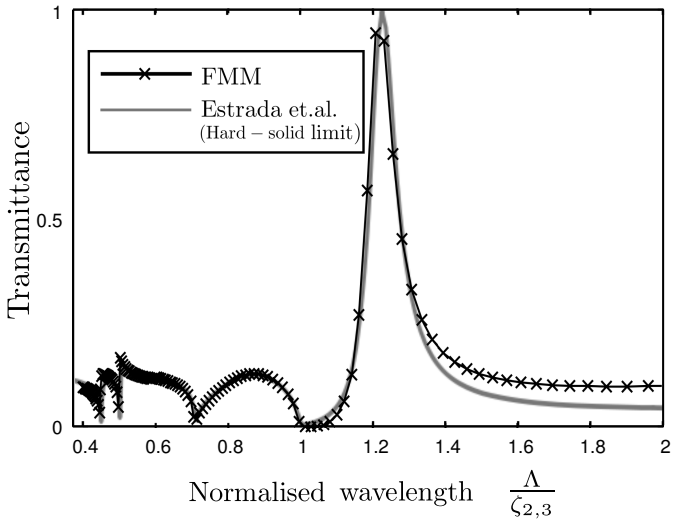

Figure 3.5: Transmittance of the perforated slab problem.

3.3.3 Scattering by spherical inclusions

We finally consider the scattering by spherical inclusions (Fig. 3.6). This is for the verification in the case that the coefficient of the Burton-Miller method α is not equal to zero. We here set the period to be $\zeta_{2,3} = 1.000$ and the radius of the sphere to be 0.450. We divided the surface of the sphere in the unit cell into 18000 triangular elements. The total degrees of freedom is 144000. The material constants shown in Table 3.4 are used for the analyses. We consider the normal incidence of the sound pressure and the frequency varied in the interval of ω is 0.1–10.0. We here set the coefficient of the Burton-Miller method to be $\alpha = -\frac{\mathrm{i}}{k^{(1)}}$. Because of the following two reasons, we conclude that the obtained results are valid:

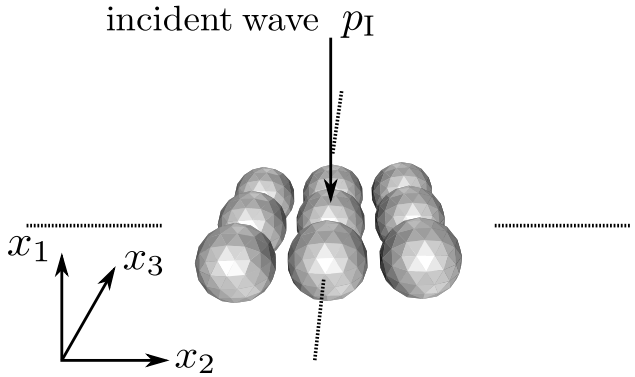

Figure 3.6: Scattering by periodic spheres.

Table 3.4: Material parameters for the periodic elastic inclusions.

	Density ρ	λ	μ
Inclusion	1.000	1.000	1.000
Exterior matrix	1.000	1.000	–

- The maximum values of the tangential component of the tractions at the surface on the sphere was 3.263×10^{-5}.
- The maximum value of the relative error of the sum of scattered energy for incident energy was 3.800%

For this problem, the maximum value of the number of iteration for GMRES and the computational time were 1556 and 17797 sec, respectively. This number of iteration is more than desirable for a simple problem of this size. This increased number of iterations is considered to be due to the hyper singular integrals in a non diagonal block in Eq.(3.21), which make the matrix considerably ill-conditioned. This observation suggests that a good preconditioner is needed in this problem.

3.4 Conclusions

We proposed a periodic FMM for acoustics-elastodynamics coupled problems. We have confirmed the validity of the proposed method through some numerical tests. However, the proposed method is not necessarily effective with respect to the computational cost especially for the problems with the complicated domain. We conclude that we have to accelerate the convergence with some techniques. We therefore investigate the Calderon preconditioning [17, 24] for the acoustics-elastodynamics coupled problems in chapter 5.

Chapter 4

Calderon's preconditioning for periodic FMM for elastodynamics in 3D

4.1 Introduction

In this chapter, preconditioning methods based on Calderon's formulae for the periodic FMM for elastodynamics in 3D are investigated. Three different types of formulations are proposed. The first type is a preconditioning just by appropriately ordering the coefficient matrix without multiplying preconditioners. Other two types utilise preconditioners constructed using matrices needed in the main FMM algorithms. We make several numerical experiments with proposed preconditioners to confirm the efficiency of these proposed methods. We also conclude that the preconditioning of the first type is faster with respect to the computational time than other preconditioning methods discussed in this thesis.

The material for this chapter is taken from Isakari et al.[24]

4.2 PMCHWT formulation for elastic problems

4.2.1 Boundary integral equations for the periodic boundary value problems

For the periodic boundary value problem described in section 2.2.1, we can formulate another boundary integral equation, which is known as PMCHWT formulation [32] in the field of electromagnetics, as follows:

$$\mathcal{A}_{\mathrm{Conv}} \begin{pmatrix} \boldsymbol{t} \\ \boldsymbol{u} \end{pmatrix} = \begin{pmatrix} \boldsymbol{u}_{\mathrm{I}} \\ \boldsymbol{t}_{\mathrm{I}} \end{pmatrix}, \tag{4.1}$$

where $\boldsymbol{u}_{\mathrm{I}}$ and $\boldsymbol{t}_{\mathrm{I}}$ are the incident wave and its traction and $\mathcal{A}_{\mathrm{Conv}}$ indicates the integral operator which is defined in the following manner:

$$\mathcal{A}_{\mathrm{Conv}} = \begin{pmatrix} -(\mathcal{U}^{(1)} + \mathcal{U}^{(2)}) & (\mathcal{T}^{(1)} + \mathcal{T}^{(2)}) \\ -(\mathcal{T}^{*(1)} + \mathcal{T}^{*(2)}) & (\mathcal{W}^{(1)} + \mathcal{W}^{(2)}) \end{pmatrix}. \tag{4.2}$$

We discretise the boundary integral equations in (4.1) into the following linear equation:

$$A_{\mathrm{Conv}} \begin{pmatrix} \boldsymbol{t} \\ \boldsymbol{u} \end{pmatrix} = \begin{pmatrix} \boldsymbol{u}_{\mathrm{I}} \\ \boldsymbol{t}_{\mathrm{I}} \end{pmatrix}, \tag{4.3}$$

and solve Eq.(4.3). In this equation A_{Conv} indicates the coefficient matrix defined as follows:

$$A_{\mathrm{Conv}} = \begin{pmatrix} -(U^{(1)} + U^{(2)}) & (T^{(1)} + T^{(2)}) \\ -(T^{*(1)} + T^{*(2)}) & (W^{(1)} + W^{(2)}) \end{pmatrix}, \tag{4.4}$$

where $U^{(m)}$, $T^{(m)}$, $T^{*(m)}$ and $W^{(m)}$ are the influence coefficient matrices which are obtained as one discretises Eq.(4.2). We here use the collocation method in the discretisation.

The periodic FMM is a fast method to calculate the integrals which appear in the boundary integral equations in (4.1). To solve (4.3) efficiently with FMM, we have to use iterative solvers with efficient preconditioners. In this chapter, we shall omit details of the periodic FMM and focus on the preconditioning issues. The reader is referred to chapter 2 for the periodic FMM in elastodynamics. We remark that we use the low frequency FMM in this thesis since most of periodic problems of interest can appropriately be solved with this formulation.

4.3 Calderon's formulae and the Calderon preconditioning

The well-known Calderon's formulae for the integral operators in Eq.(2.8)–Eq.(2.11) are given as follows:

$$\frac{\mathcal{I}}{4} = -\mathcal{U}^{(m)}\mathcal{W}^{(m)} + \mathcal{T}^{(m)}\mathcal{T}^{(m)}, \tag{4.5}$$

$$0 = \mathcal{U}^{(m)}\mathcal{T}^{*(m)} - \mathcal{T}^{(m)}\mathcal{U}^{(m)}, \tag{4.6}$$

$$\frac{\mathcal{I}}{4} = \mathcal{T}^{*(m)}\mathcal{T}^{*(m)} - \mathcal{W}^{(m)}\mathcal{U}^{(m)}, \tag{4.7}$$

$$0 = -\mathcal{T}^{*(m)}\mathcal{W}^{(m)} + \mathcal{W}^{(m)}\mathcal{T}^{(m)}, \tag{4.8}$$

where $\mathcal{I}$ is the identity operator. We can also rewrite these formulae into the following forms:

$$\begin{pmatrix} \mathcal{T}^{(m)} & -\mathcal{U}^{(m)} \\ \mathcal{W}^{(m)} & -\mathcal{T}^{*(m)} \end{pmatrix} \begin{pmatrix} \mathcal{T}^{(m)} & -\mathcal{U}^{(m)} \\ \mathcal{W}^{(m)} & -\mathcal{T}^{*(m)} \end{pmatrix} = \begin{pmatrix} \frac{\mathcal{I}}{4} & 0 \\ 0 & \frac{\mathcal{I}}{4}. \end{pmatrix}. \tag{4.9}$$

On the other hand, we can reorder the integral equations in (4.1) into the following form:

$$\begin{pmatrix} \mathcal{T}^{(1)} + \mathcal{T}^{(2)} & -(\mathcal{U}^{(1)} + \mathcal{U}^{(2)}) \\ \mathcal{W}^{(1)} + \mathcal{W}^{(2)} & -(\mathcal{T}^{*(1)} + \mathcal{T}^{*(2)}) \end{pmatrix} \begin{pmatrix} \boldsymbol{u} \\ \boldsymbol{t} \end{pmatrix} = \begin{pmatrix} \boldsymbol{u}_{\mathrm{I}} \\ \boldsymbol{t}_{\mathrm{I}} \end{pmatrix}. \tag{4.10}$$

We denote the operator which appears in Eq.(4.10) by $\mathcal{A}$.

As a consequence of Calderon's formulae in Eq.(4.9), we have the following identity when all the material constants of D_1 are equal to those of D_2:

$$\mathcal{A}^2 = \mathcal{I}. \tag{4.11}$$

Therefore, the corresponding coefficient matrix A coincides with the inverse of itself in this trivial special case, except for the error caused by discretisation.

We now examine whether a relation similar to Eq.(4.11) is satisfied or not when the material constants of D_1 are not equal to those of D_2. To this end, we take a local coordinate in the tangential plane on the boundary whose 3rd axis is directed in the direction of the normal vector $\boldsymbol{n}$. We then compute the Fourier transforms of the most singular parts of the integral operators $\mathcal{U}^{(m)}$, $\mathcal{T}^{(m)}$, $\mathcal{T}^{*(m)}$ and $\mathcal{W}^{(m)}$ within the tangential plane and denote them by $\mathcal{P}(\mathcal{U}^{(m)})$, etc. These Fourier transforms, called principal symbols in mathematics, determine the original operators to within compact operators. We then calculate $\mathcal{P}(\mathcal{A}^2)$ from $\mathcal{P}(\mathcal{U}^{(m)})$, etc.

In the calculation of these symbols, one may use the static fundamental solution since it determines the singularity of the dynamic periodic kernels. With this observation we obtain:

$$\mathcal{P}(\mathcal{U}^{(m)}) = \begin{pmatrix} \dfrac{\delta_{\alpha\beta}}{2\mu^{(m)}r} - \dfrac{(\lambda^{(m)} + \mu^{(m)})\xi_\alpha\xi_\beta}{4\mu^{(m)}(\lambda^{(m)} + 2\mu^{(m)})r^3} & \mathbf{0} \\ \mathbf{0} & \dfrac{\lambda^{(m)} + 3\mu^{(m)}}{4\mu^{(m)}(\lambda^{(m)} + \mu^{(m)})r} \end{pmatrix}, \tag{4.12}$$

where ξ_α indicates the parameter of Fourier transform, r stands for $r = \sqrt{\xi_1^2 + \xi_2^2}$ and the Greek indices α and β range form 1 to 2, respectively. Similarly, one obtains $\mathcal{P}(\mathcal{T}^{(m)})$, $\mathcal{P}(\mathcal{T}^{*(m)})$ and $\mathcal{P}(\mathcal{W}^{(m)})$ as follows:

$$\mathcal{P}(\mathcal{T}^{(m)}) = \mathcal{P}(\mathcal{T}^{*(m)}) = \frac{\mathrm{i}}{2} \begin{pmatrix} \mathbf{0} & \dfrac{\mu^{(m)}\xi_\alpha}{(\lambda^{(m)} + 2\mu^{(m)})r} \\ -\dfrac{\mu^{(m)}\xi_\beta}{(\lambda^{(m)} + 2\mu^{(m)})r} & 0 \end{pmatrix}, \tag{4.13}$$

$$\mathcal{P}(\mathcal{W}^{(m)}) = \begin{pmatrix} -\dfrac{\mu^{(m)} r \delta_{\alpha\beta}}{2} - \dfrac{\lambda^{(m)}\mu^{(m)}\xi_\alpha\xi_\beta}{(\lambda^{(m)}+2\mu^{(m)})r} & \mathbf{0} \\ \mathbf{0} & -\dfrac{(\lambda^{(m)}+\mu^{(m)})\mu^{(m)} r}{\lambda^{(m)}+2\mu^{(m)}} \end{pmatrix}. \tag{4.14}$$

Using Eq.(4.12), Eq.(4.13) and Eq.(4.14), we calculate $\mathcal{P}(\mathcal{A}^2)$ as follows:

$$\mathcal{P}(\mathcal{A}^2) = \begin{pmatrix} c_1\delta_{\alpha\beta} + c_2\dfrac{\xi_\alpha\xi_\beta}{r^2} & \mathbf{0} & \mathbf{0} & \\ \mathbf{0} & c_1+c_2 & & \\ & & c_1\delta_{\alpha\beta} + c_2\dfrac{\xi_\alpha\xi_\beta}{r^2} & \mathbf{0} \\ \mathbf{0} & & \mathbf{0} & c_1+c_2 \end{pmatrix}, \tag{4.15}$$

where c_1 and c_2 are constants given as

$$c_1 = \frac{(\mu^{(1)}+\mu^{(2)})^2}{4\mu^{(1)}\mu^{(2)}}, \tag{4.16}$$

$$c_2 = \frac{(\mu^{(1)}-\mu^{(2)})(\lambda^{(1)}\mu^{(2)2} - \lambda^{(2)}\mu^{(1)2} + \mu^{(1)}\mu^{(2)2} - \mu^{(2)}\mu^{(1)2} + \lambda^{(1)}\mu^{(1)}\mu^{(2)} - \lambda^{(2)}\mu^{(2)}\mu^{(1)})}{4\mu^{(1)}\mu^{(2)}(\lambda^{(1)}+2\mu^{(1)})(\lambda^{(2)}+2\mu^{(2)})}. \tag{4.17}$$

We remark that c_1+c_2 can be rewritten in the following form:

$$c_1+c_2 = \frac{\left((\lambda^{(1)}+\mu^{(1)})(\mu^{(1)}+\mu^{(2)}) + 2\mu^{(1)}\mu^{(2)}\right)\left((\lambda^{(2)}+\mu^{(2)})(\mu^{(1)}+\mu^{(2)}) + 2\mu^{(1)}\mu^{(2)}\right)}{4\mu^{(1)}\mu^{(2)}(\lambda^{(1)}+2\mu^{(1)})(\lambda^{(2)}+2\mu^{(2)})}. \tag{4.18}$$

From this representation, it is obvious that c_1+c_2 is always to be positive.

4.3.1 The case of $\mu^{(1)} = \mu^{(2)}$

In the special case of $\mu^{(1)} = \mu^{(2)}$, we have $\mathcal{P}(\mathcal{A}^2) = \mathcal{I}$ because $c_1 = 1$ and $c_2 = 0$ then. This yields

$$\mathcal{A}^2 = \mathcal{I} + \mathcal{K}, \tag{4.19}$$

where $\mathcal{K}$ is a compact operator. Eq.(4.19) means that the cluster point of eigenvalues of $\mathcal{A}^2$ is found only at 1 because the eigenvalues of a compact operator can accumulate only at 0. In other words, most of eigenvalues of $\mathcal{A}^2$ are near 1 and there are only finitely many eigenvalues of $\mathcal{A}^2$ whose absolute values are larger than $1+\delta$ or smaller than $1-\delta$ for $\forall\delta > 0$. Therefore, we expect that the use of (the inverse of) A, as a preconditioner for the linear equations obtained as the discretised (4.10), decreases the iteration number. We call this type of preconditioning to be of the "A^2 type".

Further consideration on (4.19) suggests another extremely simple preconditioning scheme which works if one uses GMRES [29] without restart as a solver for the linear equation. Indeed, the convergence of the unpreconditioned system is expected not to be slower than that of the same system with the A^2 type preconditioner, as far as the computational time is concerned [20]. In other words, ordering the matrix as in Eq.(4.10) is considered to be an efficient preconditioning. We call this approach the "A type" preconditioning.

To see this, we recall that GMRES minimises the residual in the Krylov subspace given by

$$M^{-1}\mathcal{K}(AM^{-1})_n = \mathrm{span}\{M^{-1}\boldsymbol{r}, M^{-1}AM^{-1}\boldsymbol{r}, M^{-1}(AM^{-1})^2\boldsymbol{r}, \cdots, M^{-1}(AM^{-1})^{n-1}\boldsymbol{r}\} \tag{4.20}$$

in the nth iteration step, where M is the (right) preconditioner, $\boldsymbol{r} := \boldsymbol{b} - A\boldsymbol{z}_0$ indicates the initial residual and $\boldsymbol{z}_0$ is the initial guess. Let us consider the Krylov subspace of A type preconditioning denoted by $\mathcal{K}(A)_{2n}$ and that of A^2 type preconditioning denoted by $A\mathcal{K}(A^2)_n$ after performing the matrix-vector product operations $2n-1$ times. They are given as follows (we note that the iteration numbers for these two approaches after the same number of matrix-vector product operations are different):

$$\mathcal{K}(A)_{2n} = \mathrm{span}\{\boldsymbol{r}, A\boldsymbol{r}, A^2\boldsymbol{r}, A^3\boldsymbol{r}, \cdots, A^{2n-2}\boldsymbol{r}, A^{2n-1}\boldsymbol{r}\}, \tag{4.21}$$

$$A\mathcal{K}(A^2)_n = \mathrm{span}\{\quad A\boldsymbol{r}, \qquad A^3\boldsymbol{r}, \cdots, \qquad A^{2n-1}\boldsymbol{r}\}. \tag{4.22}$$

Note that we have $\mathcal{K}(A)_{2n} \supset A\mathcal{K}(A^2)_n$ (proper subset), which means the following: Suppose that we have performed $2n-1$ matrix-vector product operations in A type and A^2 type preconditioning approaches. The A type preconditioning then finds the solution in a larger space in (4.21) than the A^2 type preconditioning which seeks the solution in a narrower space in (4.22). Since the matrix-vector product operation is by far the most time consuming part in the whole algorithm of the FMM accelerated BIEM, we see that the residual for the A type preconditioning is not larger than that for the A^2 type preconditioning after the same amount of computational time. In other words, the computational time for the A type preconditioned system is not longer than that for the A^2 type when the tolerance is set to be the same.

4.3.2 The case of $\mu^{(1)} \neq \mu^{(2)}$

Compared with the $\mu^{(1)} = \mu^{(2)}$ case, it is not clear if the coefficient matrix itself can be an efficient preconditioner when $\mu^{(1)} \neq \mu^{(2)}$, because (4.19) does not hold. Indeed, $\mathcal{A}^2$ is a singular operator (see Eq.(4.15)) then. We therefore calculate eigenvalues of $\mathcal{A}^2$ in order to examine whether the preconditioning approaches of the A and A^2 types are efficient or not in this case.

We first rewrite Eq.(4.15) into the following form:

$$\mathcal{P}(\mathcal{A}^2) = c_1\mathcal{I} + c_2\mathcal{P}(\mathcal{A}^{\mathrm{Singular}}), \tag{4.23}$$

where

$$\mathcal{P}(\mathcal{A}^{\mathrm{Singular}}) = \begin{pmatrix} \frac{\xi_\alpha\xi_\beta}{r^2} & \mathbf{0} & \mathbf{0} & \\ \mathbf{0} & 1 & & \\ & & \frac{\xi_\alpha\xi_\beta}{r^2} & \mathbf{0} \\ \mathbf{0} & & \mathbf{0} & 1 \end{pmatrix}. \tag{4.24}$$

One easily shows that the eigenvalues of $\mathcal{P}(\mathcal{A}^{\mathrm{Singular}})$ are 1 or 0. This shows that the eigenvalues of $\mathcal{A}^2$ accumulate only at two points given by c_1 (> 0) and $c_1 + c_2$ (> 0). Therefore, preconditioning approaches of A and/or A^2 types can be efficient also in the case of $\mu^{(1)} \neq \mu^{(2)}$ if the ratio of c_1 to $c_1 + c_2$ is not very large.

We can construct another Calderon preconditioning by eliminating the singular term (which is actually a sum of a singular integral and an identity multiplied by a constant) given by $\frac{\xi_\alpha\xi_\beta}{r^2}$ in Eq.(4.15), so that we have a preconditioned system similar to the RHS of (4.19). Namely, we seek an operator $\mathcal{M}$ which satisfies the following relation:

$$\mathcal{P}(\mathcal{A}^2\mathcal{M}) = \mathcal{I}. \tag{4.25}$$

As a matter of fact, we can achieve this by using a multiplicative block diagonal operator because this singularity exists in a block diagonal manner in the original system (4.15). To satisfy Eq.(4.25), $\mathcal{P}(\mathcal{M})$ should have the following form:

$$\mathcal{P}(\mathcal{M}) = \begin{pmatrix} c_3\delta_{\alpha\beta} + c_4\frac{\xi_\alpha\xi_\beta}{r^2} & \mathbf{0} & \mathbf{0} & \\ \mathbf{0} & c_3 + c_4 & & \\ & & c_3\delta_{\alpha\beta} + c_4\frac{\xi_\alpha\xi_\beta}{r^2} & \mathbf{0} \\ \mathbf{0} & & \mathbf{0} & c_3 + c_4 \end{pmatrix}, \tag{4.26}$$

where

$$c_3 = \frac{1}{c_1}, \quad c_4 = -\frac{c_2}{(c_1 + c_2)c_1}. \tag{4.27}$$

We next construct an operator $\mathcal{M}$ whose principal symbol is given by Eq.(4.26). We here consider a construction of $\mathcal{M}$ using a combination of operators in Eq.(2.8)–Eq.(2.11), which are also used in the FMM algorithm. To this end, we note the following relation:

$$\mathcal{P}\left((\mathcal{T}^{(1)} + \mathcal{T}^{(2)})(\mathcal{T}^{(1)} + \mathcal{T}^{(2)})\right) = \mathcal{P}\left((\mathcal{T}^{*(1)} + \mathcal{T}^{*(2)})(\mathcal{T}^{*(1)} + \mathcal{T}^{*(2)})\right) = c_5\begin{pmatrix} \frac{\xi_\alpha\xi_\beta}{r^2} & \mathbf{0} \\ \mathbf{0} & 1 \end{pmatrix}, \tag{4.28}$$

where

$$c_5 = \frac{1}{4}\left(\frac{\mu^{(1)}}{\lambda^{(1)}+2\mu^{(1)}} + \frac{\mu^{(2)}}{\lambda^{(2)}+2\mu^{(2)}}\right)^2. \tag{4.29}$$

Therefore, the following operator $\mathcal{M}$ is a possible candidate for the preconditioner:

$$\mathcal{M} = \begin{pmatrix} c_3\mathcal{I} + \frac{c_4}{c_5}(\mathcal{T}^{(1)}+\mathcal{T}^{(2)})(\mathcal{T}^{(1)}+\mathcal{T}^{(2)}) & \mathbf{0} \\ \mathbf{0} & c_3\mathcal{I} + \frac{c_4}{c_5}(\mathcal{T}^{*(1)}+\mathcal{T}^{*(2)})(\mathcal{T}^{*(1)}+\mathcal{T}^{*(2)}) \end{pmatrix}. \tag{4.30}$$

However, the operator in Eq.(4.30) may have irregular frequencies (fictitious eigenfrequencies). We therefore modify Eq.(4.30) as follows:

$$\tilde{\mathcal{M}} = \begin{pmatrix} c_3\mathcal{I} + \frac{c_4}{c_5}(\tilde{\mathcal{T}}^{(1)}+\tilde{\mathcal{T}}^{(2)})(\tilde{\mathcal{T}}^{(1)}+\tilde{\mathcal{T}}^{(2)}) & \mathbf{0} \\ \mathbf{0} & c_3\mathcal{I} + \frac{c_4}{c_5}(\tilde{\mathcal{T}}^{*(1)}+\tilde{\mathcal{T}}^{*(2)})(\tilde{\mathcal{T}}^{*(1)}+\tilde{\mathcal{T}}^{*(2)}) \end{pmatrix}, \tag{4.31}$$

where $\tilde{\mathcal{T}}^{(m)}$ and $\tilde{\mathcal{T}}^{*(m)}$ are $\mathcal{T}^{(m)}$ and $\mathcal{T}^{*(m)}$ operators evaluated for sufficiently small frequencies so that we do not have non-uniqueness problems caused by the artifact ($\mathcal{M}$). We note that Eq.(4.25) still holds for $\tilde{\mathcal{M}}$.

It is easy to see that the only cluster point of eigenvalues of $\mathcal{A}^2\tilde{\mathcal{M}}$ is 1. Therefore, AM can be an (inverse of) efficient right preconditioner, where M indicates the matrix obtained as one discretises $\tilde{\mathcal{M}}$. We call this approach the "A^2M type" preconditioning.

To summarise, we propose the following three types of Calderon's preconditioning approaches:

- The A type preconditioning solves

  $$A\boldsymbol{z} = \boldsymbol{b}$$

  as is, where $\boldsymbol{z}$ ($\boldsymbol{b}$) is the discretisation of the vector on the LHS (RHS) of (4.10). We call this approach a 'preconditioning' although there is no additional matrix multiplication involved. This is because the matrix A has an ordering different from the standard one used in (4.4).

- The A^2 type preconditioning solves

  $$A^2\boldsymbol{z'} = \boldsymbol{b} \quad \text{followed by} \quad \boldsymbol{z} = A\boldsymbol{z'}$$

- The A^2M type preconditioning solves

  $$A^2M\boldsymbol{z''} = \boldsymbol{b} \quad \text{followed by} \quad \boldsymbol{z} = AM\boldsymbol{z''}$$

  where M is the matrix obtained by discretising $\tilde{\mathcal{M}}$ in (4.31).

4.4 Numerical examples

In this section we present some numerical examples which will verify the efficiency of the preconditioning approaches proposed in section 4.3. We first state techniques common to all the examples to follow.

- We use the collocation method with locally constant elements for discretisation.
- We utilise GMRES (or Flexible GMRES known as FGMRES [29] with the conventional preconditioner) as the solver for the algebraic equations. The error tolerance for the convergence of GMRES is set to be 10^{-5} times the initial residual.
- We compute in advance the part of the matrix computed directly in the FMM algorithm (i.e., near-field interactions) and store it in memory, unless otherwise noted, because we use it at every GMRES iteration step.

- To confirm the efficiency of the proposed methods, we compare the iteration number and the computational time of the proposed preconditioning approaches to those of the conventional preconditioning method. As a conventional preconditioner we use the part of the matrix computed directly in the FMM algorithm as the (right) preconditioner. We shall henceforth denote this approach by 'Direct' in figures and tables. The inversion in the process of preconditioning is carried out approximately using GMRES (with FGMRES for the main solver) which we terminate either after 10 iterations or when the norm of the error is less than 10^{-1} times its initial value. We note that we solve Eq.(4.3) in order to make the matrix diagonally dominated when we use the conventional preconditioner. This is because this conventional preconditioner is considered to work as a block diagonal scaling, which is considered to work better with diagonally dominant coefficient matrix than with the ordering in (4.10).
- For the calculation we use Fujitsu HX supercomputer ('Thin' SMP cluster) at Academic Center for Computing and Media Studies of Kyoto University. The code is OpenMP parallelised and the number of CPUs is 16.

4.4.1 Scattering by a doubly periodic layer of spherical scatters

We first consider the scattering by a two dimensional array of elastic spheres shown in Fig. 4.1. The unit cell in this model contains one sphere, whose surface is divided into 18000 planar triangular elements (the total degrees of freedom is 108000), unless otherwise noted. We intentionally use an over refined mesh in order to see the performance of the proposed method in relatively large problems.

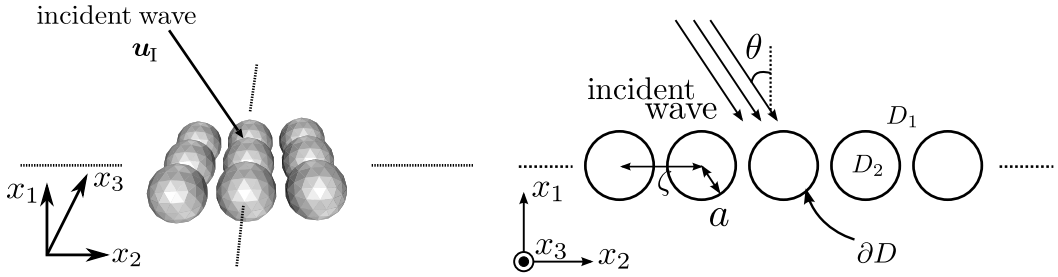

Figure 4.1: Scattering by a two dimensional array of elastic spheres. The array is perpendicular to x_1 axis. The radius of the sphere, the period and the incident angle are denoted by a, ζ and θ, respectively.

The case of $\mu^{(1)} = \mu^{(2)}$

We first consider the case of $\mu^{(1)} = \mu^{(2)}$ to test the efficiency of the A and A^2 type preconditioning approaches. The following three cases are considered.

- Infinite domain (i.e., $\lambda^{(1)} = \lambda^{(2)}$, $\mu^{(1)} = \mu^{(2)}$ and $\rho^{(1)} = \rho^{(2)}$). This is for the purpose of verification.
- **(case 1)** Lamé's constant $\lambda^{(2)}$ of the inclusion is varied and the other material constants are fixed at 1.0.
- **(case 2)** The density $\rho^{(2)}$ of the inclusion is varied and the other material constants are fixed at 1.0.

The incident wave is a plane longitudinal wave whose incident angle is $\theta = 0^\circ$ (normal incidence). The frequency of the incident wave is set to be $\omega = 8.0$. The geometrical period is set to be $\zeta_2 = \zeta_3 = 2.0(= \zeta)$, and the radius of the sphere is $a = 0.31\zeta$.

We first analysed the propagation of plane waves in the whole space in order to verify our codes. Namely, we set all the material parameters $\lambda^{(2)}$, $\mu^{(2)}$ and $\rho^{(2)}$ of the inclusion D_2 to be the same as those of the exterior domain D_1, i.e., $\lambda^{(1)}$ $\mu^{(1)}$ and $\rho^{(1)}$ in the model shown in Fig. 4.1. All the material

parameters are set to be 1.0. The analytical solution of this problem is $\boldsymbol{u} = \boldsymbol{u}_{\mathrm{I}}$ and $\boldsymbol{t} = \boldsymbol{t}_{\mathrm{I}}$. Table 4.1 shows the relative error defined as follows:

$$\epsilon = \sqrt{\frac{\sum_{i=1}^{N}\sum_{j=1}^{3}|u_{j;i}^{\mathrm{num}} - u_{j;i}^{\mathrm{ana}}|^2}{\sum_{i=1}^{N}\sum_{j=1}^{3}|u_{j;i}^{\mathrm{ana}}|^2}} + \sqrt{\frac{\sum_{i=1}^{N}\sum_{j=1}^{3}|t_{j;i}^{\mathrm{num}} - t_{j;i}^{\mathrm{ana}}|^2}{\sum_{i=1}^{N}\sum_{j=1}^{3}|t_{j;i}^{\mathrm{ana}}|^2}}, \tag{4.32}$$

where $u_{j;i}^{\mathrm{num/ana}}$ are the jth components of the displacements at the ith element of the numerical/analytical solutions and $t_{j;i}^{\mathrm{num/ana}}$ are the corresponding tractions, respectively. This table shows that the accuracy of each method is in the same range.

Table 4.1: The average of relative error for the number of elements N

N	500	2000	8000	18000
Calderon(A type)	0.169749886	8.26327056E-02	4.10175920E-02	2.73415856E-02
Calderon(A^2 type)	0.169751406	8.26305747E-02	4.10143323E-02	2.73411609E-02
Direct	0.169749886	8.26327056E-02	4.10175920E-02	2.73415856E-02

We next consider the case 1. Fig. 4.2 and Fig. 4.3 show the iteration number and the computational time for each of the preconditioning methods, respectively. These figures show that the proposed Calderon preconditioners accelerate the convergence much more effectively than the conventional one. Fig. 4.4 and

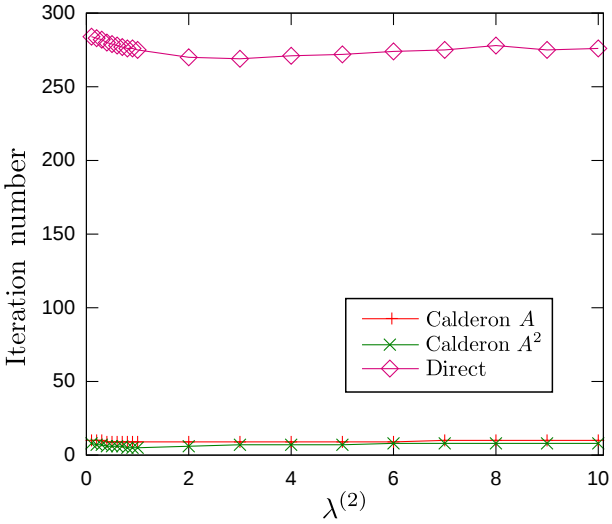

Figure 4.2: Iteration number vs Lamé's constant $\lambda^{(2)}$ of the inclusion

Fig. 4.5 are the blow-ups of the Calderon preconditioning results in Fig. 4.2 and Fig. 4.3, respectively. We see that the A^2 type preconditioning can decrease the iteration number more effectively than the A type preconditioning. However, the computational time of the A^2 type preconditioning is always larger than that of the A type preconditioning because the A^2 type preconditioning needs 2 matrix-vector product for one iteration step as we have discussed.

We next consider the case 2. We here fix all the Lamé's constants and the density of the exterior material to be 1.0. Fig. 4.6 and Fig. 4.7 show the iteration number and the total computational time, respectively. Fig. 4.8 and Fig. 4.9 are the blow-ups of the Calderon preconditioning results in Fig. 4.6 and Fig. 4.7, respectively. As in the case 1, we conclude from these results that both of the Calderon preconditioners (types A and A^2) accelerate the convergence more effectively than the conventional one and the A type preconditioning is always more efficient than the A^2 type preconditioning with respect to the computational time. Fig. 4.6 also shows that the iteration number increases as $\rho^{(2)}$ and hence the wavenumber increase. However, the iteration number with the proposed methods increases more slowly than that with the conventional preconditioning. As another observation, we note that the iteration number of all preconditioning approaches increases around $\rho^{(2)} = 2.2$ and 2.95 as seen in Fig. 4.6 and

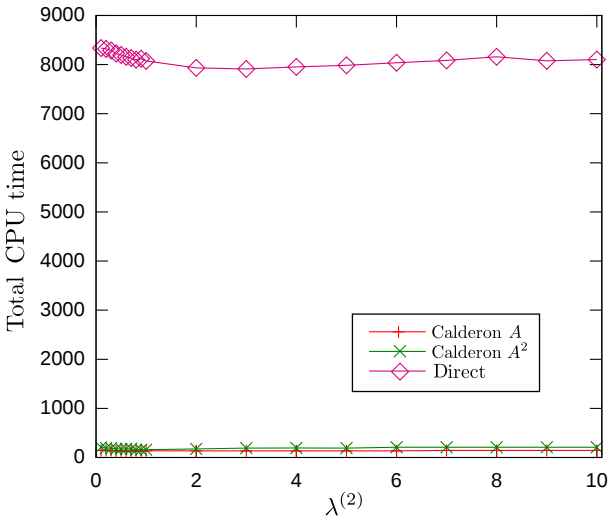

Figure 4.3: Computational time vs Lamé's constant $\lambda^{(2)}$ of the inclusion

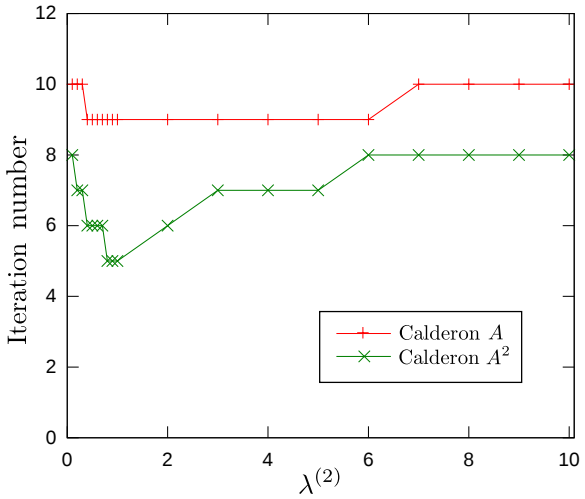

Figure 4.4: Iteration number vs Lamé's constant $\lambda^{(2)}$ of the inclusion

Fig. 4.8. We also note that the iteration number of the A^2 type increases comparable to that of the A type (Fig. 4.8) and, hence, the computational time of the A^2 type is approximately twice that of the A type around these values of $\rho^{(2)}$ (Fig. 4.9). The increase of iteration numbers is typically seen near anomalies where the solution shows sudden changes in response to small changes of frequencies, incident waves, etc. [11] We shall discuss this matter later in section 4.4.2.

The case of $\mu^{(1)} \neq \mu^{(2)}$

We next consider the case of $\mu^{(1)} \neq \mu^{(2)}$. The structure under consideration consists of steel inclusions in an infinite polyester matrix. The material parameters for this case are as shown in Table 4.2. We set the periodic length to be $\zeta_2 = \zeta_3 = 2.0(= \zeta)$ and the radius of the inclusion to be either $a = 0.15\zeta$ or 0.31ζ. For the incident wave we consider a plane P-wave of normal incidence. This problem has been studied by Maslov et al.[30] who have provided both experimental results and an approximate solution. For this model, we have computed the response in the frequency range of $\omega = 0.2$–8.2.

We first compare our numerical results obtained with the proposed preconditioning approaches with the approximate and experimental results by Maslov et al.[30] Fig. 4.10 shows the transmission and reflection coefficients vs frequency. As seen in Fig. 4.10, our results agree well with the experimental results and approximate solutions obtained by Maslov et al. and there is no difference among results

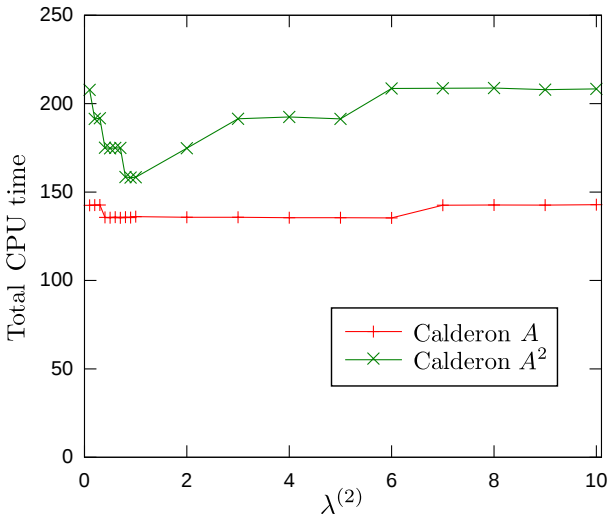

Figure 4.5: Computational time vs Lamé's constant $\lambda^{(2)}$ of the inclusion

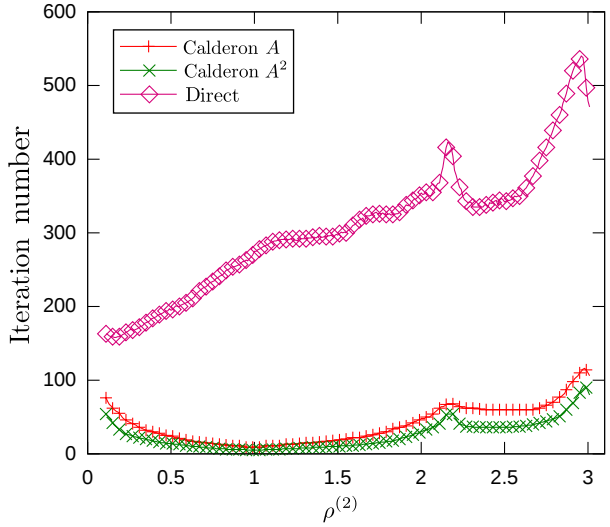

Figure 4.6: Iteration number vs density $\rho^{(2)}$ of the inclusion

Table 4.2: Material parameters used in the analysis

	Inclusion (steel)	Exterior matrix (polyester)
Density ρ	6.393	1.000
Lamé's constant λ	1.496	2.453
Lamé's constant μ	47.02	1.000

obtained with different preconditioning approaches, of course. We note that the difference between our results and their approximate solution is to be expected since their approximate solution is obtained with only a few terms of spherical harmonics and is valid only in low frequency problems where $k_{\mathrm{L}}^{(1)} a < 1$ holds.

Fig. 4.11 and Fig. 4.12 (Fig. 4.13 and Fig. 4.14) show the iteration number and total computational time in the case of $a = 0.15\zeta$ ($a = 0.31\zeta$), respectively. All of these results show that the proposed methods accelerate the convergence more effectively than the conventional one. These figures also show that the preconditioning approaches of the A^2 and A^2M types can decrease the iteration number more

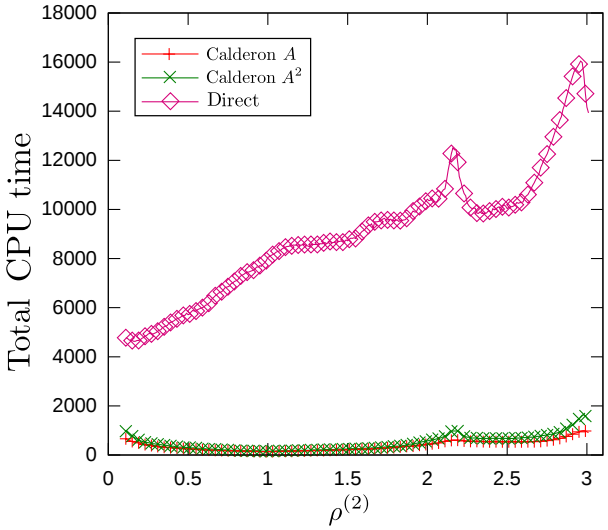

Figure 4.7: Computational time vs density $\rho^{(2)}$ of the inclusion

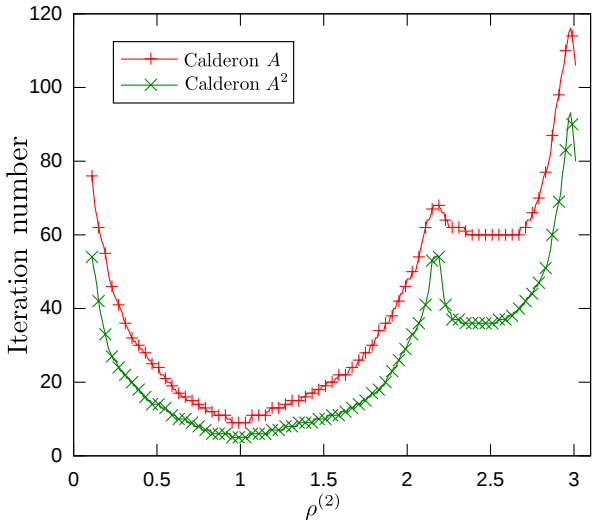

Figure 4.8: Iteration number vs density $\rho^{(2)}$ of the inclusion

than the A type preconditioning can. However, the computational time of the A type preconditioning is always less than that of other preconditioning approaches because the A^2 type preconditioning requires 2 matrix-vector product operations for every iteration and the A^2M type preconditioning needs even more products. As seen in Fig. 4.11 and Fig. 4.13, the iteration number of the A^2 and A^2M type preconditioners are almost the same. This indicates that the matrix A^2 is sufficiently well-conditioned although it contains discretised singular integrals and does not take the form of $I+K$, where I is an identity matrix and K is a matrix obtained by discretising a compact operator. This means that the eigenvalues of the preconditioned matrix need not necessarily accumulate at one single point for a preconditioner to work effectively. Indeed, we conclude that the preconditioned matrices for the A^2 type approaches are sufficiently well-conditioned although their eigenvalues accumulate at two points. It might be reasonable to expect that similar preconditioned systems will work well even if their eigenvalues have more accumulation points as far as their ratios are not very large.

Table 4.3 shows the total memory used in the case of $a = 0.31\zeta$ and $\omega = 8.2$. We note that the A^2 type approach requires less memory than the A type does because the iteration number of A^2 type is smaller than that of A, thus requiring less storage for the basis vectors of the Krylov subspace used by GMRES. We also note that the A^2M type approach needs approximately twice as much memory as the

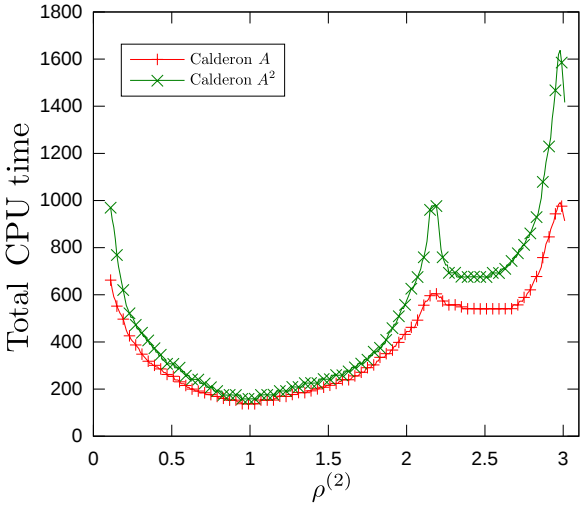

Figure 4.9: Computational time vs density $\rho^{(2)}$ of the inclusion

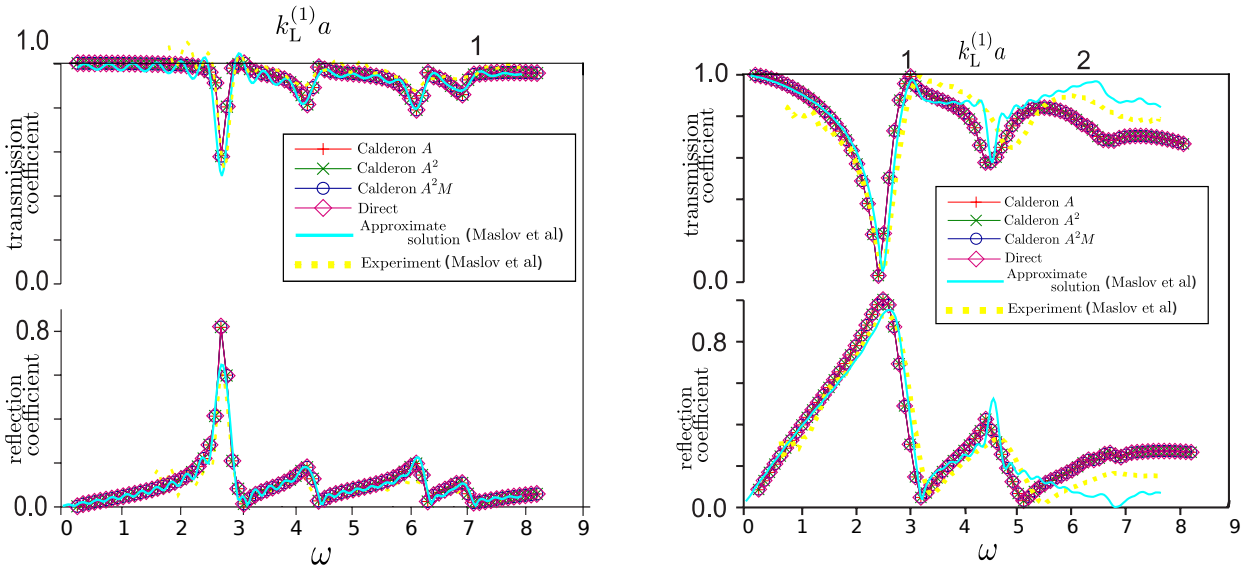

Figure 4.10: Transmission and reflection coefficients vs frequency (left: the case of $a = 0.15\zeta$, right: $a = 0.31\zeta$)

.

A or A^2 type does because the A^2M type stores the near-field interaction terms in the FMM algorithm not only for A but also for M.

Table 4.3: Total memory used in the case of $a = 0.31\zeta$, $\omega = 8.2$

Preconditioning approach	Calderon A	Calderon A^2	Calderon A^2M	Direct
Total memory used [GByte]	13.1	10.4	25.6	18.6

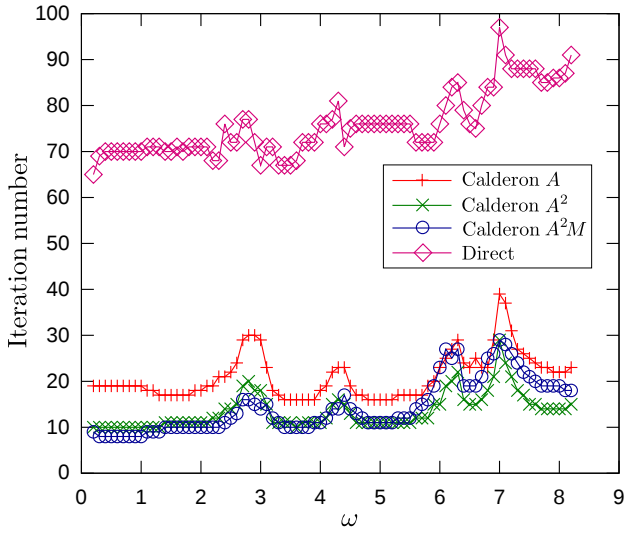

Figure 4.11: Iteration number vs frequency ω in the case of $a = 0.15\zeta$

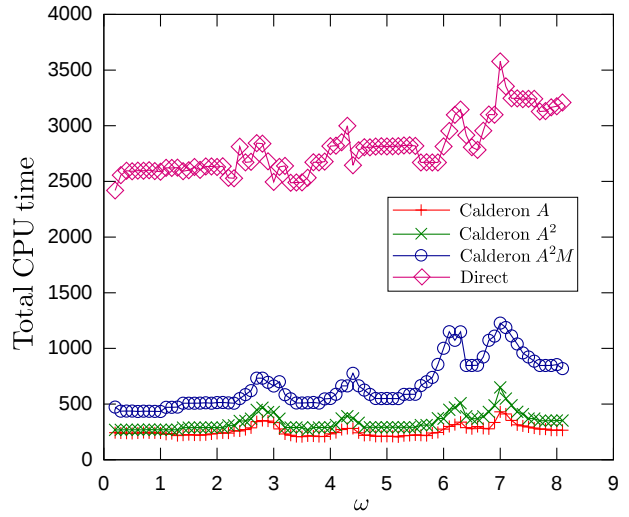

Figure 4.12: Computational time vs frequency ω in the case of $a = 0.15\zeta$

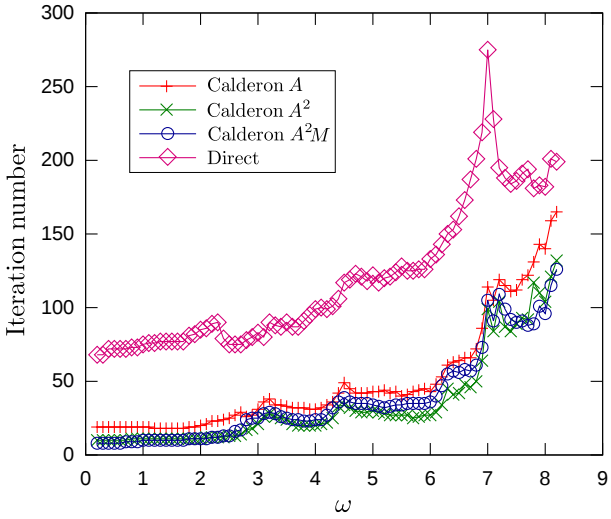

Figure 4.13: Iteration number vs frequency ω in the case of $a = 0.31\zeta$

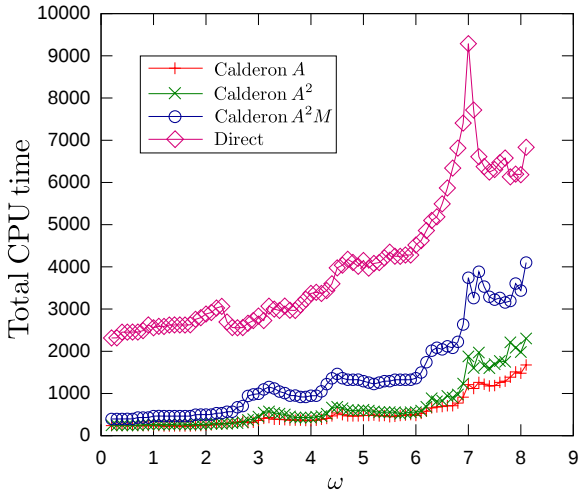

Figure 4.14: Computational time vs frequency ω in the case of $a = 0.31\zeta$

4.4.2 Performance around anomalies

It is well-known that the anomalous behaviours of periodic structures are related to the existence of modes which propagate within the lattice [11]. To further investigate the performances of the A and A^2 type preconditioning approaches around anomalies, we consider the joined half-space model shown in Fig. 4.15 where an interface wave called Stoneley's wave exists. The incident wave under consideration is as follows:

$$\boldsymbol{u}_{\mathrm{I}} = \boldsymbol{d}_{\mathrm{I}} \exp\left(\mathrm{i}k_{\mathrm{L}}^{(1)} \boldsymbol{p}_{\mathrm{I}} \cdot \boldsymbol{x}\right), \tag{4.33}$$

$$\boldsymbol{p}_{\mathrm{I}} = \boldsymbol{d}_{\mathrm{I}} = \left(q(\beta_2), \frac{\beta_2}{k_{\mathrm{L}}^{(1)}\zeta_2}, 0\right), \tag{4.34}$$

$$q(\beta_2) = \begin{cases} \sqrt{1 - \left(\frac{\beta_2}{k_{\mathrm{L}}^{(1)}\zeta_2}\right)^2}, & (\beta_2 \le k_{\mathrm{L}}^{(1)}\zeta_2, \text{ plane wave}) \\ \mathrm{i}\sqrt{\left(\frac{\beta_2}{k_{\mathrm{L}}^{(1)}\zeta_2}\right)^2 - 1}, & (\beta_2 > k_{\mathrm{L}}^{(1)}\zeta_2, \text{ evanescent wave}) \end{cases} \tag{4.35}$$

where $\boldsymbol{d}_{\mathrm{I}}$ and $\boldsymbol{p}_{\mathrm{I}}$ are unit vectors defining the directions of motion and propagation of the incident wave, respectively. Given arbitrary $\zeta_{2,3}$, we can view this problem to be periodic. We here set $\zeta_{2,3} = 1$ in addition to $\rho^{(1)} = \lambda^{(1)} = \mu^{(1)} = 0.100$, $\rho^{(2)} = \lambda^{(2)} = \mu^{(2)} = 1.000$ and $\omega = 10.00$. We have computed the response of this system in the phase difference range of $\beta_2 = 0.000$–14.00 with the phase difference resolution of 0.050. The unit cell is shown in Fig. 4.16, in which the interface is divided into 8192 planar triangular elements.

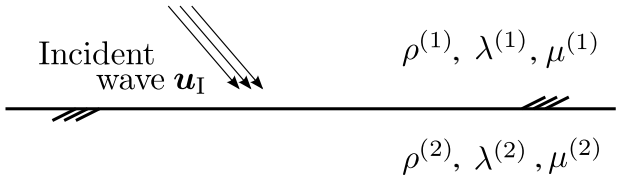

Figure 4.15: Joined half-spaces model

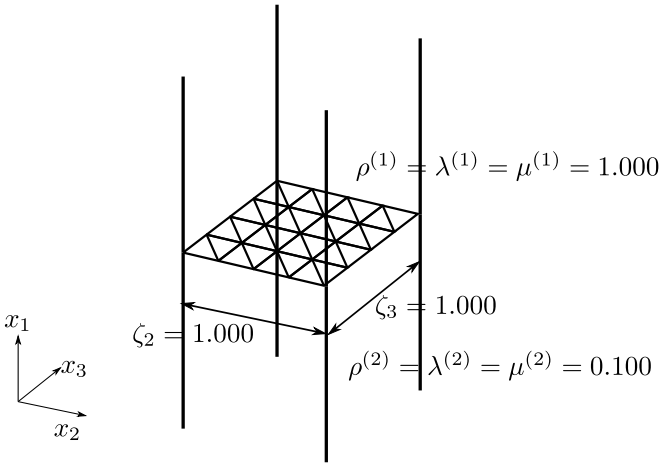

Figure 4.16: The unit cell of joined half-spaces model

The following two types of anomalies are relevant to this problem:

- There exist Rayleigh's anomalies when β_2 satisfies $(k_{\mathrm{L,T}}^{(1,2)})^2 = (\beta_2 + 2n\pi)^2 + (2m\pi)^2$ (m and n are integers). The Rayleigh's anomaly can be observed at $\beta_2 \simeq 5.776, 10.00$ in the present setting.

  As a matter of fact, the solution to our problem exists at this anomaly, but Green's function diverges and possibly causes numerical problems.

We remark that this anomaly is sometimes called 'Wood's anomaly' in mathematics, which is at variance with the engineering terminology.

- Stoneley's wave can be excited when β_2/ζ_2 coincides with the wavenumber of Stoneley's wave which is obtained as the solution to Stoneley's equation [33]. In the present case, such β_2 is found near 10.88. The incident wave in (4.33) then becomes an evanescent wave and the solution to the problem under consideration diverges at this β_2.

We shall call these β_2 "anomalous points".

Fig. 4.17 shows the relative error of the displacements on the interface (see (4.32)). The gradient of the error curve shows discontinuous behaviour at both anomalous points. When Stoneley's wave is excited, the analytical solutions diverge and the relative error also diverges. The relative error, however, is less than 1% except in the vicinity of the anomalous points. Fig. 4.18 shows the iteration number and the computational time for the A and A^2 type preconditioned system. These figures show that the iteration number does not increase around Rayleigh's anomalies, while it does when Stoneley's wave is excited. We note that the iteration number of the A type preconditioning is nearly twice as many as that of the A^2 type unless Stoneley's wave is excited. When Stoneley's wave is excited, however, the iteration number of the A^2 type preconditioning increases to the same range as that of the A type. As a result, the computational time for the A^2 type is about double of that for the A type.

To explain this phenomenon, we note that the condition number of the coefficient matrix will become very large around this frequency since the coefficient matrix is expected to have eigenvalues with very small magnitudes. In this case the A^2 type preconditioner becomes disadvantageous compared with the A type because the condition number of the A^2 type preconditioned coefficient matrix is equal to the square of that of the original (A type preconditioned) coefficient matrix. This also explains similar phenomena experienced in section 4.4.1 and later in section 4.4.3.

We finally note that the iteration number and computational time for the proposed methods are much smaller than those with the conventional method as shown in Fig. 4.19 even when β is near anomalous points.

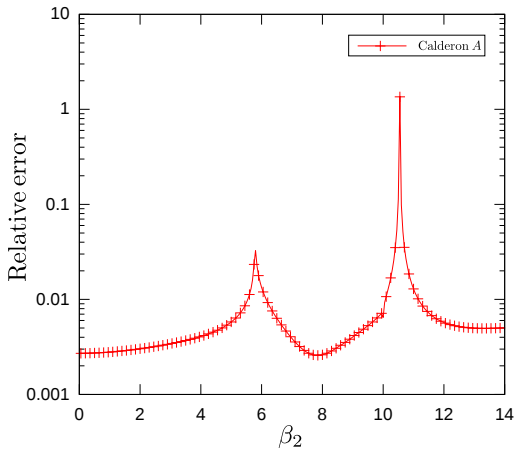

Figure 4.17: Relative error of the displacement for β_2

4.4.3 Scattering by a phononic crystal with the NaCl-type structure

We finally consider the scattering by an NaCl-type phononic crystal [34] shown in Fig. 4.20 in order to examine the applicability of the proposed methods to large scale problems. The NaCl-type phononic crystal considered here consists of two kinds of non-overlapping elastic spheres with different radii having the same periodicity as that of ions in NaCl crystals. We view the crystal to be a stack of layers each of which is a two dimensional array of spheres. We here consider eight layers each of which is perpendicular to x_1 axis and has the geometrical period of $\zeta = 1.000$. The shortest distance between the centres of the same kind of spheres is set to be $a_0 = \dfrac{\zeta}{\sqrt{2}}$ and the shortest distance between different kind of spheres is $\dfrac{a_0}{\sqrt{2}}$. The radii of small sphere a_1 and large sphere a_2 are $0.1a_0$ and $0.25a_0$, respectively. All the spheres

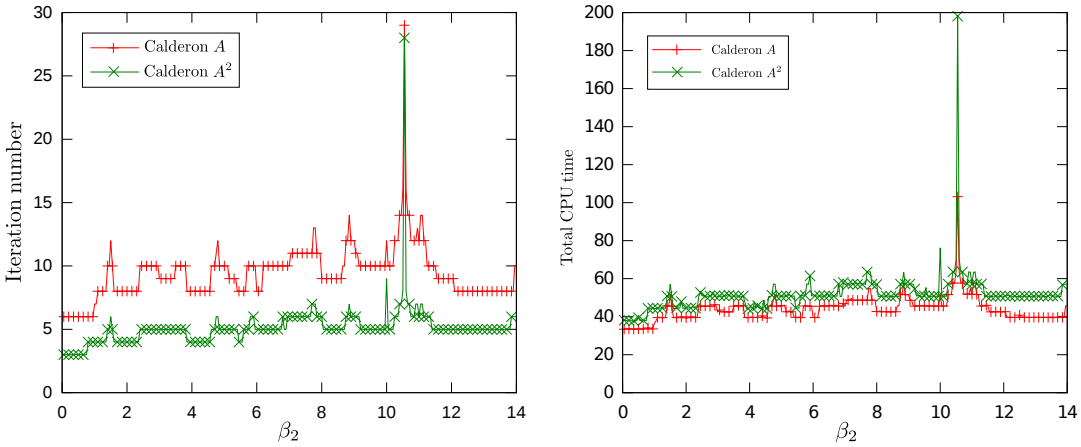

Figure 4.18: Iteration number (left) and total CPU time (right) vs β_2 in the case of joined half-space problems.

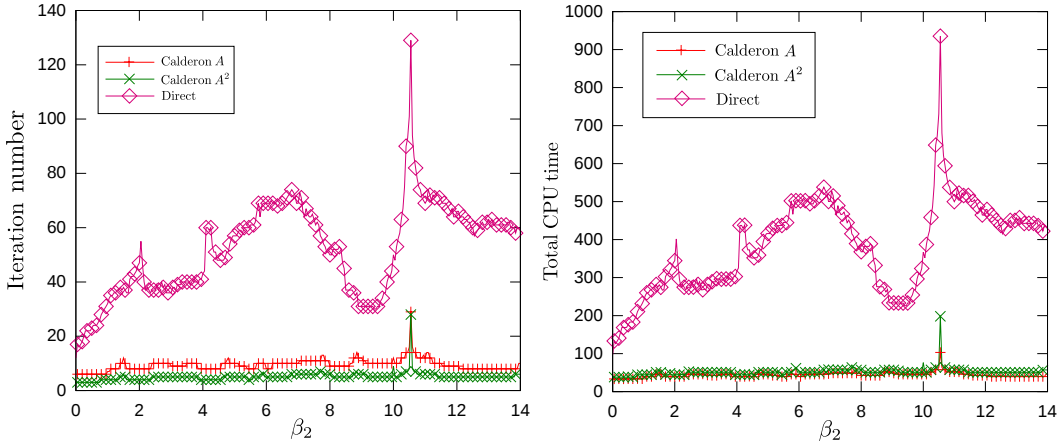

Figure 4.19: Iteration number (left) and total CPU time (right) vs β_2 in the case of joined half-space problems.

are made of lead and the host matrix is epoxy, whose material parameters are shown in Table 4.4. This model has been considered by Chen et al.[34] who have utilised the layer multiple scattering theory [35] to obtain the transmittance curve and the complex band structure of the 3D phononic crystal.

The unit cell used in our computation consists of 4 cubic level 0 FMM boxes as shown in Fig. 4.21. The surfaces of the small and large spheres are divided into 2000 and 12500 planar triangular elements, respectively, with the total number of elements and the total degrees of freedom being $232,000$ and $1,392,000$, respectively. For the incident wave we consider a plane P-wave of normal incidence. We have computed the response in the frequency range of $\omega = 0.2$–7.7. We note that this example includes relatively high frequency cases. Indeed, the nondimensional frequency of the slowest relevant wave is $k_{\mathrm{T}}^{(2)} H = 30.46$ for $\omega = 7.7$, where H is the height of the phononic crystal in the non-periodic direction x_1. The evaluation of the near-field interaction terms in FMM is done on the fly because storing all of them requires too large memory. Furthermore, we have considered only promising preconditioning approaches, i.e., A and A^2 types, because other preconditioners will be too slow to be practical in large scale problems of this size.

We first compare the transmittance vs frequency curve obtained with periodic FMM with the analytical result by Chen et al.[34] in Fig. 4.22. The agreement is satisfactory. Fig. 4.23 and Fig. 4.24 show the iteration number and the computational time for A and A^2 type Calderon preconditioners. This figure shows that the iteration number is larger with the A^2 type preconditioner than with A around normalised frequencies $k_{\mathrm{L}}^{(1)} a_0 = 1.6$ and 2.3. This resembles the behaviour we have observed in the previous section

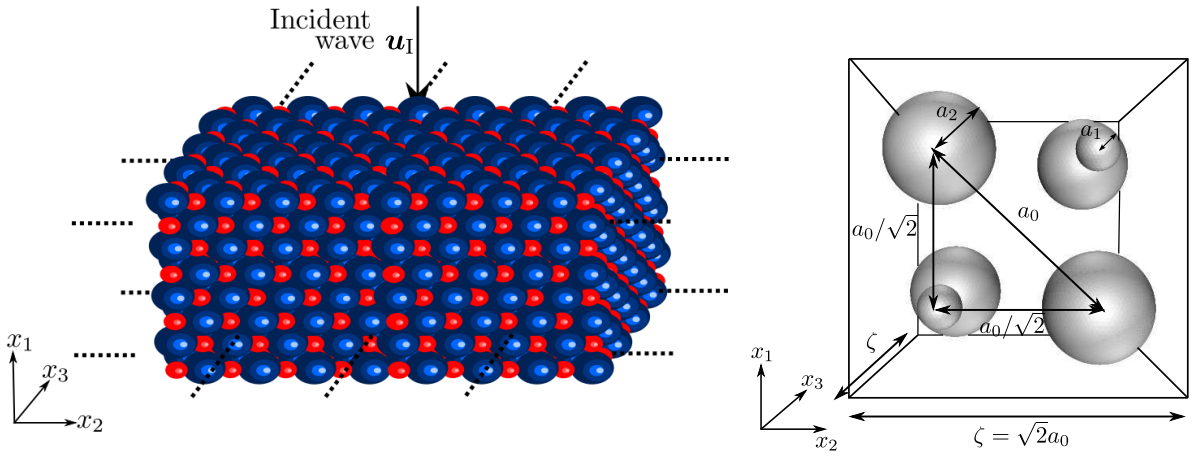

Figure 4.20: Scattering by a NaCl-type phononic crystal. The shortest distance between the same kind of spheres, the radius of the small (red) sphere, the radius of the large (blue) sphere and the period are denoted by a_0, a_1, a_2 and ζ, respectively.

Table 4.4: Material parameters used in the analysis

	Inclusion (lead)	Exterior matrix (epoxy)
Density ρ	9.831	1.000
Lamé's constant λ	26.64	2.795
Lamé's constant μ	9.329	1.000

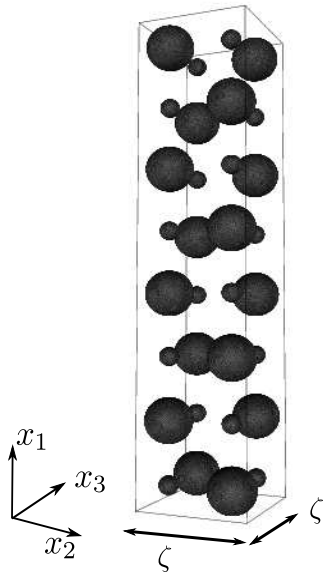

Figure 4.21: The unit cell for a NaCl-type phononic crystal. Each layer contains two large lead spheres and two small lead spheres. The whole unit cell contains 32 lead spheres. The period is denoted by ζ.

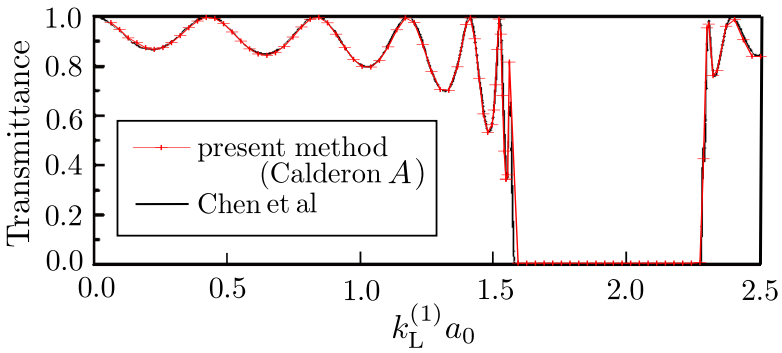

Figure 4.22: Transmittance vs normalised frequency $k_{\mathrm{L}}^{(1)} a_0$ in the case of scattering by the NaCl-type phononic crystal.

in connection with Stoneley's wave.

Indeed, a comparison with Fig. 4.22 shows that these frequencies are just below/above stopbands, where the solution shows sudden changes. We thus conclude that the increase of iteration number at these frequencies are related to the occurrence of anomalies, which explains the increase of the iteration number of the A^2 type over that of the A type as we have seen in section 4.4.2.

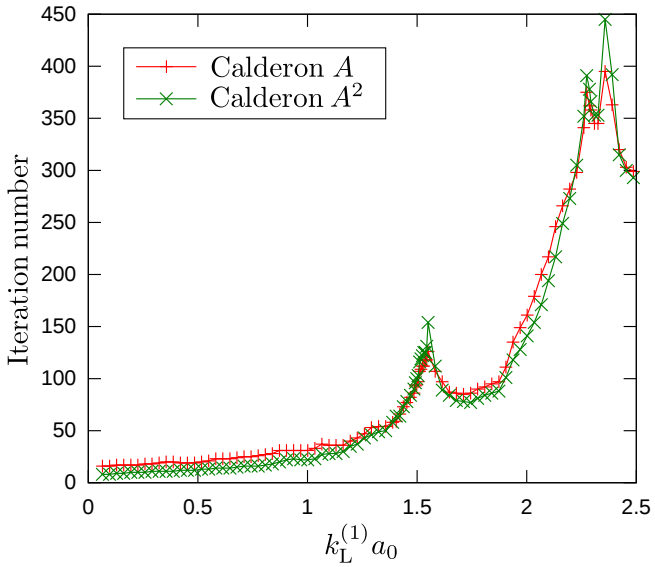

Figure 4.23: Iteration number vs normalised frequency $k_{\mathrm{L}}^{(1)} a_0$ in the case of scattering by the NaCl-type phononic crystal.

Finally, we observe from Fig. 4.23 and Fig. 4.24 that iteration number and both CPU time increase considerably for larger wave numbers even with the Calderon preconditioners. However, we still believe that these preconditioners are effective in such cases also because they keep the number of iterations almost independent of the number of unknowns. To see this, we compare the number of iterations required by the A type preconditioner with the 1,392,000 DOF mesh and with a coarser 501,120 DOF one in Fig. 4.25. As this figure shows the number of iterations are sometimes even smaller with the finer mesh.

4.5 Conclusions

We have proposed three types of Calderon preconditioning approaches for periodic FMM in elastodynamics in 3D. It is found that these Calderon preconditioners accelerate the convergence more effectively than the conventional one. In the case of transmission problems for 2 subdomains, we found, through numerical

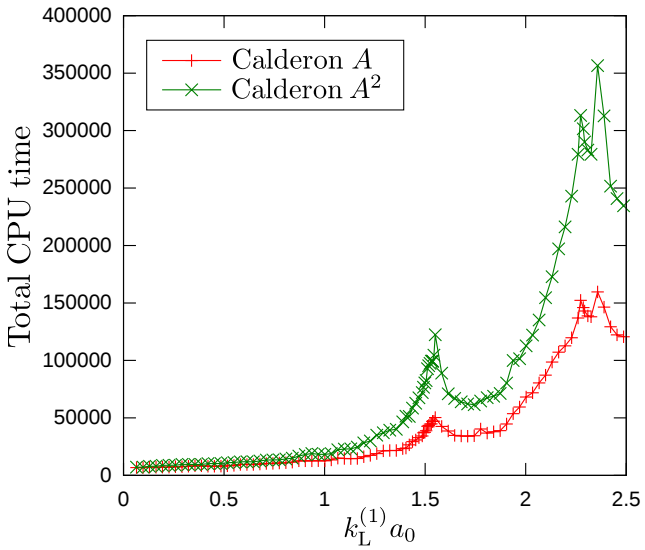

Figure 4.24: Total CPU time vs normalised frequency $k_{\mathrm{L}}^{(1)} a_0$ in the case of scattering by the NaCl-type phononic crystal.

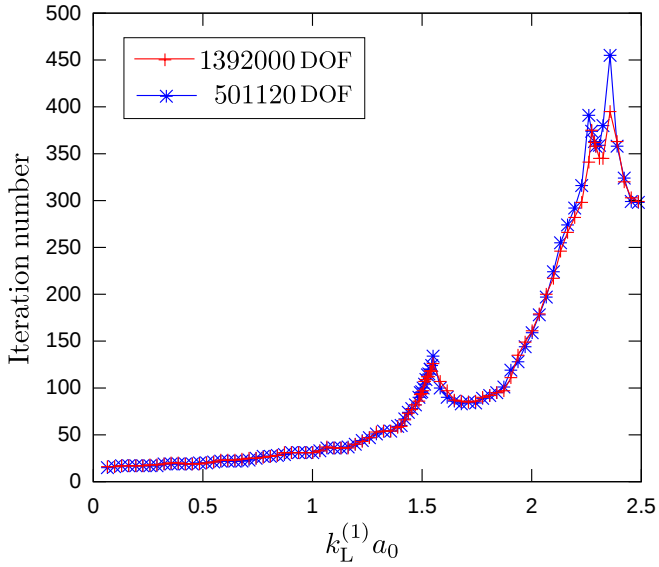

Figure 4.25: Number of iterations vs normalised frequency $k_{\mathrm{L}}^{(1)} a_0$ for A type preconditioner with different meshes

experiments, that the A type preconditioning is particularly effective since we can achieve the acceleration just by appropriately ordering the coefficient matrix. The A^2 type preconditioning is also attractive since it requires less memory than the A type and the acceleration performance is comparable to the A type. The A^2 type, however, could be slow to converge near the anomalous points because the condition number of the coefficient matrix with the A^2 type preconditioner can be much larger than that of the A type.

As subjects of further investigations on applications and enhancements of the Calderon preconditioners, we can mention the following:

- Calderon's preconditioning in more realistic phononic crystal applications.
- Investigation of Calderon's preconditioning in higher frequency problems.
- Combination of the Calderon's preconditioning with other techniques such as the complexification [36] of certain physical parameters, variants of GMRES such as the restart version, etc.

- Extension of the proposed technique to other PDEs including Maxwell's equations for electromagnetics.

Use of related preconditioning approaches such as sparse analytic preconditioners based on the quasi inverse (an inverse modulo compact) of the operator $\mathcal{A}$ [37], [38] is also among interesting future topics of investigations.

Chapter 5

Calderon's preconditioning for acoustics-elastodynamics coupled problems

5.1 Introduction

In this chapter, we investigate Calderon preconditioning approaches for the periodic FMM for acoustics-elastodynamics coupled problems. We first derive three types of boundary integral formulation for the problems, one of which is based on the PMCHWT formulation [32], and others are based on the Burton-Miller method. We then construct preconditioning approaches based on Calderon's formulae for each formulation, which use the matrices used in the FMM algorithm as (the inverse of) the preconditioner.

5.2 PMCHWT formulation and Calderon's preconditioning

We first note that Calderon's formulae hold also for the Helmholtz' operators in Eq.(3.13)–Eq.(3.16), which are represented as follows, just as in the case of elastodynamic operators in Eq.(4.5)–Eq.(4.8):

$$\frac{\mathcal{I}}{4} = -\mathcal{S}\mathcal{N} + \mathcal{D}\mathcal{D}, \tag{5.1}$$

$$0 = \mathcal{S}\mathcal{D}^* - \mathcal{D}\mathcal{S}, \tag{5.2}$$

$$\frac{\mathcal{I}}{4} = \mathcal{D}^*\mathcal{D}^* - \mathcal{N}\mathcal{S}, \tag{5.3}$$

$$0 = -\mathcal{D}^*\mathcal{N} + \mathcal{N}\mathcal{D}, \tag{5.4}$$

where $\mathcal{I}$ is the identity operator.

The PMCHWT formulation [32] for the periodic boundary value problems of acoustics-elastodynamics, stated in chapter 3 is as follows:

$$\begin{pmatrix} -\mathcal{W} - \rho^{(1)}\omega^2 \boldsymbol{n}_x \mathcal{S} \boldsymbol{n}_y^T & \mathcal{T}^* \boldsymbol{n}_y + \boldsymbol{n}_x \mathcal{D} \\ \rho^{(1)}\omega^2 \boldsymbol{n}_x^T \mathcal{T} + \rho^{(1)}\omega^2 \mathcal{D}^* \boldsymbol{n}_y & -\mathcal{N} - \rho^{(1)}\omega^2 \boldsymbol{n}_x^T \mathcal{U} \boldsymbol{n}_y \end{pmatrix} \begin{pmatrix} \boldsymbol{u}(y) \\ p(y) \end{pmatrix} = \begin{pmatrix} p_{\mathrm{I}}(x)\boldsymbol{n}_x \\ -\dfrac{\partial p_{\mathrm{I}}(x)}{\partial n} \end{pmatrix}, \tag{5.5}$$

where p_{I} is the incident sound pressure and $\boldsymbol{n}_x$ ($\boldsymbol{n}_y$) are the unit normal vector on point x (y). Also, $\mathcal{S}$, $\mathcal{D}$, $\mathcal{D}^*$, $\mathcal{N}$, $\mathcal{U}$, $\mathcal{T}$, $\mathcal{T}^*$ and $\mathcal{W}$ are the integral operators defined in Eq.(2.8)–Eq.(2.11) and Eq.(3.13)–Eq.(3.16). We denote the operator which appears in LHS of Eq.(5.5) by $\mathcal{A}$. The operator $\mathcal{A}$ can be rewritten into the following form:

$$\mathcal{A} = \mathcal{A}' + \mathcal{T}' + \mathcal{K}, \tag{5.6}$$

where $\mathcal{A}'$, $\mathcal{T}'$ and $\mathcal{K}$ are the following integral operators:

$$\mathcal{A}' = \begin{pmatrix} -\mathcal{W} & 0 \\ 0 & -\mathcal{N} \end{pmatrix}, \tag{5.7}$$

$$\mathcal{T}' = \begin{pmatrix} 0 & \mathcal{T}^* \boldsymbol{n}_y \\ \rho^{(1)}\omega^2 \boldsymbol{n}_x^T \mathcal{T} & 0 \end{pmatrix}, \tag{5.8}$$

$$\mathcal{K} = \begin{pmatrix} -\rho^{(1)}\omega^2 \boldsymbol{n}_x \mathcal{S} \boldsymbol{n}_y^T & \boldsymbol{n}_x \mathcal{D} \\ \rho^{(1)}\omega^2 \mathcal{D}^* \boldsymbol{n}_y & -\rho^{(1)}\omega^2 \boldsymbol{n}_x^T \mathcal{U} \boldsymbol{n}_y \end{pmatrix}. \tag{5.9}$$

We note that the operator $\mathcal{K}$ in Eq.(5.9) is compact. Hence, we consider improving the condition of the operator $\mathcal{A}'$ and $\mathcal{T}'$ in Eq.(5.7) without loss of the compactness of the operator $\mathcal{K}$. To this end, we consider the following operator:

$$\mathcal{M}^{-1} = \begin{pmatrix} \mathcal{U} & \mathbf{0} \\ \mathbf{0} & \mathcal{S} \end{pmatrix}. \tag{5.10}$$

Using this operator, we see that the operator $\mathcal{A}\mathcal{M}^{-1}$ has the following representation by virtue of the Calderon's formulae in Eq.(4.7) and Eq.(5.3):

$$\mathcal{A}\mathcal{M}^{-1} = \mathcal{A}'\mathcal{M}^{-1} + \mathcal{T}'\mathcal{M}^{-1} + \mathcal{K}\mathcal{M}^{-1} \tag{5.11}$$

$$= \begin{pmatrix} \dfrac{\mathcal{I}}{4} - \mathcal{T}^*\mathcal{T}^* & \mathbf{0} \\ \mathbf{0} & \dfrac{\mathcal{I}}{4} - \mathcal{D}^*\mathcal{D}^* \end{pmatrix} + \begin{pmatrix} \mathbf{0} & \mathcal{T}^* \boldsymbol{n}_y \mathcal{S} \\ \rho^{(1)}\omega^2 \boldsymbol{n}_x^T \mathcal{T}\mathcal{U} & \mathbf{0} \end{pmatrix} + \mathcal{K}\mathcal{M}^{-1}. \tag{5.12}$$

We note that the operator $\mathcal{K}\mathcal{M}^{-1}$ in Eq.(5.12) is compact since both $\mathcal{K}$ and $\mathcal{M}^{-1}$ are compact. Also, the operators $\mathcal{T}^*\boldsymbol{n}_y\mathcal{S}$ and $\rho^{(1)}\omega^2\boldsymbol{n}_x^T\mathcal{T}\mathcal{U}$, which appear in $\mathcal{T}'\mathcal{M}^{-1}$are compact. We therefore examine the eigenvalues of the operator $\mathcal{A}'\mathcal{M}^{-1}$ in Eq.(5.12). To this end, we consider the Fourier transform of the most singular parts of the operator within the tangential plane (the principal symbol, see also section 4.3), which is denoted by $\mathcal{P}(\mathcal{A}'\mathcal{M}^{-1})$. We first note that the principal symbol of $\mathcal{T}^*\mathcal{T}^*$ and $\mathcal{D}^*\mathcal{D}^*$ are given as follows:

$$\mathcal{P}(\mathcal{T}^*\mathcal{T}^*) = c^2 \begin{pmatrix} \dfrac{\xi_\alpha \xi_\beta}{r^2} & \mathbf{0} \\ \mathbf{0} & 1 \end{pmatrix}, \tag{5.13}$$

$$\mathcal{P}(\mathcal{D}^*\mathcal{D}^*) = 0, \tag{5.14}$$

where ξ_α indicates the parameter of Fourier transform, r stands for $r = \sqrt{\xi_1^2 + \xi_2^2}$ and the Greek indices α and β range form 1 to 2, respectively. Also, c is a constant defined as follows:

$$c = \frac{\mu^{(2)}}{2(\lambda^{(2)} + 2\mu^{(2)})} = \frac{1}{2}\left(\frac{c_{\mathrm{T}}}{c_{\mathrm{L}}}\right)^2, \tag{5.15}$$

where c_{L} and c_{T} are the phase velocity of the longitudinal and transverse waves of the elastic material, respectively. The principal symbol of $\mathcal{A}'\mathcal{M}^{-1}$ is then obtained as follows:

$$\mathcal{P}(\mathcal{A}'\mathcal{M}^{-1}) = \begin{pmatrix} \dfrac{\delta_{\alpha\beta}}{4} - c^2\dfrac{\xi_\alpha\xi_\beta}{r^2} & \mathbf{0} & \mathbf{0} \\ \mathbf{0} & \dfrac{1}{4} - c^2 & 0 \\ \mathbf{0} & 0 & \dfrac{1}{4} \end{pmatrix}. \tag{5.16}$$

One easily shows that the eigenvalues of $\mathcal{P}(\mathcal{A}\mathcal{M}^{-1})$ are $\dfrac{1}{4}$ or $\dfrac{1}{4} - c^2$.

With these observations, the preconditioned operator $\mathcal{A}\mathcal{M}^{-1}$ is expressed in the following form:

$$\mathcal{A}\mathcal{M}^{-1} = \mathcal{P}(\mathcal{A}'\mathcal{M}^{-1}) + \mathcal{K}', \tag{5.17}$$

where $\mathcal{K}'$ is a compact operator. We thus obtain a well conditioned operator $\mathcal{A}\mathcal{M}^{-1}$, whose cluster points of eigenvalues are at two points given by $\dfrac{1}{4}$ and $\dfrac{1}{4} - c^2$ (> 0). We also note that c^2 is less than $\dfrac{1}{4}$ since

$c_{\mathrm{T}} < c_{\mathrm{L}}$ always holds. Therefore, we expect that the use of (the inverse of) the matrix which is obtained as discretised $\mathcal{M}^{-1}$ as preconditioner decreases the number of iteration. However, the operator $\mathcal{M}^{-1}$ in Eq.(5.10) may have fictitious eigenfrequences. We therefore modify Eq.(5.10) as follows:

$$\tilde{\mathcal{M}}^{-1} = \begin{pmatrix} \tilde{\mathcal{U}} & \mathbf{0} \\ \mathbf{0} & \tilde{\mathcal{S}} \end{pmatrix}, \tag{5.18}$$

where $\tilde{\mathcal{U}}$ and $\tilde{\mathcal{S}}$ are $\mathcal{U}$ and $\mathcal{S}$ operators evaluated for sufficiently small frequencies so that non-uniqueness problems caused by the artifact ($\mathcal{M}^{-1}$) do not arise. We note that Eq.(5.16) holds also for $\tilde{\mathcal{M}}^{-1}$.

5.3 Other formulations based on the Burton-Miller method and Calderon's preconditioning

In this section, we investigate Calderon's preconditioning approaches for the formulation based on the Burton-Miller method. To this end, we first rewrite the boundary integral equations (3.21) by eliminating $\dfrac{\partial p}{\partial n}$ and $\boldsymbol{t}$ in RHS via Eq.(3.4) and Eq.(3.5) into the following form:

$$\begin{pmatrix} \dfrac{\mathcal{I}}{2} + \mathcal{D} + \alpha\mathcal{N} & -\rho^{(1)}\omega^2 \left(\mathcal{S} + \alpha \left(\mathcal{D}^* - \dfrac{\mathcal{I}}{2} \right) \right) \boldsymbol{n}_y^T \\ -\mathcal{U}\boldsymbol{n}_y & \dfrac{\mathcal{I}}{2} - \mathcal{T} \end{pmatrix} \begin{pmatrix} p(y) \\ \boldsymbol{u}(y) \end{pmatrix} = \begin{pmatrix} p_{\mathrm{I}}(x) + \alpha \dfrac{\partial p_{\mathrm{I}}(x)}{\partial n} \\ \mathbf{0} \end{pmatrix}. \tag{5.19}$$

We denote the operator which appears in LHS of Eq.(5.19) by $\mathcal{A}_{\mathrm{BM1}}$. To improve the condition of the operator $\mathcal{A}_{\mathrm{BM1}}$, we consider eliminating the hyper-singular integral $\mathcal{N}$ by virtue of the Calderon's formula in Eq.(5.4) and a diagonal scaling. To this end, we consider the following operator:

$$\mathcal{M}_{\mathrm{BM1}}^{-1} = \begin{pmatrix} -\dfrac{2\mathcal{S}}{\alpha} & \mathbf{0} \\ \mathbf{0} & \mathcal{I} \end{pmatrix}. \tag{5.20}$$

Using this operator, we can write the operator $\mathcal{A}_{\mathrm{BM1}}\mathcal{M}_{\mathrm{BM1}}^{-1}$ as follows:

$$\mathcal{A}_{\mathrm{BM1}}\mathcal{M}_{\mathrm{BM1}}^{-1} = \begin{pmatrix} \dfrac{\mathcal{I}}{2} - \mathcal{D}^*\mathcal{D}^* & \mathrm{i}\omega\sqrt{\rho^{(1)}\lambda^{(1)}}\mathcal{I}\boldsymbol{n}_y^T \\ \mathbf{0} & \dfrac{\mathcal{I}}{2} - \mathcal{T} \end{pmatrix} + \begin{pmatrix} -\dfrac{\mathcal{S} + 2\mathcal{D}\mathcal{S}}{\alpha} & -\rho^{(1)}\omega^2 \left(\mathcal{S} + \alpha\mathcal{D}^* \right) \boldsymbol{n}_y^T \\ \dfrac{2\mathcal{U}\boldsymbol{n}_y\mathcal{S}}{\alpha} & \mathbf{0} \end{pmatrix}, \tag{5.21}$$

where the second term of RHS in Eq.(5.21) is a compact operator. We now examine the eigenvalues of the operator which appears in the first term of RHS of Eq.(5.21). To this end, it suffices to investigate the eigenvalues of the operator $\mathcal{T}$. From the principal symbol of $\mathcal{T}$ (Eq.(4.13)), it can be easily shown that the cluster point of the eigenvalues of $\mathcal{T}$ is found only at 0, $\pm c$, where c is the constant defined in Eq.(5.15). With this observation, it follows that the eigenvalues of the operator $\mathcal{A}_{\mathrm{BM1}}\mathcal{M}_{\mathrm{BM1}}^{-1}$ can accumulate around the three points given by $\dfrac{1}{2}, \dfrac{1}{2} \pm c$ (> 0). We therefore expect that the use of (the inverse of) the matrix which is obtained as discretised $\mathcal{M}_{\mathrm{BM1}}^{-1}$ as preconditioner is effective. We note that we have to modify Eq.(5.20) in the same manner as Eq.(5.18), that is, replace $\mathcal{S}$ by the one for sufficiently small frequencies, to avoid a fictitious eigenvalue problem.

It is possible to construct the Calderon preconditioner for the formulation in Eq.(3.21), which is also based on the Burton-Miller method. To this end, we rearrange the column and row of Eq.(3.21) as follows:

$$\begin{pmatrix} \left(\dfrac{\mathcal{I}}{2} + \mathcal{D} \right) + \alpha\mathcal{N} & -\mathcal{S} - \alpha \left(-\dfrac{\mathcal{I}}{2} + \mathcal{D}^* \right) & \mathbf{0} & \mathbf{0} \\ 0 & \mathcal{I} & -\rho^{(1)}\omega^2\boldsymbol{n}_y^T & \mathbf{0} \\ \mathbf{0} & \mathbf{0} & \dfrac{\mathcal{I}}{2} - \mathcal{T} & \mathcal{U} \\ \boldsymbol{n}_y & \mathbf{0} & \mathbf{0} & \mathcal{I} \end{pmatrix} \begin{pmatrix} \dfrac{\partial p(y)}{\partial n} \\ p(y) \\ \boldsymbol{t}(y) \\ \boldsymbol{u}(y) \end{pmatrix} = \begin{pmatrix} p_{\mathrm{I}}(x) + \alpha \dfrac{\partial p_{\mathrm{I}}(x)}{\partial n_x} \\ 0 \\ \mathbf{0} \\ \mathbf{0} \end{pmatrix}. \tag{5.22}$$

We denote the operator which appears in LHS of Eq.(5.22) by $\mathcal{A}_{\mathrm{BM2}}$. To improve the condition of the

operator $\mathcal{A}_{\mathrm{BM2}}$, we use the following operator:

$$\mathcal{M}_{\mathrm{BM2}}^{-1} = \begin{pmatrix} -\dfrac{4\mathcal{S}}{\alpha} & 0 & \mathbf{0} & \mathbf{0} \\ 0 & \mathcal{I} & \mathbf{0} & \mathbf{0} \\ \mathbf{0} & \mathbf{0} & 2\mathcal{I} & \mathbf{0} \\ \mathbf{0} & \mathbf{0} & \mathbf{0} & \mathcal{I} \end{pmatrix}. \tag{5.23}$$

With this operator, the operator $\mathcal{A}_{\mathrm{BM2}}$ is preconditioned as follows:

$$\mathcal{A}_{\mathrm{BM2}}\mathcal{M}_{\mathrm{BM2}}^{-1} = \begin{pmatrix} \mathcal{I} & \dfrac{\alpha\mathcal{I}}{2} & \mathbf{0} & \mathbf{0} \\ 0 & \mathcal{I} & -2\rho^{(1)}\omega^2\boldsymbol{n}_y^T & \mathbf{0} \\ \mathbf{0} & \mathbf{0} & \mathcal{I} - 2\mathcal{T} & \mathbf{0} \\ \mathbf{0} & \mathbf{0} & \mathbf{0} & \mathcal{I} \end{pmatrix} + \begin{pmatrix} \dfrac{4\mathcal{D}\mathcal{S}}{\alpha} - 4\mathcal{D}^*\mathcal{D}^* & -\mathcal{S} - \alpha\mathcal{D}^* & \mathbf{0} & \mathbf{0} \\ 0 & 0 & \mathbf{0} & \mathbf{0} \\ \mathbf{0} & \mathbf{0} & \mathbf{0} & \mathcal{U} \\ -\dfrac{4\mathcal{S}\boldsymbol{n}_y}{\alpha} & \mathbf{0} & \mathbf{0} & \mathbf{0} \end{pmatrix}. \tag{5.24}$$

The cluster points of eigenvalues of the operator which appears in the first term in RHS are found only at $1, 1 \pm 2c$ (> 0), where c is the constant defined in Eq.(5.15) and the second term in Eq.(5.24) is compact. Therefore, we expect that the use of (the inverse of) the matrix which is obtained as discretised $\mathcal{M}_{\mathrm{BM2}}^{-1}$ as preconditioner accelerate the convergence of iterative solvers. We note that we have to modify Eq.(5.23) in the same manner as in Eq.(5.18), that is, replace $\mathcal{S}$ by the one for sufficiently small frequencies, to avoid a fictitious eigenvalue problem.

We note that the coefficient of the Burton-Miller method α is considerably small in high frequency range since α is typically chosen to be $\dfrac{\mathrm{i}}{k}$, where k is the wave number. Hence, the above formulations in Eq.(5.19) and Eq.(5.22) are considered to be less affected by the hyper-singular term $\alpha\mathcal{N}$ in high frequency range. In other words, solving Eq.(5.19) or Eq.(5.22) without any preconditioner or with conventional preconditioning approach, such as a block diagonal scaling, may not be too slow to converge.

5.4 Numerical examples

In this section we present numerical examples which will verify the efficiency of the preconditioning approaches stated in section 5.2 and 5.3. We consider the following two problems:

- Scattering by a periodically perforated tungsten slab immersed in water.
- Scattering by spherical inclusion immersed in water.

We have treated the same problems with the Burton-Miller method in section 3.3, where we have shown that the method is computationally expensive in these problems because of the slow convergence of iterative method. We here solve the same problems with the proposed methods shown in section 5.2 and 5.3 using the same computational conditions as have been used in section 3.3.

We shall henceforth denote the formulations stated in Eq.(3.21) by "Conventional" in figures to follow. Also, we denote the formulations in Eq.(5.5), Eq.(5.19) and Eq.(5.22) by "PMCHWT","BM1" and "BM2", respectively.

To confirm the efficiency of the proposed method, we compare the iteration number and the computational time of the proposed preconditioning approaches to those of the conventional preconditioning methods. As conventional preconditioners, we use the right preconditioner which is composed of the part of the matrix computed directly in the FMM algorithm. The inversion in the process of preconditioning is carried out approximately using GMRES (with FGMRES for the main solver) which we terminate either after 10 iterations or when the norm of the error is less than 10^{-1} times its initial value.

We note that the total degrees of freedom with the PMCHWT and BM1 are half of those of the BM2 and Conventional.

5.4.1 Scattering by periodically perforated tungsten slab immersed in water

We first consider the scattering by a tungsten slab immersed in water which is periodically perforated with circular holes (Fig. 3.3). The material and shape parameters for the slab are stated in section 3.3.2. We again consider the normal incidence. We have computed the response in the frequency range from 3.0 to 16.0 with the frequency resolution of 0.1. We divided the interface with 28054 triangular elements,

hence the total degrees of freedom are either 112216 for the PMCHWT and BM1 or 224432 for BM2 and Conventional. We set the coefficient for the Burton-Miller method α to be either 0 for Conventional or $-\frac{\mathrm{i}}{k}$ for the other formulations.

We first compare our numerical results obtained with the proposed preconditioning approaches with that of the hard solid limit model by Estrada et al.[31] Fig. 5.1 shows the transmittance curve vs normalised wavelength. The results with the proposed preconditioning approaches well agreed with the reference solution except for the low frequency range as was the case in chapter 3. Also, the results with the PMCHWT formulation is slightly different from those with the Burton-Miller methods, although the agreement is satisfactory.

Fig. 5.2 and Fig. 5.3 show the iteration number and the computational time for each preconditioning approach. These figures show that the proposed method can accelerate the convergence more effectively than the conventional ones. We note that "Conventional" is slow to convergence compared with the other formulations although it does not contain hyper singular integrals. We also note that "BM1+Direct" and "BM2+Direct" is seen to be effective since the matrices obtained as discretised $\mathcal{A}_{\mathrm{BM1,2}}$ (Eq.(5.19), Eq.(5.22)) are relatively well-conditioned, especially in the high frequency range, as we have discussed. However, the proposed Calderon preconditioning approaches are more effective than the conventional preconditioning approaches in almost all cases and the computational time with "BM1+Calderon" is always the smallest. With these observations, we conclude that the proposed methods are effective even when the material constant of the inclusion is extremely different from those of the exterior matrix (see Table 3.3).

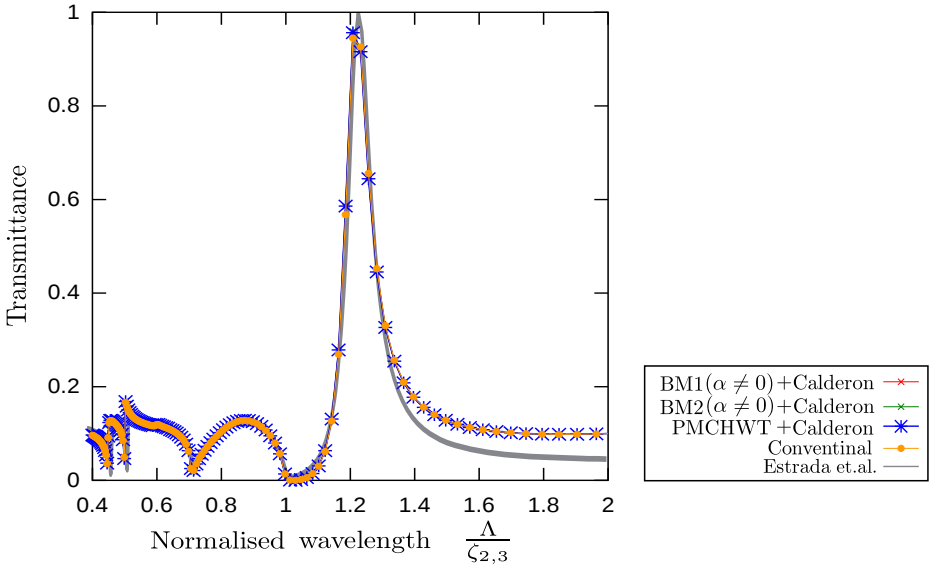

Figure 5.1: Transmittance vs normalised wavelength in the case of scattering by periodically perforated tungsten slab.

5.4.2 Scattering by spherical inclusion immersed in water

We then consider the problems of scattering by spherical inclusion immersed in water discussed in section 3.3.3.

Fig. 5.4 and Fig. 5.5 show the iteration number and the computational time for each preconditioning approach. The proposed approach "BM1+Calderon" is always the fastest and "PMCHWT+Calderon" is faster than any other conventional approaches except at a few points in high frequency range. "BM2+Calderon" is faster than "BM2+Direct". However, it is slow to converge compared even with the conventional preconditioning approach with the other formulations, i.e., "BM1+Direct" or "PMCHWT+Direct". This is partly because the total degrees of freedom for BM2 is twice as that for the other formulations. Furthermore, "PMCHWT+Direct" is considered to be relatively fast for this problem because of the following reasons.

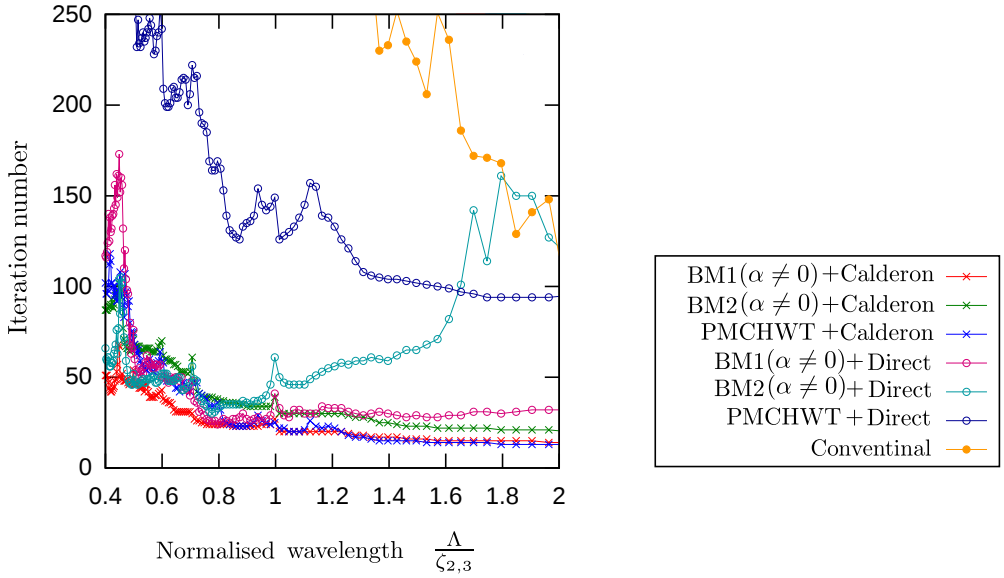

Figure 5.2: Iteration number vs normalised wavelength in the case of scattering by periodically perforated tungsten slab.

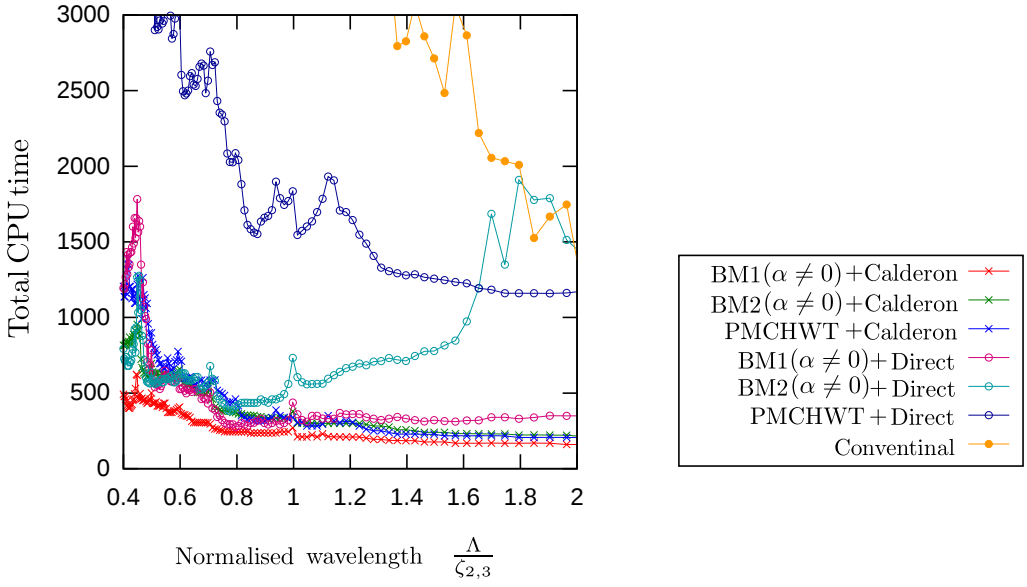

Figure 5.3: Total CPU time vs normalised wavelength in the case of scattering by periodically perforated tungsten slab.

- The coefficient matrices obtained as discretised Eq.(5.5) is highly diagonal dominant since the hyper singular terms, i.e., $\mathcal{N}$ and $\mathcal{W}$, are located at the diagonal block.
- The values of the matrix components in Eq.(5.5) resulting from $\mathcal{N}$ are considered to be comparable in magnitude to those from $\mathcal{W}$ since the material constants of the inclusion are in about the same range as those of the exterior domain (see Table 3.4). These values are located around the diagonal band in the coefficient matrix.

We finally note that the computational time for "BM1+Calderon" is considerably smaller than that for "PMCHWT+Calderon" though the iteration number for these two approaches are comparable. This is

because of the difference of the cost for operating (the inverse of) the preconditioner. We only have to compute $\mathcal{S}$ for "BM1+Calderon" preconditioner in Eq.(5.20), while we have to compute both $\mathcal{S}$ and $\mathcal{U}$ for "PMCHWT+Calderon" preconditioner in Eq.(5.10). From these observations, we conclude that "BM1+Calderon" is particularly effective.

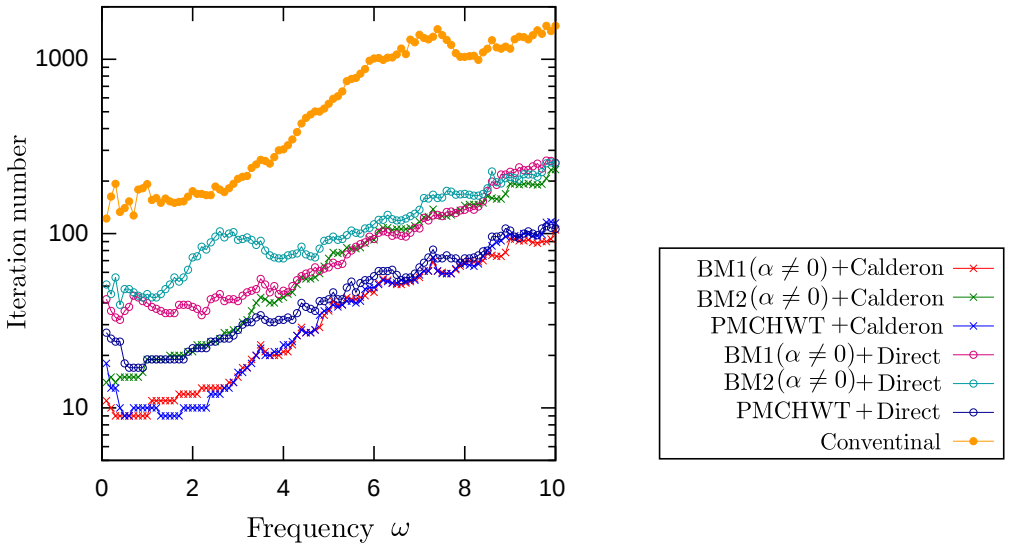

Figure 5.4: Iteration number vs frequency in the case of scattering by spherical inclusion.

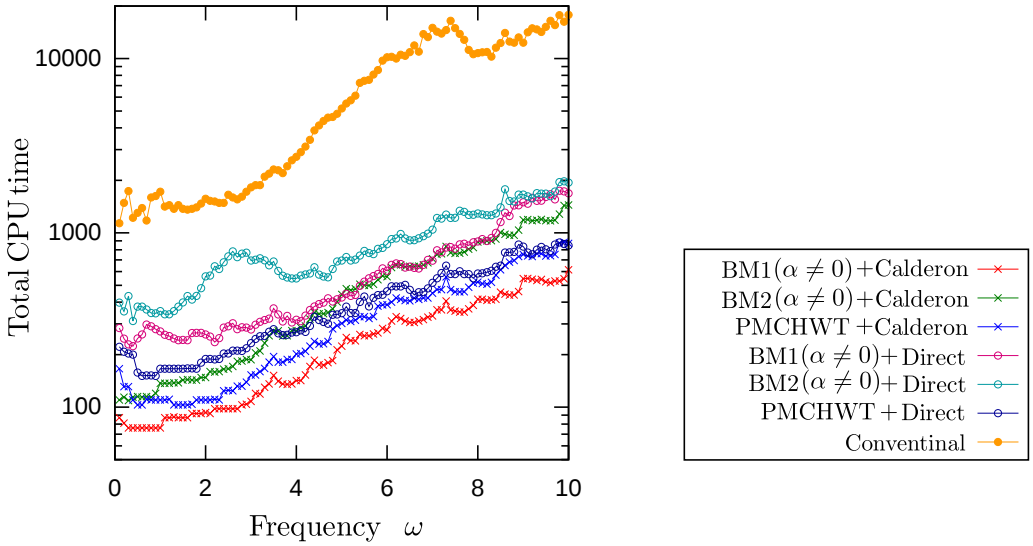

Figure 5.5: Total CPU time vs frequency in the case of scattering by spherical inclusion.

5.5 Conclusion

We have proposed Calderon preconditioning approaches for periodic FMM for acoustics-elastodynamics coupled problems. It is found that the proposed methods can accelerate the convergence of the iterative method more effectively than the conventional ones. It is also found that the proposed method is effective even for the problems with high contrast of the material constants between inclusions and exterior matrix.

Chapter 6

Conclusions

In this thesis, we have investigated periodic FMMs and Calderon's preconditioning in acoustics and elastodynamics. The conclusions from each of the chapters are summarised as follows:

- Chapter 2
  In chapter 2, we have investigated a periodic fast multipole boundary integral equation method for three dimensional elastodynamics as an extension of the previous studies for Helmholtz' equation [13] and Maxwell's equations [14]. Through numerical examples, we have confirmed the efficiency of the proposed method and the occurrence of the Wood's anomaly in the field of elastodynamics.

- Chapter 3
  In chapter 3, we have investigated a periodic FMM for acoustics-elastodynamics coupled problems in 3D. The accuracy of the proposed method is confirmed through numerical examples related to phononic crystals immersed in water.

- Chapter 4
  In chapter 4, we have proposed three types of Calderon preconditioning approaches for periodic FMM in elastodynamics in 3D stated in chapter 2. It is found that these Calderon preconditioners accelerate the convergence more effectively than the conventional one. We found, through numerical experiments, that the A type preconditioning is particularly effective since we can achieve the acceleration just by appropriately ordering the coefficient matrix. The A^2 type preconditioning is also attractive since it requires less memory than the A type and the acceleration performance is comparable to the A type, except near anomalies.

- Chapter 5
  In chapter 5, we have proposed Calderon preconditioners for acoustics-elastodynamics coupled problems stated in chapter 3. We have derived the PMCHWT formulation for problems of this type and a Calderon preconditioning approach, which uses the matrices which are also used in the FMM algorithm. We have also investigated the Calderon preconditioners for the formulations based on the Burton-Miller method. We found, through numerical experiments, that the proposed method can accelerate the convergence of the iterative method more effectively than the conventional ones. We also found that the proposed method is effective even for the problems with large contrasts between the material constants of inclusions and the exterior matrix.

With these investigations, we can now solve a variety of periodic boundary value problems for acoustics and elastodynamics related to phononic crystals with sufficient accuracy. The proposed method is fast enough to solve large scale problems with millions of DOF in a realistic time frame.

As further investigation for related problems, we can mention the following:

- A periodic FMM for a locally resonant sonic material (LRSM) [39]. This material is a kind of phononic crystal with inclusions coated by elastically soft materials such as rubber and is known to exhibit stopband with a geometrical period much smaller than the relevant wavelength. We need another formulation to deal with LRSM since the wave velocity of the coating is too small compared with that of the inclusion to apply the current version of periodic FMM.

- A periodic FMM for a piezoelectric phononic crystal [40]. To deal with this material we have to investigate a periodic FMM for electoromagnetics-elastodynamics coupled problems. Also, we have

to modify our elastodynamic formulation to deal with anisotropic material since the piezoelectric materials exhibit anisotropic behaviour.

- Combination of the Calderon's preconditioning with other techniques such as the complexification [36] of certain physical parameters, variants of GMRES such as the restart version, etc.
- Use of related preconditioning approaches such as sparse analytic preconditioners based on the quasi inverse (an inverse modulo compact) of the operator $\mathcal{A}$ [37], [38].

Bibliography

[1] N. Nishimura. Fast multipole accelerated boundary integral equation methods. *Applied Mechanics Reviews*, Vol. 55, pp. 299–322, 2004.

[2] V. Rokhlin. Rapid solution of intergral equations of classical potential theory. *Journal of Computational Physics*, Vol. 60, pp. 187–207, 1985.

[3] L. Greengard and V. Rokhlin. A fast algorithm for particle simulations. *Journal of Computational Physics*, Vol. 73, No. 2, pp. 325–348, 1987.

[4] T. Fukui and J. Katsumoto. Fast multipole algorithm for two dimensional helmholtz equation and its application to boundary element method. In *Proceedings of 14th Japan National Symposium on Boundary Element Methods*, pp. 81–86, 1997.

[5] V. Rokhlin. Rapid solution of intergral equations of scattering in two dimensions. *Journal of Computational Physics*, Vol. 86, pp. 414–439, 1990.

[6] H. Fujiwara. The fast multipole method for integral equations of seismic scattering problems. *Geophysical Journal International*, Vol. 133, pp. 773–782, 1998.

[7] K. Yoshida. Applications of fast multipole method to boundary integral equation method. *Ph.D. thesis for Kyoto Univ., Japan*, 2001.

[8] L. Brillouin. *Wave propagation in periodic structures*. Dover Pubns, 2003.

[9] J.D. Joannopoulos, S.G. Johnson, J.N. Winn, and R.D. Meade. *Photonic crystals*. Princeton University Press, 1995.

[10] J.B. Pendry. Negative refraction makes a perfect lens. *Physical Review Letters*, Vol. 85, No. 18, pp. 3966–3969, 2000.

[11] Y. Otani and N. Nishimura. Behaviour of periodic fast multipole boundary integral equation method for Maxwell's equations near Wood's anomalies. In *Imaging microstructures: mathematical and computational challenges: proceedings of a research conference, June 18-20, 2008, Institut Henri Poincaré, Paris, France*, Vol. 494, p. 43. Amer Mathematical Society, 2009.

[12] S.P. Shipman and D. Volkov. Existence of guided modes on periodic slabs. *Discrete and Continuous Dynamical systems, Supplement Volume*, pp. 784–791, 2005.

[13] Y. Otani and N. Nishimura. An FMM for periodic boundary value problems for clacks for Helmholtz' equation in 2D. *International Journal for Numerical Methods in Engineering*, Vol. 74, pp. 381–406, 2007.

[14] Y. Otani and N. Nishimura. A periodic FMM for Maxwell's equations in 3D and its applications to problems related to photonic crystals. *Journal of Computational Physics*, Vol. 227, pp. 4630–4652, 2008.

[15] M. S. Kushwaha, P. Halevi, L. Dobrzynski, and B. Djafari-Rouhani. Acoustic band structure of periodic elastic composites. *Phys. Rev. Lett.*, Vol. 71, No. 13, pp. 2022–2025, 1993.

[16] K. Sakoda. *Optical properties of photonic crystals*, Vol. 80. Springer Verlag, 2005.

[17] O. Steinbach and WL Wendland. The construction of some efficient preconditioners in the boundary element method. *Advances in Computational Mathematics*, Vol. 9, No. 1, pp. 191–216, 1998.

[18] S.H. Christiansen and J.C. Nédélec. A preconditioner for the electric field integral equation based on Calderon formulas. *SIAM journal on numerical analysis*, Vol. 40, No. 3, pp. 1100–1135, 2003.

[19] X. Antoine and Y. Boubendir. An integral preconditioner for solving the two-dimensional scattering transmission problem using integral equations. *International Journal of Computer Mathematics*, Vol. 85, No. 10, pp. 1473–1490, 2008.

[20] K. Niino and N. Nishimura. Preconditioners based on Calderon's formulae for 1 periodic boundary value problems for Helmholtz' equation in 2D (Japanese). *Transactions of the Japan Society for Computational Methods in Engineering*, Vol. 9, pp. 1–6, 2009.

[21] K. Niino and N. Nishimura. Preconditioning based on Calderon's formulae for periodic fast multipole methods for Helmholtz' equation. *Journal of Computational Physics*, Vol. 231, pp. 66–81, 2012.

[22] H. Isakari, H. Yoshikawa, and N. Nishimura. A periodic FMM for elastodynamics in 3D and its applications to problems related to waves scattered by a doubly periodic layer of scatters (Japanese). *Journal of Applied Mechanics*, Vol. 13, pp. 169–178, 2010.

[23] H. Isakari, H. Yoshikawa, and N. Nishimura. A periodic FMM for Helmholtz–elastodynamics coupled problems (Japanese). *Transactions of the Japan Society for Computational Methods in Engineering*, Vol. 11, pp. 59–64, 2011.

[24] H. Isakari, K. Niino, H. Yoshikawa, and N. Nishimura. Calderon's preconditioning for periodic FMM for elastodynamics in 3D. *International Journal for Numerical Methods in Engineering*, 2011(accepted).

[25] AJ. Burton and GF. Miller. The application of integral equation methods to the numerical solution of some exterior boudary-value problems. *Proceedings of the Royal society of London. Ser A, A mathematical and physical sciences*, Vol. 323, pp. 201–210, 1971.

[26] M. Abramowitz and I.A. Stegun. *Handbook of mathematical functions with formulas, graphs, and mathematical tables*, Vol. 55. Dover publications, 1964.

[27] NA. Gumerov and R. Duraiswami. *Fast Multipole Methods for the Helmholtz Equation in Three Dimensions*. Elsevier, 2005.

[28] Y. Otani and N. Nishimura. An FMM for orthotropic periodic boundary value problems for Maxwell's equations. *Waves in Random and Complex Media*, Vol. 19, No. 1, pp. 80–104, 2009.

[29] Y. Saad. *Iterative Methods for Sparse Linear Systems*. Society for Industrial and Applied Mathematics, Philadelphia, PA, USA, 2003.

[30] K. Maslov, VK. Kinra, and BK. Henderson. Elastodynamic response of a coplanar periodic layer of elastic spherical inclusions. *Mechanics of Materials*, Vol. 32, pp. 785–795, 2000.

[31] H. Estrada, V. Gómez-Lozano, A. Uris, P. Candelas, F. Belmar, and F. Meseguer. Sound transmission through plates perforated with two periodic subwavelength hole arrays. *Journal of Physics: Condensed Matter*, Vol. 23, p. 135401, 2011.

[32] W.C. Chew, E. Michielssen, JM Song, and JM Jin. *Fast and efficient algorithms in computational electromagnetics*. Artech House, Inc., 2001.

[33] A.C. Eringen and ES Suhubi. Elastodynamics, vol. II. *Academic, New York*, Vol. 1, No. 2.3, p. 2, 1975.

[34] Huanyang Chen, Xudong Luo, and Hongru Ma. Scattering of elastic waves by elastic spheres in a NaCl-type phononic crystal. *Phys. Rev. B*, Vol. 75, No. 2, p. 024306, Jan 2007.

[35] I. E. Psarobas, N. Stefanou, and A. Modinos. Scattering of elastic waves by periodic arrays of spherical bodies. *Phys. Rev. B*, Vol. 62, No. 1, pp. 278–291, Jul 2000.

[36] N. Engheta, W.D. Murphy, V. Rokhlin, and M.S. Vassiliou. The fast multipole method (FMM) for electromagnetic scattering problems. *Antennas and Propagation, IEEE Transactions on*, Vol. 40, No. 6, pp. 634–641, 1992.

[37] X. Antoine, A. Bendali, and M. Darbas. Analytic preconditioners for the boundary integral solution of the scattering of acoustic waves by open surfaces. *Journal of Computational Acoustics*, Vol. 13, No. 3, pp. 477–498, 2005.

[38] X. Antoine, A. Bendali, and M. Darbas. Analytic preconditioners for the electric field integral equation. *International journal for numerical methods in engineering*, Vol. 61, No. 8, pp. 1310–1331, 2004.

[39] Z. Liu, X. Zhang, Y. Mao, YY Zhu, Z. Yang, CT Chan, and P. Sheng. Locally resonant sonic materials. *Science*, Vol. 289, No. 5485, p. 1734, 2000.

[40] S. Benchabane, A. Khelif, J.Y. Rauch, L. Robert, and V. Laude. Evidence for complete surface wave band gap in a piezoelectric phononic crystal. *Physical Review E*, Vol. 73, No. 6, p. 065601, 2006.